BALOGUN, Y. 2021. *Numerical and experimental study of the impact of temperature on relative permeability in an oil and water system*. Robert Gordon University, PhD thesis. Hosted on OpenAIR [online]. Available from: https://doi.org/10.48526/rgu-wt-1357866

# Numerical and experimental study of the impact of temperature on relative permeability in an oil and water system.

BALOGUN, Y.

2021

*The author of this thesis retains the right to be identified as such on any occasion in which content from this thesis is referenced or re-used. The licence under which this thesis is distributed applies to the text and any original images only – re-use of any third-party content must still be cleared with the original copyright holder.*

OpenAIR @RGU

This document was downloaded from https://openair.rgu.ac.uk

CC BY NC

# Numerical and Experimental Study of the Impact of Temperature on Relative Permeability in an Oil and Water System

Yakubu Balogun

PhD 2021

# Numerical and Experimental Study of the Impact of Temperature on Relative Permeability in an Oil and Water System

Yakubu Balogun

A thesis submitted in partial fulfilment of the
requirements of the
Robert Gordon University
for the degree of Doctor of Philosophy

February 2021

# DEDICATION

This work is dedicated to the Almighty God for His unfailing grace and mercies. The work is also dedicated to my dear and ever supportive wife- Oluwatoyin Priscilla (LT) and my adorable daughters – Ella & Elsie; you girls make fatherhood fun!

# ACKNOWLEDGEMENT

I wish to express my sincere and unalloyed gratitude to my wonderful and supportive supervisory team, Dr Draco Iyi for starting me on the right footing and holding my hands when needed and allowing me to fly when I could; Dr Nadimul H. Faisal for your motivating words at every meeting and particularly the words from you and Dr Prabhu during the challenging COVID-19 lockdown; Prof. Babs for grooming me with a strong hand to self-actualisation in the world of research. Dr Gbenga Oluyemi for the times spent with me in the lab listening to the unending stories of faulty and failing equipment yet never tiring to help.

Toyin you know I appreciate your patience and support; holding our girls when I had to stay until 10 pm in the university without complaining, and without you this PhD journey would not have been possible. To my little princesses, Ella and Elsie, I appreciate your patience and understating when daddy could not spend quality time – PhD is over now, time to have fun! To my elder brother turned mentor and role model, Ademola Balogun, you made it possible both financially and morally. I want to thank my mother and mother-in-law, Mrs Ololade Balogun and Mrs Akinbola Esther for your never-ending prayers. My appreciation goes to my sisters Ola, Lizzy and Nike for your prayers, and my younger brother for always believing I can achieve almost anything.

My sincere appreciation goes to the Robert Gordon University for giving me the scholarship and needed funding for my PhD programme. Special thanks to the support staff in the School of Engineering; Dr Ros and Kirsty for never getting tired of our never-ending challenges. To the technical support team head Alan McLean and other technical staff – David Smith, Martin Johnstone and Allan MacPherson, I am grateful for your support. When the going was tough, Ms Ruissein was there – thanks to my PhD friend you make collaborative research fun! To Dr Mamdud Hussein for trainings on fundamentals of CFD – I will not forget, Dr Ibiye Iyalla for your support and all my colleagues in the hub; Yatin, Ofasa, Ovoke, Paul, Demmy, Emmanuel, Bola, Awalu, Maryam, and Mutiu – I enjoyed our time together.

I acknowledge the support from the Deeper Life Bible Church, Aberdeen – Pastor Israel Adebayo for your prayers and support, Tony Mbata for your time and support during my machine learning troubles and my fellow G-light Ambassadors

– Emem, Onoja, Blessing, Grace, Ope, Darius, Temi, Dayo, Dele, Olamide, Beloveth – you all rock!

I thank many other people whose names are not mentioned but have contributed in one way or another to making my PhD journey a success.

# ABSTRACT

Relative permeability is affected by several flow parameters, predominantly operating temperature and fluid viscosity. Fluid viscosity changes with temperature, which correspondingly affects the relative permeability. Temperature is believed to have a considerable effect on oil–water relative permeability, thus a vital input parameter in petroleum reservoir development modelling. The actual effect of temperature on oil–water relative permeability curves has been a subject of debate within the scientific community. This is based on contradictory experimental and numerical results concerning the effect of temperature on oil–water relative permeability in literature.

This work investigates the effect of temperature on the multiphase flow physics in a porous media under varying temperature conditions. A computational fluid dynamics approach was adopted for a pore-scale study of the temperature effect on oil recovery factor under a water- and oil-wet condition. For the oil–water relative permeability investigation, a series of coreflooding experiments were conducted with well-sorted unconsolidated silica sandpacks, adopting the unsteady-state relative permeability method. The series of experiments were performed at different temperatures (range between 40 to 80 °C). Three levels of injection flowrates (0.5, 0.75 and 1.0 mL/min) and two oil viscosities (43 cP motor and 21 cP mineral oil – at 60 °C) were used in the study. A history matching approach using the commercial software Sendra was used to determine the oil-water relative permeability for each respective temperature, flowrate, and oil viscosity. A support vector regression algorithm was later implemented for the machine learning modelling aspect of this work which can predict reliable temperature dependent oil–water relative permeability.

The pore-scale results showed that the displacement behaviour of water and oil-wet system is strongly affected by the contact angle with a profound effect on the oil recovery factor. The water-wet system resulted in about 35 – 45 % more oil recovery than the oil-wet system, with the unrecovered oil mainly adhering to the wall region of the pore bodies of the oil–water system. The results from all the experimental cases showed that the oil–water relative permeability is a function of temperature, water injection flowrate and oil viscosity. In addition, the experimental findings show a decreasing residual oil saturation of the more viscous fluid with increasing injection flowrate. The end-point water relative permeability varies slightly for the set of experiments with the values higher for the less viscous oil under the same flowrate condition. Generally, the profile of oil and water relative permeability curve changes with varying oil viscosity and water injection flowrate at the same operating condition. This behaviour shows that the viscosity of oil is an important factor to be considered when selecting displacement flowrate to guarantee high oil production. Furthermore, an increment in temperature results in a corresponding rise in the relative permeability of both oil and water.

Comparison of the experimental and machine learning results showed a good match and consistency across all datasets. In addition to the machine learning model, this study proposes a modified empirical model using nonlinear least square regression for application in unconsolidated porous media. The output from this model can be applied for relative permeability prediction, preliminary evaluation in experimental design and as a valuable benchmarking tool for future laboratory experiments under varying temperature conditions.

**Key words:** Multiphase flow, Relative permeability, Temperature, Porous media flow, Machine learning, Support vector regression, Predictive model, Empirical model, Numerical modelling, CFD modelling

# TABLE OF CONTENTS

# TABLE OF FIGURES

# LIST OF TABLES

# NOMENCLATURE

| | |
|---|---|
| A | Area ($cm^2$) |
| K | Permeability ($m^2$ or D) |
| L | Length (cm) |
| NPV | Number of pore volume |
| P | Pressures (Atm) |
| q | Flowrate ($cm^3/s$) |
| $S_{or}$ | Irreducible oil saturation |
| M | Mobility ratio |
| S | Saturations |
| t | Time (s) |
| T | Temperature (K) |
| v | Volume ($cm^3$) |
| V | Velocity (m/s) |
| Greek symbols | |
| $\emptyset$ | Porosity (dimensionless) |
| $\lambda$ | Fluid mobility |
| $\sigma$ | Interfacial tension (dyne/cm) |
| $\propto$ | Volume fraction (dimensionless) |
| $\mu$ | Viscosity(cp) |
| $\rho$ | Density ($Kg/m^3$) |
| Subscript | |
| b | Bulk |
| o | Oil |
| or | Residual oil |
| p | Pore |
| c | Capillary |
| r | Relative |
| w | Water |
| $w_i$ | Initial water |

# Chapter 1: INTRODUCTION

**Overview**

This chapter is divided into 3 main sections. The first section provides the context and motivation for the study, the second section provides a summary of the study's rationale, aim and objectives. The third section outlines and highlights the content in the subsequent chapters of the thesis.

## 1.1 RESEARCH CONTEXT AND MOTIVATION

Multiphase flow and heat transfer in porous media have been the focus of prolific research for decades as it arises in diverse engineering applications including thermal enhanced oil recovery, soil remediation, contaminant transport and fuel cells, etc. However, owing to the complex transport phenomena involved, multiphase flow coupled with heat transfer in porous media remain poorly understood and analytically intractable. This is because it involves inherently complex and nonlinear physical parameters, multiphase flow convolution – with exact solutions of the flow models being limited coupled with numerous simplifying assumptions. Consequently, solving practical engineering problems usually involves multi-dimensional effects requiring a solution of multiple coupled sets of nonlinear differential equations.

A porous media is a material consisting of rigid skeletal bodies and void spaces. The skeletal part of the porous body is referred to as the "matrix" or "frame" while the void spaces are called “pores” and usually occupied by fluids either liquid and/or gas. The interconnected pore spaces within the media aids the flow of fluids (Bastian, 1999). A pictorial representation of a porous system after a flood run is shown in Figure 1.1 below with the endcap used for the experiment at the top.

Figure 1.1: An image of a porous medium

The existence of porous materials appears in diverse areas and facets of humanity, occurring both naturally and synthetically (fabricated). Natural occurrences of porous media include rocks and soil (e.g. aquifers and oil reservoirs), biological tissues (e.g. bones and wood), while fabricated occurrences include cements, paper, ceramics, etc. Porous materials can be grouped into 3 broad categories: artificial, biological and geological. A regular assemblage of spheres or fibres is an example of artificial media, which has been used for different studies due to its simplicity. However, naturally occurring media are more complex and heterogeneous in existence. Biological media on the other hand includes bones, tissues and membranes and these are naturally occurring. The last category, geologic media, includes subsurface water aquifers and petroleum reservoirs, which are of practical applications in both ground water hydrology, contaminant studies and petroleum exploration and production (Abdussamie, 2009; Pan, et al., 2004).

Multiphase flow and heat transfer in porous media are of particular importance to several engineering applications, including radioactive waste disposal, carbon capture and storage, petroleum recovery, fluidised beds, environmental engineering, thermal engineering, biomedical engineering and soil remediation. Adequate knowledge of the physical properties of the porous structure, coupled with the existing interaction between the fluids and solid matrix is essential in understanding and evaluating the performance and application of any given porous medium. In a petroleum reservoir with oil, water and/or gas flowing, the concept of relative permeability explains the likelihood of a particular fluid phase flowing in the presence of the other fluids. The relative permeability is a critical parameter in the evaluation of any petroleum reservoir recovery performance.

### 1.1.1 **Heat transfer in porous media**

Heat transfer is the transfer of thermal energy from one physical system to another. The temperature of the body is a major determining factor affecting the rate of heat transfer between the systems coupled with the properties of the medium (thermal conductivity) where the transfer takes place. There are 3 fundamental mechanisms which aid the transfer of heat during the injection process of hot fluid into a porous medium:

- The physical movement of the injected fluid transports energy;
- Thermal conduction from the hotter end of the porous media to the regions of lower temperature; and
- Convective heat transfer between the injected fluid and original fluid/s in the medium.

According to Mohammadmoradi (2016) a knowledge of the heat transfer mechanics in a porous medium is needed for an accurate operation of thermal enhanced oil recovery methods. Thermal enhanced oil recovery mainly involves changing the reservoir makeup or rock/fluid properties due to the operating thermal gradient. An effective transfer of heat aids fluid viscosity reduction, fluid mobility and ultimate recovery. Two core parameters used to ascertain how efficiently thermal energy can be transported in a porous medium are the effective thermal conductivity (ETC) and effective thermal diffusivity (ETD). In a porous medium, factors such as morphology, porosity and fluid saturation generally affect the effective thermal conductivity. Several research efforts have been made to predict the thermal properties of porous media via experimental, theoretical and numerical or through a coupling effort of both (Arthur, 2015).

Multiphase flow and heat transfer system in a porous medium involves both convective and conductive heat transfer mechanisms to improve thermal performance of any system. Therefore, both mechanisms are important considerations. An accurate description of the modes of heat transfer, properties of the porous material, flow regimes and geometry will support the analysis of temperature distribution and heat transfer.

## 1.2 GAP IN KNOWLEDGE

In a multiphase flow regime within a porous system, the relative permeability of a phase is the ratio the phase effective permeability to the porous media absolute permeability. It has been shown that relative permeability is affected by several factors: viscosity, interfacial tension, fluid saturation, wettability, and rock petrophysical properties. All these properties are affected by temperature. Therefore, it is logical to believe that temperature will have some significant effect on relative permeability. Figure 1.2 illustrates relative permeability curves for an oil-water system.

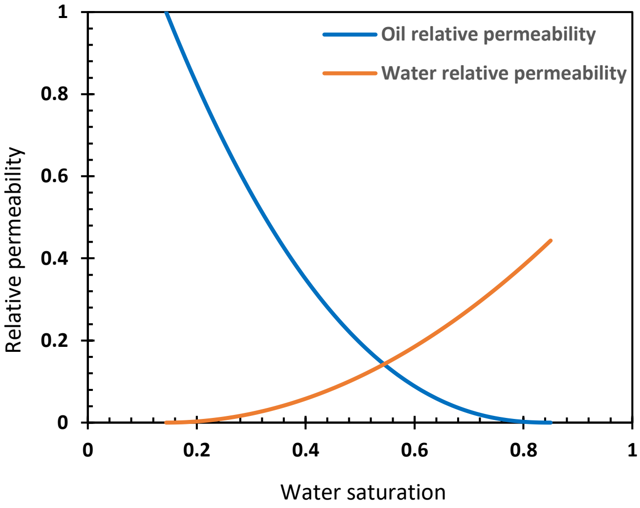

Figure 1.2: Typical oil-water relative permeability curve

Currently, the same values of oil-water relative permeability are used in reservoir simulators at different temperatures. This would potentially lead to significant errors and unreal values in the predictions. At elevated temperatures, some rock grains may expand while some particles are detached and re-mobilized in unconsolidated media. This results in the opening of more pore spaces or blockages of the pore throat and increments in pore constriction thereby reducing the intrinsic permeability of the rock (Miller & Ramey Jr, 1985; Mohammadmoradi, 2016). Thermal stress induced when there is a sharp temperature contrast in a system is believed to affect the properties of the media and needs to be understood to aid engineering applications. This study aims to improve the understanding of these phenomenon and advance the predictive capabilities of current approaches for better use in various applications.

Although relative permeability is believed to vary with temperature, there is controversy on the effect and thus the same set of relative permeability is often applied in the prediction of reservoir performance modelling at varying temperature (Qin, et al., 2018). While some authors believe that the relative permeability does not change with temperature (Sufi, et al., 1982; Polikar, et al., 1990); arguing that the observed variation in values is a function of other fluid-fluid or fluid-rock interactions and not necessarily the temperature factor, others disagree maintaining that the same relative permeability cannot be used for different temperature conditions (Torabzabeh & Handy, 1984; Watson & Ertekin, 1988; Maini, et al., 1989). This research would enhance the understanding of the temperature effects on relative permeability in a porous media.

## 1.3 RESEARCH AIM AND OBJECTIVES

The aim of this study is to evaluate the flow physics experimentally and numerically, with particular focus on relative permeability in oil-water porous media systems at high temperature and utilise the generated data to develop a data-driven model for future predictions. To achieve this aim, the specific objectives are as follows:

i. To numerically investigate the complex pore-scale interactions and transport phenomena of a multiphase fluid system of varying interfacial tension and matrix wettability. This will help to quantify the effect on oil recovery factor and improve thermal recovery field practice.

ii. To design and fabricate an experimental test-rig to provide reliable temperature dependent data for relative permeability computation. This experimental setup would allow for a detailed parametric study and generation of dataset for model development.

iii. To experimentally investigate the effect of oil viscosity and water injection flowrate on oil-water relative permeability.

iv. To experimentally investigate the effect of temperature on oil-water relative permeability and oil production over time.

v. To develop a data-driven model with a reliable and robust predictive capability for oil-water temperature dependent relative permeability which can serve as a benchmarking tool for future experimental work or field scale operations.

## 1.4 ORIGINAL CONTRIBUTIONS

This research work has been carried out to contribute to the body of knowledge by providing a better understanding of the influence of temperate on multiphase flow in porous media. During this research, the author has:

i. Presented a qualitative and quantitative evaluation of oil recovery factor under different media wettability. Application of the research findings is focused on thermal recover processes with combined effect of wettability and interfacial tension.
ii. Designed and fabricated an experimental test rig with adjoining instrumentation for unsteady-state coreflooding to study temperature dependent oil-water relative permeability. The development of the experimental test-rig is to the author’s knowledge a significant contribution.
iii. Quantified and evaluated the effect of oil viscosity, water injection flowrate and operating temperature on oil-water relative permeability providing a better understanding for the complex phenomenon.
iv. Derived empirical constants to be applied in analytic model published in literature for temperature dependent oil-water relative prediction. This has been validated using an independent experimental dataset from literature.
v. Formulated a machine learning model using Python programming language which applied the support vector regression algorithm with the experimental dataset generated from the experiments conducted.

The findings in this research establishes a better understanding of the intricate multiphase physics in a porous media with consideration for varying temperature. The machine learning and empirical modelling would serve as valuable tools for benchmarking future high temperature relative permeability laboratory experiments while equally been used for preliminary evaluation purposes prior to experiments or field-scale operations. These contributions are summarised in Figure 1.3 and have led to publications as listed in Section 1.5.

## 1.5 LIST OF PUBLICATIONS

**Published Article:**

i. Mahon Ruissein, **Balogun Yakubu**, Oluyemi Gbenga and Njuguna James (2020). Swelling performance of sodium polyacrylate and poly (acrylamide-co-acrylic acid) potassium salt. *SN Applied Sciences* volume 2, Article number: 117

**Manuscripts submitted for review:**

i. Iyi Draco, **Balogun Yakubu**, Faisal Nadimul and Oyeneyin Babs (2019). *A Numerical Investigation of Heat Transfer in a Vertical Porous Channel: The Effect of Thermophysical Properties.* Submitted to Journal of Petroleum Science and Engineering -Elsevier (Revised copy under review).
ii. Iyi Draco, **Balogun Yakubu**, Faisal Nadimul and Oyeneyin Babs (2019). *Numerical Modelling of Oil-Water Immiscible Flow and Heat Transfer in a Porous Media.* Submitted to SN Applied Sciences - Springer (Revised copy under Review).
iii. Iyi Draco, **Balogun Yakubu**, Faisal Nadimul and Oyeneyin Babs (2019). *CFD modelling of Wettability, Interfacial Tension (IFT) and Temperature effect on Oil Recovery at Pore-Scale.* Submitted to Journal of Petroleum Science and Engineering - Elsevier (Accepted, In print).
iv. **Balogun Yakubu,** Iyi Draco, Faisal Nadimul, Oyeneyin Babs, Oluyemi Gbenga and Mahon Ruissein (2020). *Experimental investigation of the effect of injection rate and oil viscosity on two phase oil-water relative permeability.* (Manuscript in preparation).
v. **Balogun Yakubu,** Iyi Draco, Faisal Nadimul, Oyeneyin Babs, Oluyemi Gbenga and Mahon Ruissein (2020). *Experimental investigation of the effect of injection temperature on two-phase oil-water relative permeability*. Submitted to Fuel Journal - Elsevier (Revised copy under review).
vi. **Balogun Yakubu,** Iyi Draco, Faisal Nadimul, Oyeneyin Babs, Oluyemi Gbenga Mahon Ruissein and Anthony Mbata (2020). *Predicting the effect of temperature on oil-water relative permeability: A machine learning modelling approach*. Submitted to Journal of Petroleum Science and Engineering - Elsevier (Under review).

**Conference/seminar Presentations:**

i. **Balogun Yakubu,** Iyi Draco, Faisal Nadimul and Oyeneyin Babs (2017). *Numerical Modelling of Oil-Water Immiscible Flow and Heat Transfer in a Porous Media.* Presented at the Third UK InterPore Conference on Porous Media, September 4-5, 2017, The University of Warwick, UK
ii. **Balogun Yakubu,** Iyi Draco, Faisal Nadimul and Oyeneyin Babs (2019). *CFD modelling of Wettability, Interfacial Tension (IFT) and Temperature effect on Oil Recovery at Pore-Scale.* Presented at the Robert Gordon University, Graduate School Symposium Aberdeen, UK.
iii. **Balogun Yakubu,** Iyi Draco, Faisal Nadimul and Oyeneyin Babs (2020). *Experimental and machine learning study of temperature dependent oil-water relative permeability*. Presented at the monthly seminar of the Petroleum Engineering Research Group (PERG), Robert Gordon University, Aberdeen, UK.

**Posters:**

1. **Balogun Yakubu,** Iyi Draco, Faisal Nadimul and Oyeneyin Babs (2018). *Investigation of the Heat Transfer Characteristics in a Vertical Porous Channel of varying Thermophysical Properties: A Numerical Approach*. Poster presented at the Society of Petroleum Engineers (SPE) Networking Seminar, Aberdeen UK.
2. **Balogun Yakubu,** Iyi Draco, Faisal Nadimul and Oyeneyin Babs (2019). *CFD modelling of Wettability and Temperature effect on Oil Recovery at Pore-Scale level*. InterPore2019 Valencia, Spain, 6 May – 10 May

## 1.6 PROJECT ROADMAP

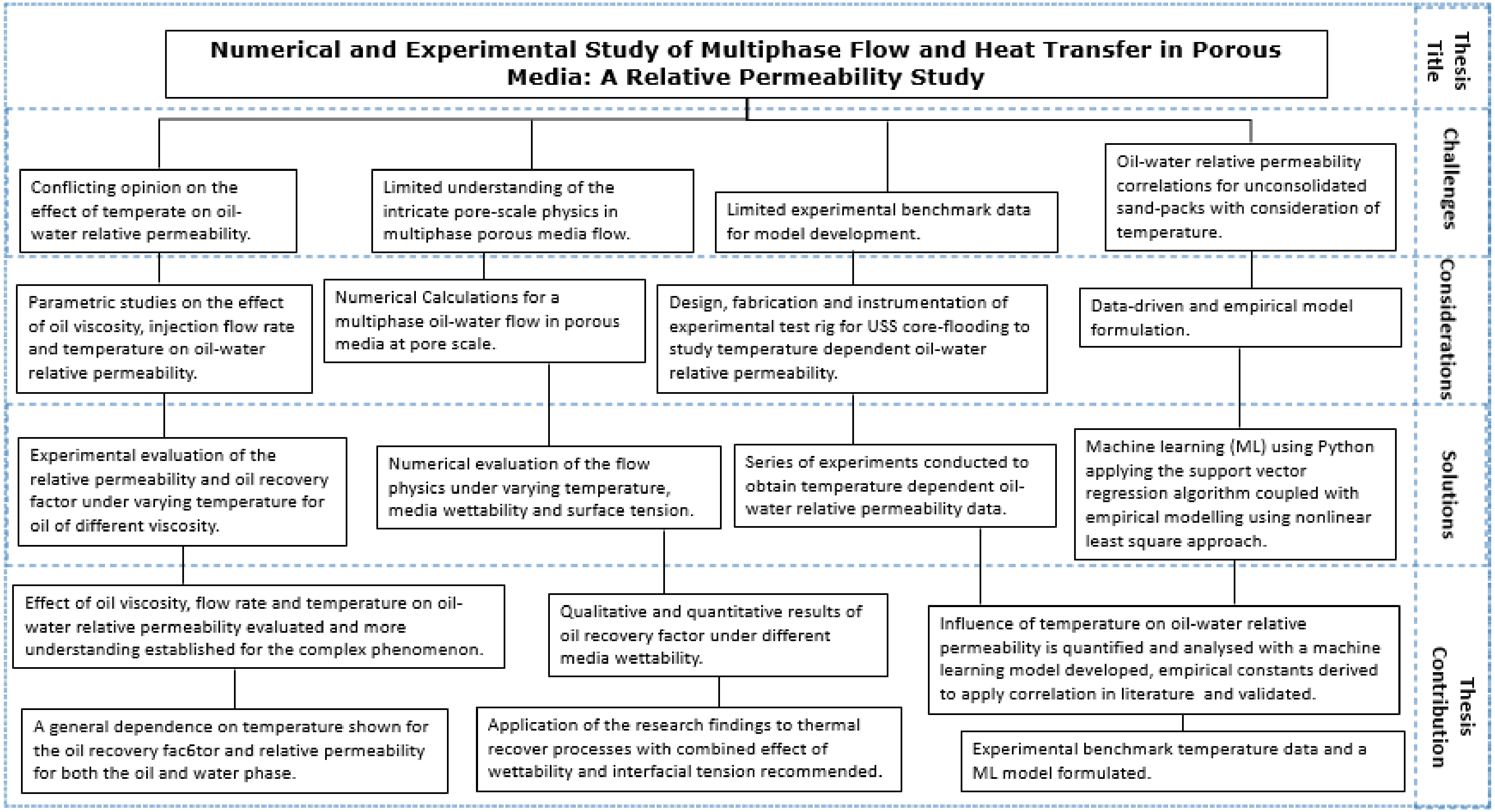

Figure 1.3: Research road map highlighting the work completed as part of this research study and its contribution to knowledge

## 1.7 THESIS OUTLINE

*Chapter 1*: Introduction. This section contains the fundamental description of a porous media, providing the motivation/justification, aim and objectives of the research work. Last section is the outline of the thesis.

*Chapter 2*: Literature Review. This chapter presents a comprehensive review of the background literature on relative permeability to establish the knowledge gap in the field. This chapter also presents the different experimental techniques used for the laboratory measurements of relative permeability with comparative advantages and disadvantages of each method.

*Chapter 3*: Experimental Procedures. This chapter describes the experimental apparatus, sandpack and fluid systems with the methods used for the research including analysis techniques.

*Chapter 4:* Numerical Methodology. This chapter presents the computational fluid dynamics (CFD) approach with governing equations and simulation methods implemented in the study. It also presents a brief summary of the machine learning methodology.

*Chapter 5:* This chapter covers the results and discussion from the CFD approach on the micro-scale investigation of wettability and interfacial tension effect with temperature in a 2D porous media. This chapter also contains the results from the mixture model CFD study on the effect of temperature on two-phase oil-water relative permeability and lastly a detailed report of the Eulerian model numerical simulation of multiphase flow and heat transfer in porous with applications in petroleum reservoirs.

*Chapter 6:* This chapter presents experimental results obtained from high temperature coreflooding experiments to estimate two-phase relative permeability. Detailed experimental data coupled with results from the numerical simulator for special core analysis (SCAL) are also captured in this chapter. A modified empirical model and validation of model are also included in this chapter.

*Chapter 7:* This chapter reports the machine-learning modelling aspect of the work using the experimental data generated for oil-water relative permeability through the implementation the support vector machine (SVR) algorithm.

*Chapter 8:* This chapter presents the conclusion and recommendations for future work.

# Chapter 2: LITERATURE REVIEW

**Overview**

This chapter is divided into 4 main sections. The first section reviews the general concepts in a multiphase system, providing a brief explanation of the relative permeability concept. The second section discusses in detail the different methods, both experimental and numerical correlations while highlighting the procedures and their comparative advantages and disadvantages. The third section is used to itemise some models that couples temperature effect in their derivation while the last section reviews a wide spectrum of literature on the different factors affecting relative permeability.

## 2.1 MULTIPHASE FLOW IN POROUS MEDIA

As defined by Bastian (1999), a phase is a chemically homogeneous part of a system under consideration that is separated from others by a definite physical boundary. In a single–phase regime, the porous media pore spaces are occupied by only a single fluid (e.g. oil) or by two or more completely miscible fluids (e.g. fresh water and salt water). In fluid mechanics, multiphase flow refers to the concurrent flow of:

(a) Fluids with varying states or phase such as liquid/gas or solid/liquid; and

(b) Fluids of the same state or phase but separate chemical properties mainly a liquid-liquid flow such as oil in water.

Under a multiphase scenario in porous media, individual phases are considered to have a specified volume fraction and flow velocity field. The following sub-sessions provide an overview of the principles involved in the modelling of multiphase fluid flow through porous media.

### 2.1.1 Effective permeability

The preferential transmission of a particular fluid phase within a porous media whilst coexisting with other immiscible fluids is termed "effective permeability". The main determining factor of the effective permeability of a phase is the relative saturation of the fluid present and the characteristics of the medium. The effective permeability of a phase β can be expressed as (Eq. 2.1):

$$q_\beta = \frac{k_\beta A \Delta P}{\mu_\beta L} \quad 2.1$$

Where q is the flowrate, k is the permeability, A is the surface area, ΔP is the pressure difference, μ is the fluid viscosity and L is the length.

### 2.1.2 **Relative permeability**

In multiphase flow systems, the relative permeability of a phase is the ratio of the phase effective permeability to the absolute permeability of the porous media. The relative permeability is a dimensionless property denoted as $k_r$. The relative permeability of a phase β can be expressed below as:

$$k_{r\beta} = \frac{k_\beta}{k} \quad 2.2$$

In a multiphase flow system containing oil, water or gas, the sum of their respective relative permeability is between 0 and 1; that is, $k_{ro} + k_{rw} \leq 1$. Typical oil-water relative permeability data is represented in the form of the Figure 2.1 below. As the water saturation increases, the relative permeability to the oil phase reduces and the relative permeability to the water phase increases until it reaches the residual oil saturation when the oil phase is immobile. Analysis of typical relative permeability curves shows that:

i. The relationship between the phase saturation and relative permeability is nonlinear.
ii. For the water phase, the irreducible water saturation ($S_{wi}$) is the endpoint saturation where the contained water is immobile and relative permeability is 0.
iii. In the case of the oil phase, the analogous point is the residual oil saturation ($S_{or}$) where oil relative permeability is 0 and oil ceases to flow in the porous medium.
iv. Concurrent flow of oil and water gives values of $k_{ro}$ and $k_{rw}$ between 0 and 1.

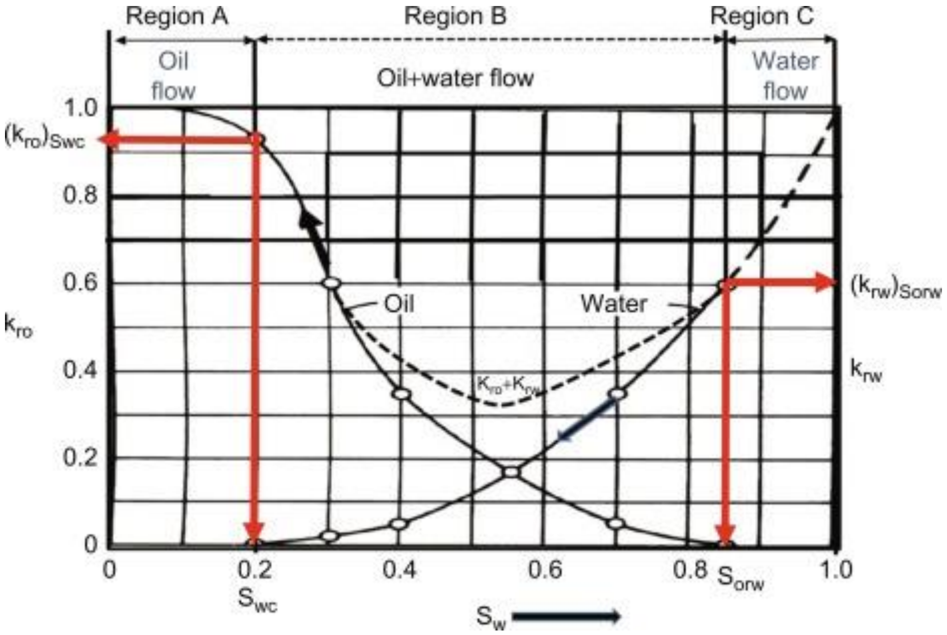

Figure 2.1: Relative permeability curve (Tarek, 2019)

The transient relationship between the oil-water relative permeability and saturation for a porous media under water injection with the media filled with only water and oil is summarised in the Table 2.1 below.

Table 2.1: Relationship between oil-water relative permeability and saturation (Abdus & Iqbal, 2016)

| Stage of waterflood | Oil saturation ($S_o$) | Oil relative permeability ($k_{ro}$) | Water saturation ($S_w$) | Water relative permeability ($k_{rw}$) |
|---|---|---|---|---|
| At the start of waterflood | $S_{oi}$ | 1 | $S_{wi}$* | 0 |
| During waterflood | $S_{oi} < S_o < S_{or}$ | $0 < k_{ro} < 1$ | $S_{wi} < S_w < 1 - S_{or}$ | $0 < k_{rw} < 1$ |
| At the end of waterflood | $S_{or}$* | 0 | $1 - S_{or}$ | 1 |

**Endpoint saturation*

## 2.1.3 **Mobility ratio**

Mobility of a particular fluid phase is the ratio of its effective permeability to the viscosity. Large phase mobilities means the fluids can flow at higher velocities than fluids with small mobilities. Water, for example, has a low viscosity compared to highly viscous oil and will thus have a larger mobility than the oil. In a waterflood scenario operating under a piston-like displacement, the mobility ratio is defined as the mobility of the displacing fluid at average residual oil saturation divided by the mobility of the displaced fluid at irreducible water saturation (Green & Willhite, 1998). This can be expressed mathematically as (Eq. 2.3):

$$M = \frac{\lambda_D}{\lambda_d} = \frac{\lambda_w}{\lambda_o} = \frac{(k_{rw}/\mu_w)_{s_{or}}}{(k_{ro}/\mu_o)_{s_{wi}}} \qquad 2.3$$

where M is the mobility ratio and $\lambda_D$, $\lambda_d$, $\lambda_w$, $\lambda_o$ are the mobility of the displacing fluid, displaced fluid, water and oil phase respectively, $\mu_o$ and $\mu_w$ are the viscosity of the water and oil respectively.

In an immiscible displacement scenario, the mobility ratio is an important parameter that describes the rate and efficiency of the process. A positive mobility ratio is typically considered for values less than one with values above one termed as unfavourable. With increasing mobility ratio above one, the flow becomes unstable, and viscous fingering can occur (Donaldson & Alam, 2008; Green & Willhite, 1998). Figure 2.2 illustrates a favourable mobility ratio and an unfavourable mobility ratio scenario.

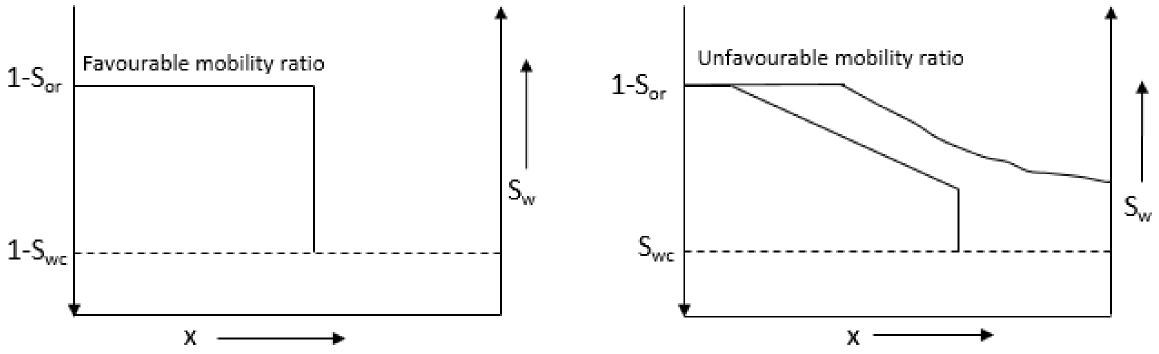

Figure 2.2: A favorable mobility ratio with water displacing oil, a mobile oil bank is developed ahead of the advancing water (left). An unfavorable mobility ratio with the water flowing faster than oil resulting in discontinuities in the water saturation, adapted after Apostolos et al. (2016)

### 2.1.4 **Surface and interfacial tension**

When a liquid is in contact with gas, there exist a tensile force on the contact surface referred to as the surface tension. If the interacting fluids are both liquid, interfacial tension is used instead. This property of immiscible fluids in contact with one another makes the surface acts like an elastic membrane/sheet under tension. This multiphase flow property causes the attractive forces between the molecules of two liquids present at the surface. While this property is referred to as "interfacial tension" (IFT) for liquid-liquid or liquid-solid interactions, it is called the surface tension when one of the two phases is a gas. In a multiphase scenario, each surface tension acts upon its respective interface, defined by the contact angle, “θ”, to the surface. Details of the contact angle is given in the next section and shown in Figure 2.3 below.

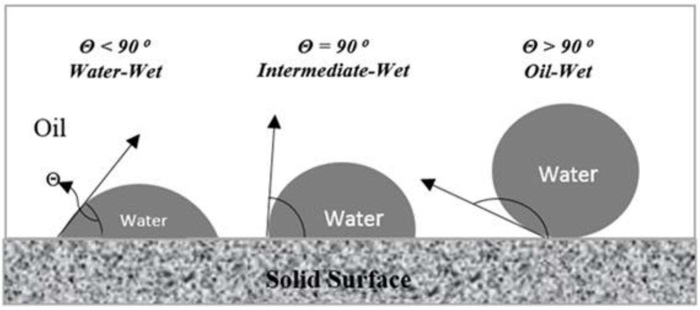

Figure 2.3: Schematic representation of contact angles of water on a solid surface

### 2.1.5 **Wettability**

Wettability is the propensity of one fluid to preferentially spread on or adhere to a solid surface when two or more immiscible fluids are flowing concurrently in the system. Wettability is a multiphase flow property that reflects the interaction between the fluid and the walls of the solid matrix. In an oil reservoir, with a fluid phase of brine, oil and/or gas, and the solid phase being the rock matrix, one of the fluid phases preferentially wets the solid matrix based on the interactions within the system. The phase that wets the matrix is termed as the wetting phase and the other the non-wetting phase. In an oil-water system, water wets the solids matrix while oil wets the solid matrix in a gas-oil system. In a system containing the three fluid phases, water is always the wetting phase while gas is considered the non-wetting phase. Determination of the solid wettability condition is done by measuring the contact angle of the fluid with the solid phase which is always measured through the denser phase and is related to interfacial tension using Eq. 2.4 (John, 2010):

$$\sigma_{os} - \sigma_{ws} = \sigma_{ow} cos\Theta \qquad 2.4$$

where $\sigma_{os}$, $\sigma_{ws}$ and $\sigma_{ow}$ are the interfacial tensions in dyne/cm between the oil-solid, water-solid and oil-water phase respectively while $\Theta$ is the contact angle at the oil–water–solid interface in degrees.

Figure 2.4 shows the result from a CFD simulation for different contact angles to illustrating the different wettability conditions on a sand grain within a pore throat; red represents oil while blue represents water.

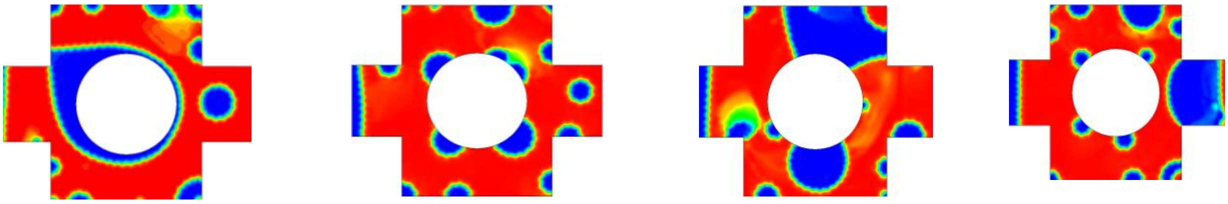

0°: Totally water wet (<90 °) 70°: Fairly water wet (<90 °) 90 °: Neutrally wet 120°: Oil wet (>90 °)

Figure 2.4: Wetting/contact angles for different wetting properties

The range of values for some common surface tensions for oil, water and gas in the petroleum industry are given in **Error! Reference source not found.** below (Paul, 2012; John, 2010).

Table 2.2: Interfacial tension for common fluid-fluid interfaces

| Fluid pair interface | Interfacial tension (mN/m or dyne/cm) |
|---|---|
| Air-water | 72-100 |
| Oil-water | 15-40 |
| Gas-oil | 35-65 |

Different laboratory methods are used for wettability measurements with reliable measurements obtained at reservoir conditions. Table 2.3 presents examples of contact angles for different wetting conditions.

Table 2.3: Examples of contact angle for different fluid systems (Paul, 2012)

| Wetting condition | Contact angle (in degrees) |
|---|---|
| Strongly water wet | 0–30 |
| Moderately water wet | 30–75 |
| Neutrally wet | 75–105 |
| Moderately oil-wet | 105–150 |
| Strongly oil-wet | 150–180 |

## 2.1.6 **Capillary pressure**

When two immiscible fluids are in contact, the pressure difference across the interface between them is termed as “capillary pressure” ($P_c$) which arises from the capillary forces that are mainly surface tension and interfacial tension (Tarek, 2019). In a porous media, the capillary pressure is the pressure differential between the non-wetting phase and the wetting phase, and it is always non-zero. It can be expressed as:

$$P_c = p_{non-wetting\,phase} - p_{wetting-phase} \qquad 2.5$$

In a typical porous media, the capillary pressure is a function of the combined effect of the surface and interfacial tensions, porous media geometry and pore size as well as the wettability condition of the media. The capillary pressure affects the displacement process of one fluid by another in a porous media. Therefore, to maintain a porous system that is partially occupied by the non-wetting fluid, the non-wetting phase pressure has to be maintained at a value higher than that in the wetting phase (Tarek, 2019).

### 2.1.7 Phase saturation

As mentioned earlier, multiphase flow occurs when several phases co-exist in a control volume simultaneously. The fluid system might have one or more of its components existing in more than one phase, or the phases existing in very different components. It is apparent that the presence of different phases within the same volume makes the volume of each phase to be less than the total volume. The saturation of a particular fluid, known as the phase saturation, is the ratio of the fluid volume to the total pore volume. The phase saturation of each present phase is typically a number between 0 and 1.

## 2.2 RELATIVE PERMEABILITY MEASUREMENTS

The multiphase flow of fluid through porous media is a complex phenomenon which is often poorly understood with relative permeability being one of the most important factors influencing fluid behaviour through a porous medium. The fundamental concept of permeability was established by the classic Darcy equation for single-phase fluid flow scenario in a sand filter and has now been extended to multiphase flow by the introduction of the concept of relative permeability. Henry Darcy established the equation in the form of an empirical law for fluid flow in 1856 through experimentation. He used an experimental setup made up of a cylinder packed with sand grains having uniform sizes as the porous media was held in place by screens at both ends and saturated with water. From the experiments, he was able to establish the relationship between the flowrate for the water through the porous media, head loss between the ends of the cylinder, and the cross-sectional area. Relative permeability on the other hand is an indication of the complicated pore-level displacement physics coupled with the fluid-fluid and solid-fluid interaction and properties. Relative permeability can be measured through laboratory experiments or estimated using empirical correlations and pore-scale models (Blunt, 2001). The use of empirical correlations and pore-scale models relies on experimentally derived data for development and validation. While ample research attention has been given to two-phase relative permeability, three-phase relative permeability has not received much attention mainly due to its measurements in the laboratory being prohibitively complicated, costly, and time-consuming (Alizadeh & Piri, 2014).

Prediction of three-phase relative permeability curves have been achieved via several empirical correlations proposed by extrapolating two-phase relative permeability data (Baker, 1988; Blunt, 1999). Ranaee et al. (2016) carried out a comparative assessment of three-phase relative permeability models and demonstrated the reliable predictive capabilities of three-phase relative permeability models derived solely from two-phase flow experimental data without any three-phase flow data included. The study concluded that two-phase relative experimental data can be employed to calibrate three-phase oil relative permeability models. It is intuitive however to state that these empirical correlations are as reliable as the experimental data used for their formulation, highlighting the necessity for more experimental data in order to build new correlations that considers the different factors affecting the flow physics. Relative permeability correlations are discussed in Chapter 3 of this thesis.

### 2.2.1 **Experimental measurement of relative permeability**

Several techniques, ranging from laboratory experiments, mathematical models and empirical correlations have been adopted for relative permeability measurements. Laboratory measurement of relative permeability typically involves the use of a small porous sample and the simulation of one-dimensional two-phase flow in the sample from an inlet to an outlet. There are 3 different experimental measurement methods for relative permeability namely, steady-state (SS), unsteady-state (USS) and centrifuge. Comparative studies have shown that these methods produce dissimilar results, which may be attributed to the fact that a single approach may not be representative of the various flow regimes in the porous system, making different approaches a necessity (Singh, et al., 2001). A method that theoretically mimics the fluid displacement process in an underground reservoir is the unsteady-state method. Detailed explanations of the different methods with their corresponding advantages and disadvantages are presented in the following section.

#### 2.2.1.1 **Steady-state method**

The SS approach involves the concurrent injection of all fluid phases (water and oil or water, oil, and gas) into a porous medium at different metered fractional flows. With each run for the pre-set fractional flows, the flow domain is allowed to reach SS, (indicated by constant stable pressure drop across the sample). With the assumption that fluid saturations are uniform across the porous medium, respective fluid relative permeability can then be calculated from classic Darcy's law stated above. The SS experiment usually starts with the porous system fully saturated with one of two fluids before the fractional flow injection (Figure 2.5). Some of the challenges in the SS method are:

- The SS method assumes a uniform saturation profile along the sample. However, this assumption is rendered invalid in situations where gravitational or capillary forces are dominant.
- The SS procedure is not an exact representation of the recovery process in an underground reservoir. The realistic case involves displacement of one fluid by the other instead of concurrently injection both fluids.
- The SS technique is time-consuming and costly to achieve. Reported studies shows that it takes several hours to days to reach SS for one runs of the experiment (Alhammadi, et al., 2019).

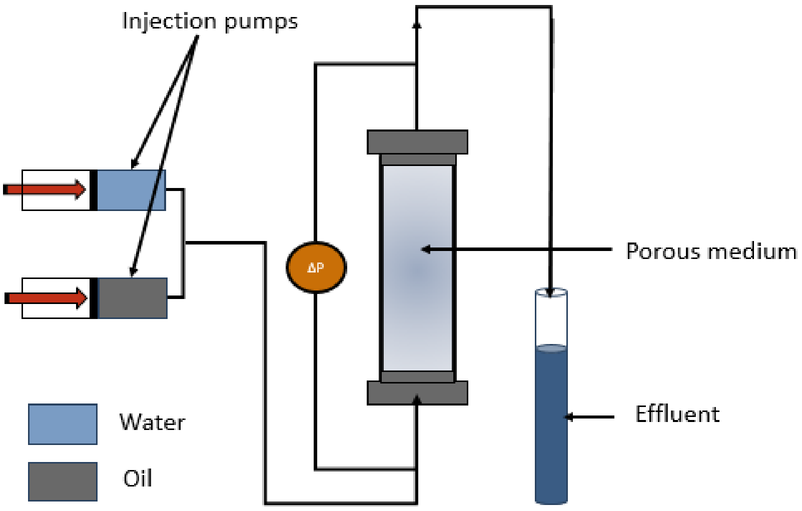

Figure 2.5: Schematic of a steady-state waterflood experiment

### 2.2.1.2 **Unsteady-state method**

The USS method otherwise referred to as the dynamic displacement method involves the injection of a single fluid into the porous media during each displacement process while monitoring the recovery of the phases at the outlet with the corresponding pressure drop across the sample taken. The USS method normally starts with the porous sample fully saturated with one fluid and measuring the differential pressure across the sample in the process. The differential pressure value is a critical parameter used to compute the relative permeability. Next, a displacing fluid is injected into the sample at a specified flowrate to displace the first phase. When water is used to displace oil, it is called imbibition while the process of displacing water with oil is drainage, a schematic of the process is shown in Figure 2.6. During the displacement process, the recovered fluid, injection flowrate and the differential pressures across the sample are monitored with respect to time and the injection volume recorded as number of pore volumes (NPV).

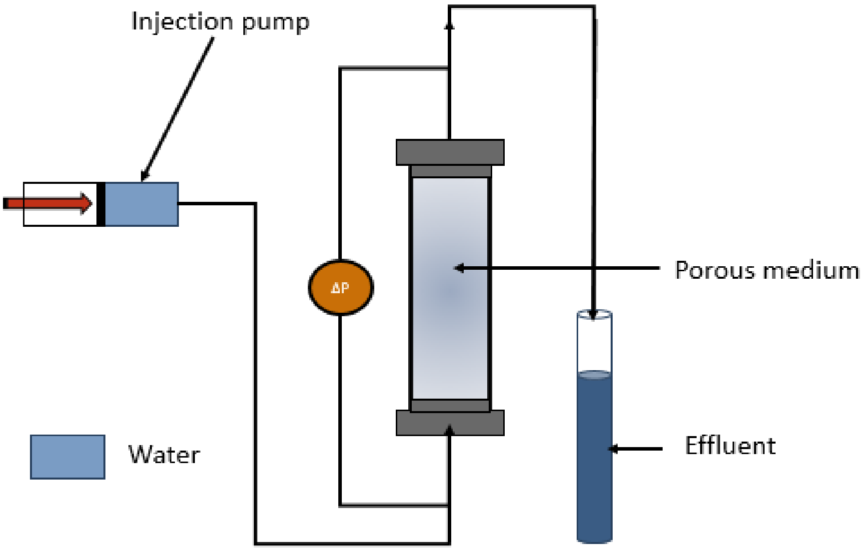

Figure 2.6: Schematic of the unsteady-state flow experiment

Unlike the SS method, the USS is an indirect technique for computing the relative permeability. It involves the application of the Buckley-Leverett theory (Buckley & Leverett, 1942) for linear displacement of immiscible and incompressible fluids (Honarpour & Mahmood, 1988). Due to the time being considerably lesser, the USS is the most widely used method for relative permeability measurements, however, this method is prone to experimental and interpretation errors (Ali, 1997). Interpretation of USS experimental data for relative permeability calculations involves various mathematical (Johnson, et al., 1959), graphical (Jones & Roszelle, 1978) and numerical history matching techniques (Archer & Wong, 1973; Roland, et al., 2016).

Johnson et al. (1959) presented a method referred to as the JBN method for calculating individual fluid phase relative permeability from waterflood experiment on a linear porous medium. They stated that after testing, the method was found to be both rapid and reliable for normal-sized core samples. The accuracy of using this approach was improved by Tao and Watson (1984) with the development of a Monte Carlo error analysis capable of investigating the effect of other experimental operating parameters on the accuracy of relative permeability estimates. A major issue with the JBN method is the non-inclusion of capillary pressure force that was improved upon by Li et al. (1994) with a new analytical method developed to include capillary pressure for oil-water relative permeability calculations. Further extension of the JBN method was made by Chen and DiCarlo (2016) by having a section-wise pressure drop measurements to correct for the capillary end effects.

More recent researchers have shown that the one-step experiments (only one injection pressure or flowrate) adopted in the JBN experiments is inaccurate and should be discarded (Roland & Guillaume, 2016). They maintained that JBN interpretations are based on transient flow dominated by viscous fingering and/or channelling, which is not a true representation of the pore-scale relative permeability. Details of the recommended procedures can be found in the reference.

Some of the challenges in the USS method are:

- The occurrences of capillary end effect result in non-uniform saturation profile at the outlet during USS experiments.
- Viscous fingering, channelling and instabilities resulting from the high flowrate used.
- In some instances, the time between the water breakthrough and complete flood-out is very short making space for relative permeability calculations within a small range.

- A precise measurement of the breakthrough time is critical for different interpretation techniques giving rise to inaccurate results when the wrong breakthrough time is recorded.

#### 2.2.1.3 **Centrifuge method**

The use of the centrifuge has been adopted as intrinsically USS and indirect method for relative permeability measurement. The process involves the rotation of a pre-saturated porous sample held inside a centrifuge bucket without confining pressure at elevated angular velocity. As the porous sample is being rotated in the centrifuge bucket, the fluids inside are exposed to a known centrifugal force and a calibrated graduated tube is used to measure the rate of liquid displacement. Data from the experimental run are used to calculate for the relative permeability through mathematical models (Van, 1982). The application of centrifuge method for relative permeability is based on what is called the "Hagoort's method" (Hagoort, 1980). Assumptions of the approach include: negligible capillary effects, an instantaneous start-up, and constant gravitational effects in the sample (Heaviside & Black, 1983). The method has a major disadvantage in that only the relative permeability of the displaced phase is given, and centrifugal forces rather than viscous forces displace the oil phase. On the other hand, this approach is believed to have an advantage over the USS because the effect of viscous fingering is eliminated and it is the preferred technique to simulate the gravity drainage process (Honarpour & Mahmood, 1988; Hagoort, 1980).

### 2.2.2 **Empirical correlations for temperature dependent relative permeability**

Indirect methods have been adopted to study and predict the fluid relative permeability in petroleum reservoirs with linkages drawn between different multiphase properties. Water saturation and capillary pressure data were used to predict relative permeability models in previous studies (Wyllie, 1951; Baker, 1988; Burdine, 1953; Corey, et al., 1956; Sigmund & McCaffery, 1979; Parker, et al., 1987; Lomeland, et al., 2005; Mehdi, et al., 1982).

While a lot of research effort has been put into developing these models, there has been few attempts made into investigating the effect of temperature on relative permeability through an indirect method and incorporating the temperature factor in the presented models. One of the authors that have attempted the relative permeability study through indirect techniques is Ehrlich (1970) who focused on the contact angle variation with temperature to study the effect of temperature on two-phase relative permeability analytically. Using the temperature multiphase flow parameter linkage, Amaefule et al. (1982) focused on the effect of temperature on IFT and proposed an explicit model for oil and water relative permeability as a function of IFT.

The effect of temperature and interfacial tension on oil-water relative permeability was studied experimentally using consolidated porous samples by Torabzabeh and Handy (1984) and the experimental data generated used by Kumar et al. (1985) with an empirical correlation presented for the relative permeability to the oil and water phase. Kumar et al. (1985) presented empirical correlations to model the relative permeability dependence on temperature both in high and low interfacial tension systems based on experimental data on water-oil residual saturations and relative permeability relationship with temperature, interfacial tension and capillary number. Data used for the correlation were categorised into two different clusters as the low IFT and high IFT system, thereby estimating the phase relative permeability under different circumstances. The authors emphasised that the model presented contained some variable coefficients affected by temperature and other rock/fluid properties.

Several other researchers have presented empirical oil and water relative permeability models as a function of pressure, fluid viscosity ratio, injection flowrate and temperature. However, only the developed models that consider the effect of temperature on the relative permeability curves have been compiled and summarised in Table 2.4 with the temperature range and other experimental/operating conditions under which the studies were conducted.

### 2.2.3 **Machine learning modelling approach**

With the emergence of high computing power coupled with smart computational techniques the ability to undertake highly convoluted modelling problems has been made possible. Artificial intelligence (AI), machine learning (ML) and deep learning have gained more attention in recent years due to the reliability and cost-saving comparative advantage derived from the application. Although empirical models have been widely employed for predictive problems, they are however limited in handling complex and nonlinear relationships (Kisi & Parmar, 2016).

Furthermore, ML does not require explicit conditioning in its formulation and thus can be applicable over a wide range of parameters as the patterns could be found independent of specific operating conditions. ML is the science of making computers, learn and act like humans with ability to improve their learning over time without being explicitly programmed to do so (Hanga & Yevgeniya, 2019). The key objectives of every ML implementation are prediction generation, clustering/segmentation, extraction of association rules as well as decision making from supplied data (Mohammed, et al., 2016).

In the oil and gas industry, ML has been found to be of great potential in the area of data analysis and interpretations, particularly in developing drilling plans, fault diagnosis, facilities monitoring, fault prediction and implementing real-time optimisation plans with minimum cost (Ccoicca, 2013). Different ML algorithms have been employed including support vector machine (SVM) for classification or regression, linear regression for prediction, logistic regression in cases with binary dependent variables; artificial neural networks (ANN) for complex pattern as well as optimisation algorithms such as particle swarm optimisation (PSO) and genetic algorithms (GAs). A more detailed review of the different algorithms is contained in the review by Hanga and Yevgeniya (2019). Typical cases of soft computing applications include the application of ANN for production forecasting by Amirian et al. (2018), enhanced oil recovery process optimisation by Nait et al. (2019), optimisation of water alternating gas injection process by Nait et al. (2018a) and a decision three approach to reservoir flood control by Chuntian and Chau (2002).

SVMs are a type of supervised machine learning algorithms mainly used for the execution of classification and regression problems. An SVM typically builds a hyperplane or set of hyperplanes to categorise all inputs in a high-dimensional or even infinite space. The data points closest to the classification margin are called support vectors. The goal of the SVM algorithm is to find an optimum hyper-plane with maximum distance from the support vectors. Figure 2.7 illustrates a simple case of a two-category classification problem in a two-dimensional input space.

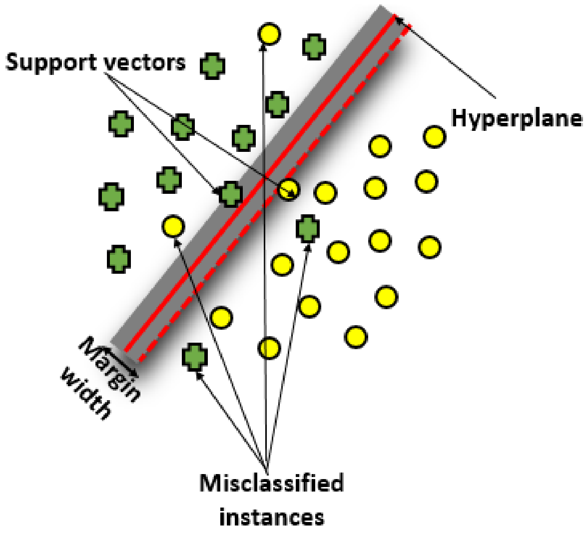

Figure 2.7: Simple linear SVM scenario adapted from Burges (1998)

An SVM model is a robust strategy and is considered by many as the best classifier that results in satisfactory generalisation of performance (Rafiee-Taghanaki, et al., 2013; Robert & Jorge, 2012; Übeyli, 2010). SVM has found high application use in the oil and gas industry due to its ability to handle highly convoluted, uncertain, and nonlinear behaviour of a host of parameters typical of the sector (Nowroozi, et al., 2009). More information on the application of SVM in the petroleum industry is presented in the review by Ccoicca (2013).

Gholami et al. (2012) employed the SVM algorithm for permeability prediction in three gas wells with very reliable results of $R^2$ value of 0.97 generated. The study compared the result of the SVM with the regression neural network (GRNN) and stated that higher accuracy and speed was obtained for the SVM approach. A similar approach was implemented by Mohammad et al. (2015) for prediction of the reservoir lithology using petrophysical well logs and Serapião (2006) for classification of drilling operation stages using mud-logging parameters. Yasin (2016) used the SVM coupled with cross validation algorithm for crude oil price predictions.

Chaki et al. (2014) implemented the Modular ANN (MANN) methodology for reservoir sand volume prediction. Both reservoir and seismic data were used in the model and the authors reported that the proposed workflow is superior to ANN with regards to higher correlation coefficient and reduced error measures. The least squared support vector machine (LSSVM) has been used in the estimation of: thermal conductivity of $CO_2$ gas by Shams et al. (2015), crude oil saturation pressure by Farasat et al. (2013), minimum miscibility pressure of $CO_2$ in a reservoir by Shokrollahi et al. (2013), gas condensate reservoir dew point pressure by Arabloo et al. (2013), and compressibility factor for natural gas compressibility by Fayazi (2014).

A limited number of studies have been conducted on the implementation of predictive ML algorithms for temperature dependent oil-water relative permeability. Arigbe et al. (2019) formulated a deep neural network (DNN) methodology for real-time relative permeability prediction in porous system of varying wettability considering the changes in fluid phase saturation with no consideration for the varying reservoir temperature. Results from the DNN predictions were compared with correlations by Wyllie, Corey, Parker, Stone, Baker, Honarpour and field data from an oil reservoir in the North Sea and showed higher accuracy for both oil and water relative permeability (Figure 2.8). However, reservoir temperature was not factored in as one of the influencing parameters in the model development. The LSSVM was implemented for a temperature dependent oil and water relative permeability by Nait et al. (2019) and Esmaelli et al. (2019).

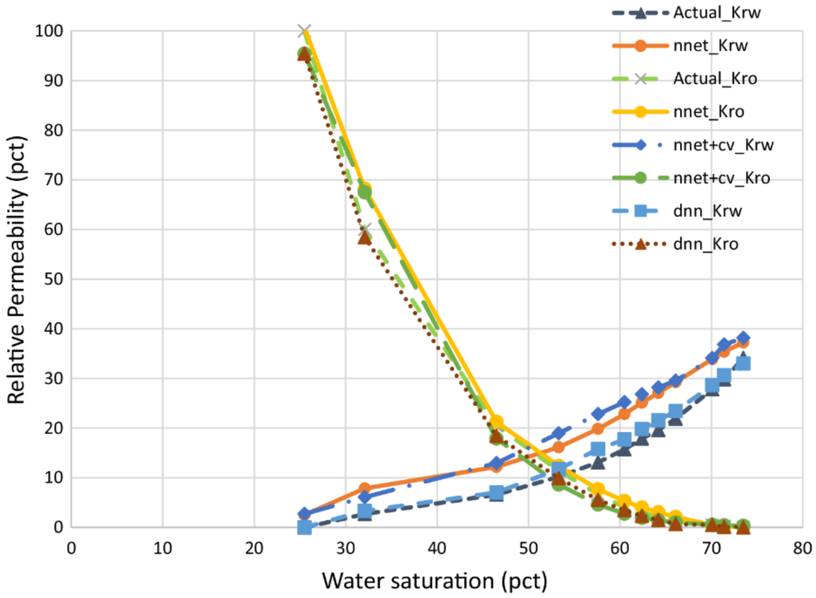

Figure 2.8: Experimental and predicted relative permeability models using machine learning with and without cross validation (Arigbe, et al., 2018)

Esmaelli et al. (2019) presented a LSSVM coupled with the simulated annealing optimisation technique for temperature dependent oil and water relative permeability with datasets mined from published literature. The result was compared with empirical models proposed by several scholars and revealed that the LSSVM proves to be more reliable, robust and accurate over the dataset used.

A similar study was conducted by Nait et al. (2019) with LSSVM, and radial basis neural network (RBFNN). The predictive algorithms were coupled with four optimisation algorithms involving PSO, GA, differential evolution (DE) and grey wolf optimisation (GWO). The study reported that the formulated RBFNN-GWO model is the most accurate for the temperature dependent oil and water relative permeability prediction. The authors stated that the RBFNN-GWO model can be used only in cases where the data satisfy the conditions of formulation.

Table 2.4: Relative permeability models with temperature effect

| Model | Water and oil relative permeability | Porous media and fluid used | Operating conditions |
|---|---|---|---|
| Bennion et at. (2006) | $60^{o}C < T < 100^{o}C$ $k_{rw} = 0.021(1 - S_N)^5$<br>$k_{ro} = (S_N)^{2.2}$<br>$S_N = (0.6 - S_w)0.45$<br>$150^{o}C < T < 275^{o}C$ $k_{rw} = 0.055(1 - S_N)^{2.5}$<br>$k_{ro} = (S_N)^3$<br>$S_N = (0.85 - S_w)0.7$ | Heavy oil<br>USS<br>History matching | $10 \leq T \leq 280^{o}$<br>$8000 \leq \mu_o \leq 1000000\ cP$<br>$0.12 \leq S_{or} \leq 0.72$<br>$0.11 \leq S_{wi} \leq 0.43$ |
| Mosavat et al. (2016) | $k_{rw} = S_{wc}^{a}$<br>$k_{ro} = (1 - S_{wc}^{b})(1 - S_{wc})^{c}$<br>$a = 1.32 + 0.00123(\mu_o/\mu_w) - 7.47 \times 10^{-7}(\mu_o/\mu_w)^2$<br>$b = 1.02 + 0.000298(\mu_o/\mu_w) - 1.38 \times 10^{-7}(\mu_o/\mu_w)^2$<br>$c = 2.22 + 0.00318(\mu_o/\mu_w) - 1.22 \times 10^{-7}(\mu_o/\mu_w)^2$ | Silica sand<br>Heavy oil<br>USS<br>History matching | $23 \leq T \leq 100^{o}$<br>$19.5 \leq \mu_o \leq 1860\ cP$<br>$0.2 \leq S_{or} \leq 0.413$<br>$0.05 \leq S_{wi} \leq 0.105$ |
| Torabi et al. (2016) | $k_{rw} = 0.0466(0.0588P_D)^{-1.28676} \times e^{0.34443(2-q_D)} \times (0.0025\mu_D)^{-0.34267S_{we}^2}$<br>$k_{ro} = (0.0588P_D)^{-0.0291} \times e^{-0.01254(2-qD)} \times (1 - S_{we})^2 \times \left(1 - S_{wc}^{0.1(0.025\mu_D)^{-0.818}}\right)$<br>$P_D = \frac{P_{exp}}{P_{std}} \mu_D = \frac{\mu_o}{\mu_{std}} q_D = \frac{q_{exp}}{q_{std}}$ | Consolidated core<br>Heavy oil<br>Light oil<br>USS<br>JBN | $27 \leq T \leq 45^{o}$<br>$24.3 \leq \mu_o \leq 400.2\ cP$<br>$0.463 \leq S_{or} \leq 0.539$<br>$0.092 \leq S_{wi} \leq 0.138$ |
| Zhang et al. (2017) | $k_{rw} = k_{rw}^{0-50C}(e_1 + e_2 T + \frac{e_3}{T} + \frac{e_4}{T^2})\left(\frac{S_w - S_{wi}}{1 - S_{wi} - S_{or}}\right)^{a_3 T + a_4}$<br>$k_{ro} = \left(\frac{1 - S_w - c_1 \ln(T) - c_2}{1 - b_1 T - b_2 - c_1 \ln(T) - c_2}\right)^{a_1 T + a_2}$ | Consolidated core<br>Light oil<br>USS<br>JBN and Corey model | $25 \leq T \leq 100^{o}$<br>$4 \leq \mu_o \leq 48\ cP$<br>$0.153 \leq S_{or} \leq 0.324$<br>$0.234 \leq S_{wi} \leq 0.482$ |

## 2.3 FACTORS AFFECTING RELATIVE PERMEABILITY

Several factors have varying effect on the relative permeability curves. These include micro-scale features ranging from media wettability, fluid-fluid IFT and pore size distribution of the porous media as well as macro-scale properties such as viscosity, flowrate and temperature. All these factors can potentially change the shape of relative permeability curves. The change of media wettability can affect the distribution of fluids while the change in interfacial tension of flowing phases can significantly alter the flow characteristics within the porous system.

### 2.3.1 Effect of temperature on relative permeability

Maini and Batycky (1985) used composite core samples from real heavy oil reservoirs drilled both horizontally and vertically to investigate the effect of flow direction on relative permeability at varying temperatures from 25 to 272 $^{o}$C. Dynamic displacement experiments were carried out and relative permeability computation done by history matching with results showing a decrease of residual oil with an increase in the irreducible water saturation at high temperature. The study also reported that the oil relative permeability at irreducible water saturation decreases as the operating temperature increases. No temperature dependency was reported for the water relative permeability.

Closmann et al. (1985) performed SS experiments for relative permeability test on tar/brine systems at elevated temperatures. The study reported that for the thermally unaltered tar, the relative permeability curve shifts toward the low water saturation region. For the thermally altered tar, the relative permeability curve shows a close match with the Leverett oil permeability curve for water-wet unconsolidated sands. The effect of temperature gradient on relative permeability measurement was investigated by Watson and Ertekin (1988) under temperature values ranging from room temperature to 149 $^{o}$C. Experimental results showed that the irreducible water saturation increases while the residual oil saturation decreases with temperature. It was also reported that with an increase in the injection temperature, the computed values of oil and water relative permeability decreases. Both the oil and water relative permeability decrease at a larger rate with an increase in the temperature gradient.

Maini and Okazawa (1987) performed a series of USS two-phase experiments on unconsolidated silica sand using Bodo stock tank oil with relative permeability computed by history matching technique. The conclusion from the study is similar to earlier reports with relative permeability increasing with temperature. Three-phase flow experiments were performed for measuring relative permeability at elevated temperatures and pressures by Maini et al. (1989) using Ottawa sand as porous media with refined mineral oil, distilled water and nitrogen gas as the fluid phases. A SS approach was adopted for the different experiments at an elevated temperature of 100 $^{o}$C and pressure of 3.5 MPa. Unlike the earlier two-phase experiments, no dependence on temperature was reported in this study with the findings showing that the three-phase water and gas relative permeability are functions of their respective saturations only and did not change with the direction of saturation change. The oil relative permeability on the other hand was reported to vary as the saturation of the other fluids changed.

Kumar and Inouye (1994) carried out USS experiments aimed at developing and evaluating simpler low-temperature analogues of the high temperature relative permeability data using similar viscosity ratio and wettability. The JBN method was used for computing the relative permeability and results showed that the endpoint saturation changes with viscosity ratio but remains unchanged under varying temperature.

Sufi et al. (1982) presented an experimental study on the temperature effects on oil-water relative permeability and reported that the relative permeability curves remain unchanged with temperature. The same observation was reported by Miller and Ramey (1985) after conducting dynamic-displacement laboratory experiments on unconsolidated and consolidated porous media with water and a refined white mineral oil to measure relative permeability to oil and water. The experiments were carried out on cores of 5.1 cm in diameter and 52 cm in length with temperatures ranging from room temperature to about 149 °C. Results presented show essentially no changes in the relative permeability curves with temperature variations. They argued that factors such as viscous instabilities, capillary end effects or possible challenge in maintaining material balances might have affected previous reported results.

Akin et al. (1998) alluded to the argument of Miller and Ramey by stating that there is the need for examining the correctness of applying the JBN method for heavy oil-water relative permeability calculations while investigating the effect of temperature on relative permeability through numerical and experimental examples. They stated that the use of the JBN technique results in an erroneous result showing some temperature dependence of relative permeability curves. USS relative permeability experiments were performed for heavy oil and brine at different temperatures of 22 and 66 $^{o}$C. They showed that a single set of relative permeability curves is representative of both the ambient and high temperature for the experiments performed and thus concluded that relative permeability is not a function of temperature. Report of Polikar et al. (1990) also supports this claim as no significant temperature effects were found for their experiments on Athabasca bitumen-water system.

Zhang et al. (2017) conducted a series of coreflooding experiments on 5 sandstone core samples having different permeability values at different temperatures to investigate the relationship between relative permeability curves and temperature. Considering the fact that laboratory state conditions cannot perfectly represent fluid flow behaviour under reservoir condition, they proposed a way of translating the laboratory results to reservoir scales by combing the JBN method with empirical method. The study observed a significant increment in the shape of oil and water relative permeability curves with a rise in temperature for the various core samples with different permeabilities (Figure 2.9). With an increase in temperature, residual oil saturation was observed to decrease nonlinearly while the irreducible water saturation increased linearly but decreases with reducing permeability.

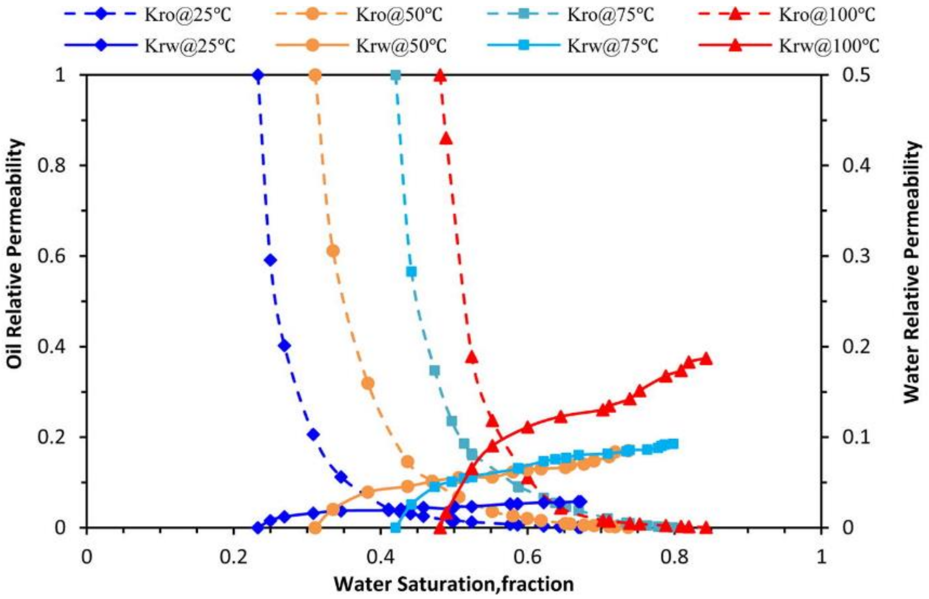

Figure 2.9: Variation of relative permeability curve under different temperatures, after Zhang et al. (2017)

Bennion et al. (2006) presented an oil-water relative permeability correlation with temperature effect for an unconsolidated bitumen producing formation in Canada. The study was an extensive review of existing water-oil relative permeability experimental data carried out under temperatures ranging from 10 to 275 °C. The study aim was to develop correlations for estimating water-oil relative permeability characteristics and residual oil saturations mainly for preliminary evaluation analysis. It was shown that with an increase in temperature, residual oil saturation decreases in a nonlinear pattern while the water saturation increases. Sensitivity of the relative permeability to brine was observed at temperatures below 100 °C.

The effect of initial water saturation, fluid composition and temperature on relative permeability was investigated by Hamouda et al. (2008) experimentally with 10 core samples having permeabilities of about 3 – 4 mD and porosities of 43 – 51 %. Results from the experiments showed that the residual oil saturation decreases for temperatures up to 80 °C while at 130 °C, it increased to about 45 % in value. The reversal and increment in residual oil saturation are believed to be caused by possible oil trapping resulting from the detachment of fines and their migration when temperatures exceeded 80 °C thereby creating dead ends and creating localised high residual oil saturation in the media. Relating the relative permeability curves to wettability of the media indicates a water-wet condition when the relative permeability shifts to the right at temperatures up to 80 °C while at higher temperature of about 130 °C, an oil-wet tendency can be inferred from the relative permeability curves. A shift in media wettability with temperature is also reported by Schembre et al. (2005) with the porous surface becoming more water-wet with temperature apparently due to fines detachment. Further studies by Hamouda and Karoussi (2008) stated that inferring relative permeability by media wetness might be misleading as the fine detachment and migration during flooding due the fluid-rock interactions become more repulsive at higher temperatures.

Akhlaghinia et al. (2014) conducted coreflood experiments on consolidated sandstone core samples to measure relative permeability using heavy oil, methane and carbon dioxide and used the JBN technique to calculate two-phase relative permeability. A series of experiments were conducted at 3 different temperature values of 28, 40 and 52 °C for different fluid pair to investigate temperature effect on relative permeability curves. Experimental results showed a linear increase of about 65% and 50% in the water relative permeability for temperatures ranging from 28 to 40 °C and 40 to 52 °C respectively. While the oil relative permeability curve increased at a rate of about 70 % with a temperature change from 28 to 40 °C and decreased by about 30 % with a temperature increase from 40 to 52 °C.

Vega and Kovscek (2014) carried out a series of SS coreflood experiments on low-permeability consolidated core samples to investigate the dependency of the respective phase relative permeability on operating temperature ranging from 45 to 230 °C. The study reported a systematic shift to increased water-wet state with increasing temperature. It was observed that this water wetness affects the relative permeability with the water-phase relative permeability shifting to the right as the temperature increases. A similar temperature range was investigated by Zeidani and Maini (2016) with Athabasca reservoir oil using the displacement experimental approach and history matching technique. Their reported results showed a decrease in oil saturation with an increase in temperature.

Ashrafi et al. (2014) investigated the dependency of oil-water relative permeability for heavy oil systems with temperature using unconsolidated media made up of glass beads and sandpacks. Their study reported that both the oil and water relative permeability are not affected by temperature. While changes to the fluid relative permeability were observed, the study suggests that the relative permeability variations with temperature is mainly due to the oil to water viscosity ratio changes with temperature. The study therefore concludes that temperature dependency of relative permeability is due more to different conditions such as viscous instabilities or fingering in higher permeable cores as well as viscosity ratios than fundamental flow properties.

Waxy crude oil samples and natural reservoir cores of permeabilities ranging from 300 to 1000 mD were used to study the effect of temperature and rock permeability on oil-water relative permeability curves by Cao et al. (2016). The experimental USS displacement method was carried out and the results obtained showed that temperature has a great influence on water-oil relative permeability curves. The findings reported that as the temperature decreased from 85 $^{o}$C to 50 $^{o}$C, there is a 40 % decrease in the initial water saturation while the residual oil saturation increased to 2.5 times in both the low and high permeability core samples. Two reasons suggested for these observations were mainly attributed to an increase in the oil viscosity due to wax deposition and the changing media wettability due to wax adsorption on the substrate.

Qin et al. (2018) reported experimental results on the effects of temperature on oil-water relative permeability in heavy-oil reservoirs in unconsolidated porous systems stating that irreducible water saturation linearly increases as temperature increases while the residual oil saturation decreases nonlinearly. In agreement with previous reports, this study showed that the water-wettability of the porous systems is increased, and that the overall relative permeability curves shift to the right with increasing temperature with both oil and water relative permeability increasing but that the increase ratio of water is less than that of oil. A summary table of the experimental studies, methods, operating conditions and temperature dependency on relative is presented in Table 2.5.

Table 2.5: Summary of literature reports on the effect of temperature on relative permeability

| | Reference | Materials | | Method | Operating conditions | | Effect of temperature on relative permeability |
|---|---|---|---|---|---|---|---|
| | | Porous media | Fluid | | Temperature (°C) | Pressure (psi) | |
| 1 | Sufi et al. (1982) | Unconsolidated sandstone | Refined oil | USS (JBN and Welge) | Up to 149 | 2000 | No effect |
| 2 | Torabzadeh and Handy (1984) | Berea sandstone | Dodecanese | USS and SS | $21 \leq T \leq 177$ | 650 | $K_{ro}$ increases and $K_{rw}$ decreases |
| 3 | Miller and Ramey (1985) | Ottawa and Berea sands | Refined oil | - | $19 \leq T \leq 149$ | 500 | No effect |
| 4 | Maini and Batycky (1985) | Sandstone | Heavy oil | USS, History matching | $25 \leq T \leq 272$ | 1100 | Reduction in $K_{ro}$ and $K_{rw}$ remain unchanged |
| 5 | Kumar et al. (1985) | Berea sandstone<br>Peace River sand | Dodecanese | Theoretical | Up to 177 | - | $K_{ro}$ increases and $K_{rw}$ decreases<br>$K_r$ curve affected |
| 6 | Closmann et al. (1988) | Berea sandstone | Unaltered, thermally altered and deasphalted tar | SS | $62 \leq T \leq 169$ | - | - |
| 7 | Watson and Ertekin (1988) | Ottawa silica | Refined oil | SS | $104 \leq T \leq 149$ | - | Reduction of $K_{ro}$ and $K_{rw}$ due to formation of third Phase |
| 8 | Maini et al. (1989) | Berea sand | Refined oil | USS (history matching) | 100 | - | $K_r$ curve affected |
| 9 | Polikar et al. (1990) | Athabasca sandstone | Heavy oil | SS and USS | $100 \leq T \leq 250$ | - | No effect |
| 10 | Kumar and Inuouye (1994) | Unconsolidated sandstone | White, refined and heavy oil | USS (JBN) | $24 \leq T \leq 160$ | - | - |
| 11 | Akin et al. (1998) | Ottawa sandstone and sandpack | Mineral oil | Simulation | $22 \leq T \leq 66$ | - | No effect |

|  | Reference | Materials |  | Method | Operating conditions |  | Effect of temperature on relative permeability |
|---|---|---|---|---|---|---|---|
|  |  | Porous media | Fluid |  | Temperature (°C) | Pressure (psi) |  |
| 12 | Esfahani and Haghighib (2004) | Dolomite and limestone | Light oil | USS (JBN) | $16 \leq T \leq 104$ | - | Increasing temperature makes rocks oil-wet |
| 13 | Schembre et al. (2005) | Diatomite cores | Mineral and crude oil | USS | $120 \leq T \leq 180$ | - | Media becomes more water wet with $K_{rw}$ and $K_{ro}$ affected by temperature |
| 14 | Sola et al. (2007) | Dolomite | Heavy oil | USS | $38 \leq T \leq 260$ | 2500 | $K_{ro}$ becomes more linear and $K_{rw}$ reduces |
| 15 | Hamouda et al. (2008) | Chalk core sample | n-decane | Jones and Rosezelle | Up to 130 | - | Kr shifts to right at about 80 °C as more water wet but shifts to oil wet state at about 130 °C |
| 16 | Hamouda and Karoussi (2008) | Chalk core samples | - | Simulation | $23 \leq T \leq 130$ | - | Effects due to experimental artefacts |
| 17 | Ashrafi et al. (2014) | Unconsolidated sandpacks | Athabasca bitumen | USS History matching | Up to 300 | 25 bar | $K_r$ affected by temperature |
| 18 | Kovscek and Vega (2014) | Siliceous shale | Dehydrated dead oil | SS | $45 \leq T \leq 230$ | - | $K_{rw}$ shifts to the right as temperature increases |
| 19 | Akhlaghinia et al. (2014) | Consolidated sandstone core | Heavy oil | JBN method | $28 \leq T \leq 52$ | - | $K_{rw}$ and $K_{ro}$ increases as temperature rises to about 40 °C, $K_{ro}$ decreases when temperature reaches 52 °C |
| 20 | Zeidani and Maini (2016) | Unconsolidated sandpack | Athabasca reservoir oil | USS History matching | Up to 220 | - | Residual oil saturation decreases with temperature |
| 21 | Cao et al. (2016) | Consolidated reservoir cores | Waxy crude oil | USS | $50 \leq T \leq 85$ | 22 MPa | $K_{rw}$ and $K_{ro}$ increases with temperature |
| 22 | Qin et al. (2018) | Unconsolidated sandpacks | Heavy oil | USS | $45 \leq T \leq 200$ | 70MPa | - |

### 2.3.2 **Effect of wettability on relative permeability**

There exists a fundamental assumption that petroleum reservoir are always strongly water-wet. This is because the reservoir was originally a water-bearing aquifer prior to the migration of oil from the source rock through migratory pathways to displace some contained water and fill the reservoir now containing both oil and water. As stated by Chinedu et al. (2008), while it is correct that water is contained in the pore volumes of the reservoir with the migrated oil, determination of the final wettability is dependent on the constituents of the oil. The final wettability is affected by whether the oil contains polar compounds and high molecular paraffin while also being affected by the distribution of minerals, reservoir rock type as well as the salinity of the connate water. This position was further buttressed by Blunt et al. (2002) stating that few, if any, petroleum reservoirs are strongly water-wet as oil-wetness characteristics is observed in many soils contaminated by oil. A reason for this wettability alteration as stated by Buckley et al. (1998) is that a continued contact of the oil phase with the solid surface results in the adherence of the surface-active components of the oil to the solid surface thereby changing the surface wettability.

Understanding the wettability condition of the oil-bearing formation is vital for optimising oil recovery. The oil-water wetting preference of the formation affects many facets of reservoir performance, mainly in waterflooding and enhanced oil recovery methods. Therefore, wrongly assuming a water-wet reservoir condition can lead to irreversible reservoir damage (Wael, et al., 2007).

USS coreflood experiments for relative permeability dependence on wettability was carried out under reservoir pressure conditions and original fluid saturations for an elevated temperature range of 38 – 260 °C by Sedaee et al. (2007) on core samples from carbonate reservoirs. History matching and the JBN method were used in the analysis of the data from the experiments with the results showing that the relative permeability of both fluids is a function of temperature. Possible wettability alterations at elevated temperature were suggested to have resulted in the change of the oil relative permeability curve with an increase in temperature. This study highlighted a disagreement with previous studies using sandstone core samples that reported an increase of irreducible water saturation and decrease in residual oil saturation with temperature increase.

Zhang and Tor (2006) studied how temperature and ionic contents affect the wettability and oil recovery from carbonates rocks (Figure 2.10). A series of experiments were performed by spontaneous imbibition of water with different sulphate concentrations into homogenous chalk cores having a permeability range between 2 – 5 mD at varying operating temperatures. They reported that for moderate water-wet and preferential oil-wet chalk samples, by increasing the sulphate concentration in the injection fluid, the oil recovery was significantly improved. They also observed a better efficiency in the wettability alteration process in the presence of sulphate with an increase in temperature.

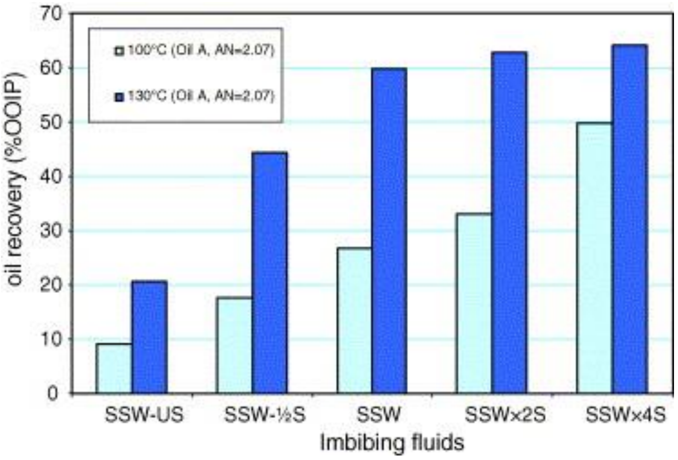

Figure 2.10: Comparison of the effects of temperature and wettability altering additives on oil recovery (Zhang & Tor, 2006)

Another study on carbonate reservoirs was carried out by Kallel et al. (2016) with findings on the effect of wettability distributions on oil recovery from microporous carbonate reservoirs as seen in Figure 2.11. A qualitatively wettability alteration scenario was implemented in a two-phase flow network model capturing a diversity of pore shapes. Reported results reveal that wettability effects are considerably more significant in the carbonate network, because the wettability of the micro-pores affects oil recovery.

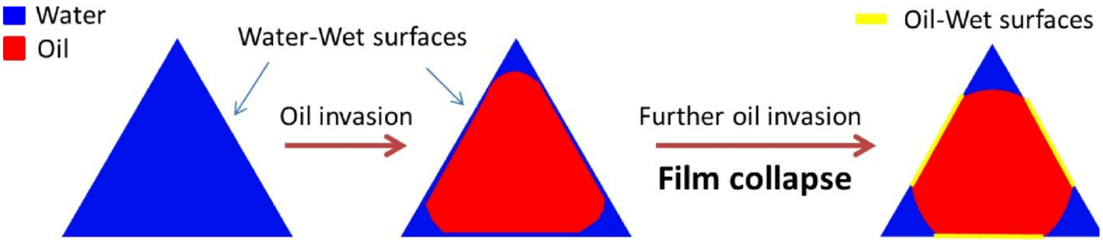

Figure 2.11: Schematic representation of the wettability alteration process in a triangular pore cross-section

Thermal recovery methods involving the injection of steam or hot water have been reported to change the wettability of reservoir rocks according to Donaldson and Alam (2008). Some research on the thermal effect on reservoir wettability is presented in Tang and Morrow (1997) experimental study on sandstone in which they reported that the rock wettability becomes hydrophilic with an increase temperature (Tang & Morrow, 1997). A comparable study was reported by Dangerfield and Brown (1985), which showed that an originally hydrophilic rock was changed to become hydrophobic owing to the prolonged oil deposit on the surface of the rock changing the wettability due to the adsorption of ionic compounds of crude oil. Schembre et al. (2006) experimentally investigated how oil recovery and wettability alteration is caused by waterflooding at elevated temperature, using 9 reservoir core samples of permeability ranging from 0.2 to 0.7 mD and porosity of 45 to 65 % at temperatures between 45 to 230 °C. The experimental results showed that a temperature increase resulted in a significant increase in the imbibition rate and oil recovery, while also shifting the wettability index from intermediate and weakly water-wet to strongly water-wet. The same authors conducted high temperature experiments to study the interrelationship of temperature and wettability on relative permeability. Various studies have showed that with increasing temperature, there is a systematic shift of the core samples tested towards a water-wet state. This change has a corresponding effect of the relative permeability and they concluded that the changes in relative permeability is connected to the effect of temperature on the rock-fluid interactions.

Olugbenga and Manuel (2014) investigated the effects of wettability on relative permeability, capillary pressure and irreducible saturation using an experimental approach with the application of a porous plate. The study reported how the wettability alteration of a media from water to oil-wetness affects the multiphase flow properties. Water-wet samples with permeability ranging from 50 – 233 mD and porosities ranging from 23 to 33 % were tested with an air-brine fluid-mix and results showed irreducible wetting phase saturations of 19 to 21 %. They later altered the wettability to oil-wet using a surfactant with the test yielding a wetting phase (oil) irreducible saturation of 25 to 34 %. They concluded that a change of the wettability from water-wet to oil-wet results in an improvement of the wetting phase (oil) recovery.

### 2.3.3 **Effect of interfacial tension on relative permeability**

The effect of IFT on oil recovery is well documented in the literature with almost all the studies reporting a dependence of the phase relative permeability with IFT (Al-Wahaibi & Muggeridge, 2006; Blom, et al., 2000; Amir & Mehran, 2016; Latifa Al-Nuaimi & Mehran, 2018). Dynamic displacements experiments were performed on unconsolidated porous systems by Al-Wahaibi and Muggeridge (2006) to investigate the effect of IFT on relative permeability for four mixtures. The experimental results presented showed that with a decrease in IFT, there is a corresponding increase in the non-wetting (gas) phase relative permeability. Longeron (1980) performed a series of two-phase gas/oil relative permeability coreflood experiments to investigate the effect of IFT (ranging from 0.001 to 12.6 mN/m) at high pressure and temperature conditions. Their findings supported the claim that there is a relationship between IFT values and relative permeability and alluded to the findings of Shen et al. (2010) concerning a critical IFT value of 0.04 mN/m, below which the effect was more pronounced. A similar observation was reported by Asar and Handy (1988) under IFT conditions ranging between 0.03 to 0.82 mN/m.

Shen et al. (2010) studied the dependence of relative permeability on IFT and developed an improved SS procedure for water–oil relative permeability curves. Findings from the studies showed that there are certain critical values of IFT greater than 3 mN/m where its impact on relative permeability is minimal while values lesser than 3 mN/m gives an increase of relative permeability to both water and oil phases with decreasing IFT (Figure 2.12). The study also presented a functional correlation between water–oil two-phase relative permeability and IFT.

Henderson et al. (1997) investigated the influence of fluid flowrates and IFT on relative permeability and their findings showed an increase in relative permeability with increase in flowrates and reduction in IFT. The same parameters (flowrate and IFT) were investigated by Blom et al. (2000) with a methanol/n-hexane fluid pair at low IFT range of between 0.31 and 0.006 mN/m. The study reported that IFT and superficial velocity has a strong influence on the fluid relative permeability.

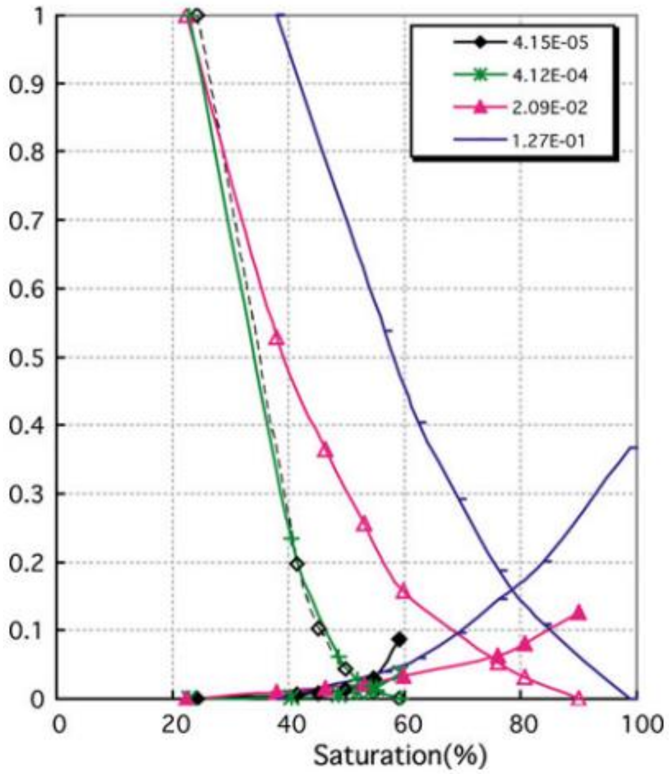

Figure 2.12: Varying water–oil relative permeability curves under different interfacial tension (Shen, et al., 2010).

### 2.3.4 **Effect of viscosity and flowrate on relative permeability**

Theoretically, it is assumed that phase relative permeability is not function of injection flowrate. However, with the flowrate having a corresponding effect on the phase saturation which in turn influences the relative permeability, this assertion could be argued otherwise. In a two-phase regime, only two possible saturation paths exist; increase in one phase saturation results in a corresponding decrease in the other phase saturation. A more complicated scenario is encountered in three-phase systems owing to the fact that the two-phase saturations can change independently which can result in an infinite saturation path (Kianinejad, Xiongyu, & David, 2015). Oak (1990) investigated two- and three-phase relative permeability in water-wet sandstone cores for different saturation histories. The study reported that three-phase relative permeability to water is primarily affected by the water saturation and almost the same as two-phase water relative permeability. Further observations also showed that three-phase gas relative permeability is a function of gas saturation while the oil phase varied with all saturations. Alizadeh and Piri (2014), reached a similar conclusion in more recent experimental studies on the saturation effect on relative permeability.

Experimental studies conducted by Henderson et al. (1997) reported a variation in the relative permeability with respect to the flowrate while other studies (Chen & Wood, 2001; Alizadeh, et al., 2007; Wang & Buckley, 1999) maintain that no sensitivity exist between relative permeability and flowrate.  In a two-phase flow of oil and water into a water-wet porous media under SS conditions, it is expected that both fluids exit the outlet face at the same pressure. However, this is not the case, as there exists a build-up of the water phase (higher saturation) at the outlet face due to capillarity. The non-uniform saturation profile occurring at the outlet is referred to as "capillary end effect". Ignoring the effect of this phenomenon has been found to give rise to erroneous results and measures which has to be taken into consideration to minimise or eliminate this effect (Huang & Honarpour, 1998). Andersen et al. (2017) developed an analytical model for the evaluation of capillary end effects during single-phase injection and provided a possible solution for a two-phase scenario with a high flowrate. On the other hand, high flowrate has a negative effect, as it deviates from Darcy flow and the possibility of creating preferential flow pathways in the porous media due to channelisation. This phenomenon might occur when local fluid-induced stresses surpass a critical threshold thereby dislodging grains and consequently altering the porosity and permeability of the medium along the induced flow paths. Furthermore, flowing at high rates means a system that is significantly higher than the characteristic reservoir displacement rates (Odeh & Dotson, 1985). Numerous investigations have been carried out to study the effect of varying flowrates; these studies reported conflicting results. In order to eliminate or minimise these effects, Dos Santos et al. (1997) proposed some criteria to consider in choosing a range of injection flowrates for laboratory coreflood experiments. The criteria presented are in the form of dimensionless parameters that considers the core length, diameter and media property to calculate the optimal injection flowrate or displacement velocity. While the assumption that relative permeability is not affected by injection rate, it has been reported by some researchers for the drainage process (Chen & Wood, 2001; Qadeer, et al., 1998), however, the validity of this assumption is not clear for the imbibition process (Akin & Demiral, 1997; Virnovsky, et al., 1998 ).

The effect of injection rate on oil-water relative permeability was investigated by Chen and Wood (2001) by measuring imbibition relative permeability under SS method for mixed-wet sandstone core samples. Direct application of Darcy's equation was used for the computation of the relative permeability and the effect of capillary pressure filtered out by using only the section of the core sample unaffected by capillary end effects. Results from both cases showed no significant shift of the relative permeability curves under varying flowrates (Figure 2.13). The results are however at variance with that of Henderson et al. (1997) who reported that relative permeability of both phases increase as the flowrate increases. The flowrates considered in this study were chosen to be representative of the regions of the reservoir, specifically for producing wells.

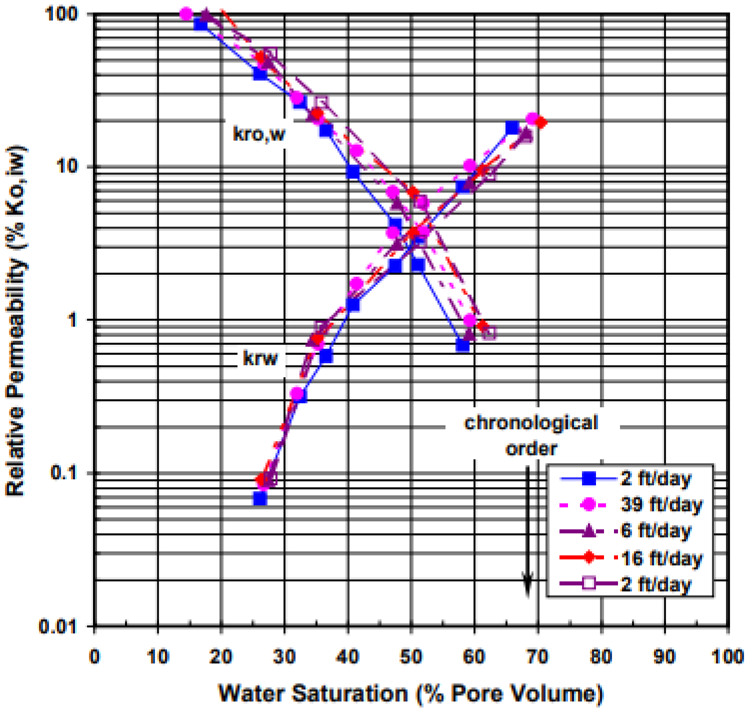

Figure 2.13: Water-oil imbibition relative permeability at different flowrates for a mixed-wet sandstone core (Chen & Wood, 2001)

Alizadeh et al. (2007) investigated the effect of flowrate on relative permeability curves on very tight Iranian carbonate. The waterflood experimental results showed that the relative permeability to water is not affected by the flowrate while the oil relative permeability reduces at lower flowrates. Wang and Buckley (1999) performed a series of coreflood experiments on strongly water-wet Berea cores and reported that for the wide range of flowrates considered; the water relative permeability remains constant at residual oil saturation. Nguyen et al. (2006) implemented a dynamic network model to study the intricate interaction between flowrate and pore–throat aspect ratio on relative permeability and residual saturation. Their results showed that the extent of the flowrate effect on waterflood relative permeability and residual saturation is largely a function of the pore–throat aspect ratio. A higher magnitude of flowrate effect was observed for porous systems having high aspect ratios (large pores and small throats) compared to low aspect ratios.

Wang et al. (2006) studied the effect of oil viscosity on heavy oil/water relative permeability curves using USS displacement experiments in sandpacks under usual injection flowrate for heavy oil production process. The study reported a shift of relative permeability curves of both fluids under the same injection flowrate and different oil viscosities. With an increase in the oil viscosity, it was observed that there was a corresponding increase in the residual oil saturation and a decrease in the irreducible water saturation.

Sami (2014) carried out a two-phase relative permeability test on both heavy and light oil samples with different viscosities and brine of varying salinities. The study explored the sensitivity of the two-phase relative permeability curves, residual oil saturation and oil recovery with different values for the salinity and viscosity of the fluids. The results showed that the residual oil saturation and water relative permeability endpoints are all affected by the oil viscosity and/or brine salinity. As the oil viscosity increases, the residual oil saturation generally increases and the relative permeability to water decreases.

Torabi et al. (2016) performed a series of USS coreflooding experiments to investigate the effect of different vital fluid flow parameters such as operating temperature, oil viscosity, flowrate and pressure on oil-water relative permeability after which new correlations were proposed for computing oil-water relative permeability. The results presented in their study indicated that the water and oil relative permeability increases significantly with an increase in temperature. A decrease in the oil viscosity was reported to cause an increase in both the oil and water relative permeability. Additionally, experimental results showed that as the injection flowrate increases, oil relative permeability increases as well while water relative permeability reduces.

### *Summary*

As seen in the review conducted, numerous studies have been carried out to investigate the effect of temperature, injection flowrate and other parameters on two-phase relative permeability in porous media with contradictory results; while some reported a dependence of the relative permeability curve on the injection flowrate, others reported no effect. Another observation from existing literature is that only a handful of researchers have given detailed information on the composition of the synthetic brine used in their experiments. Studies have shown that the composition of connate water and invading brines could have a major effect on the media wettability and in turn the oil recovery and relative permeability at reservoir temperature (Salehi, et al., 2017; Bagci, et al., 2001 ).

There exist different reports on both sides of dependent and non-dependent relationship between relative permeability and temperature. A significant observation worthy of note is that relative permeability is sensitive to temperature variation only under a certain temperature range after which the trend changes as the temperature rises further. As reported by Akhlaghinia et al. (2014) at a certain temperature, the relative permeability trend reverses which indicates that the oil relative permeability changes up to an optimum temperature around 40 to 52 $^{o}$C after which the trend reverses with a further increase in the temperature. While researchers maintained that there exist some changes without acknowledging the optimum temperature, others stated there is no change. It is obvious that results from literature review, analysis and experiments do not establish a definite trend of the relative permeability with temperature variation. It is thus necessary to investigate the dependency of relative permeability curves with temperature variations, howbeit not with experiments but with a numerical simulation tool, CFD.

Based on the review done, it can be concluded that there exist a series of complex interrelationships between the fluids and the porous material properties through which they flow, and ample research focus is being conducted to explain these occurrences. Attempts have been made to establish the fundamental understanding of these phenomena through controlled laboratory experiments and numerical modelling by applying different governing equations; these equations are as well equally complex and solving them cannot be achieved through basic analytic approaches. It is the aim of this research to add to the knowledge pool that have attempted to demystify these complexities and difficulties in the respective solutions.

# Chapter 3: EXPERIMENTAL METHODOLOGY

**Overview**

This chapter presents the details of the coreflooding experiments conducted during this study. The main aim of the coreflooding experiments was to investigate the effect of temperature and other parameters on the respective relative permeability curves. The preparation process of each sandpack, laboratory setup and experimental procedure for flooding are detailed in this chapter.

## 3.1 COREFLOODING EXPERIMENTS

Experiments conducted during this research consists of a series of different coreflooding experiments using the high temperature, two-phase USS coreflooding apparatus in the Well Control laboratory at the Robert Gordon University, Aberdeen. The first part of this chapter presents a detailed description of the experimental apparatus with the various component. A detailed description and characterisation of the materials (fluids and sandpack samples) used for the experiments are given in the second section after which the coreflooding experimental procedures is outlined. The specifications and operating conditions with accurate details of the laboratory instruments used are also presented.

## 3.2 EXPERIMENTAL APPARATUS

The experimental apparatus used for this research is designed to perform different multiphase flow coreflooding experiments and, in this instance, has been used for two-phases (oil and water) immiscible USS relative permeability measurements at elevated temperatures. The material selection was done in such a way that critical wetted parts are made of highly corrosion resistant material, making the system rust free even under elevated temperature conditions with high chloride concentrations. The setup was modified from the original design and assembly by Idahosa (2016) in the study of rate-dependent polymer adsorption in porous media.

The main features of the current experimental setup are:

1. Ability to inject oil of different viscosities and brine.
2. Operating in non-isothermal condition up to 300 $^{o}$C.
3. Performing transient measurements of the following parameters:

a. Number of pore volume injected,
b. Cumulative displaced fluid production volumes, and
c. Differential pressure across the sandpack.

A schematic representation of the flow system is presented in the Figure 3.1 while a picture of the oven with the sandpack and adjoining tubing shown in the Figure 3.2. Overall, the experimental setup is made up of 4 main sections: the fluid injection system, coreholder, production system and the data logging/monitoring. A detailed description of the various sections and their respective specific apparatus are presented in Section 3.2 and 3.3.

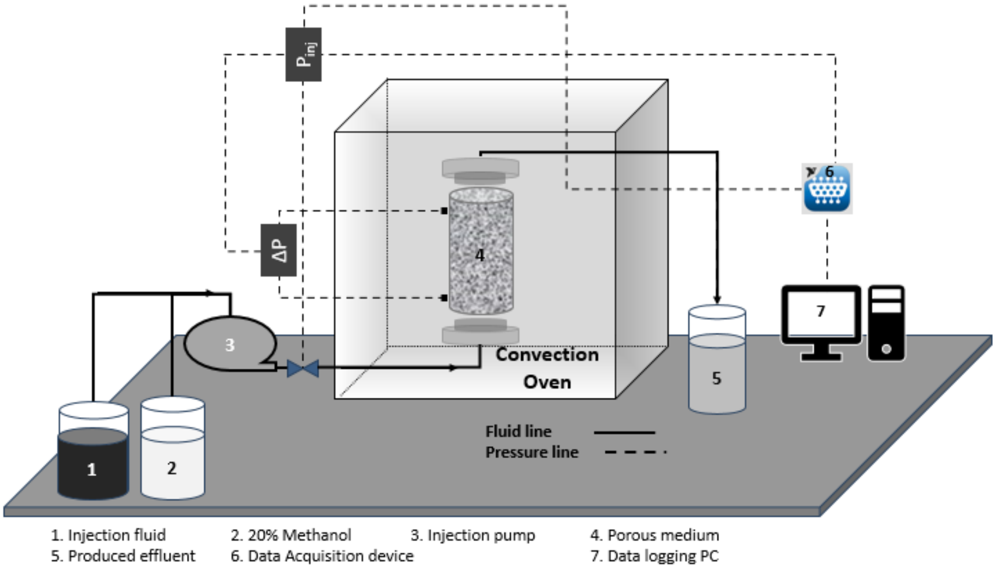

Figure 3.1: Schematic diagram of the coreflooding experimental setup

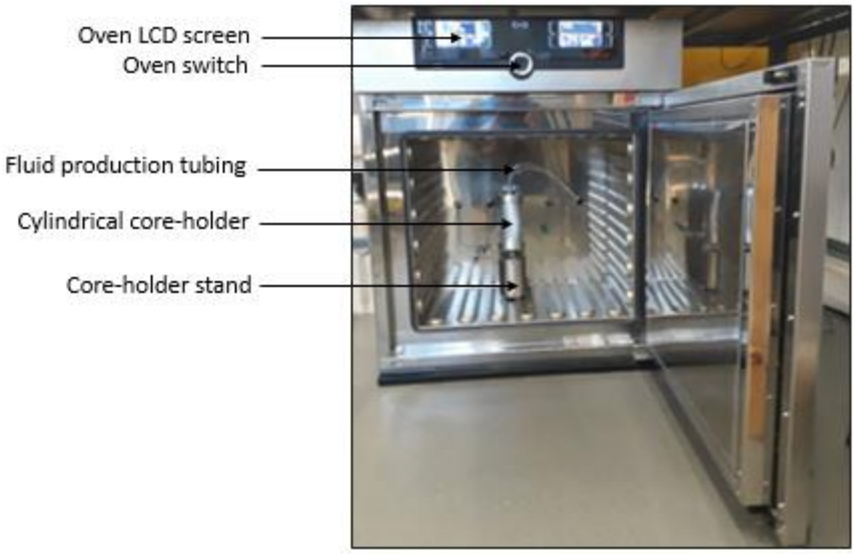

Figure 3.2: Pictorial representation of the coreflooding experimental setup

### 3.2.1 **Injection system**

The upstream component for injection is essentially a multi-solvent High-Performance Liquid Chromatography (HPLC) dual piston pump supplied with 220V. The pump is made of 316 stainless steel fitted with two 50 mL pump heads with the capability of running at a wide range of flowrate from 0.1 to 100 mL/min with 0.1 mL increments and pressure range of 0-1000 psi with consistent performance at a flow accuracy of $\pm$2 %. The two pump heads are connected to separate fluid bottles; one serving as the reservoir for the injection fluid (e.g. oil and brine), while the other is the flushing fluid made-up of 20 % methanol solution. The pump has an adjustable upper and lower pressure limit which was set at 0 and 5860 psi for the experiments. This feature makes the pump to stop automatically if the pressure drops below the preset lower pressure limit or if it exceeds the upper pressure limit. A major component of this pump model is the digital stepper motor design to prevent flowrate drift over time at varying temperature (common with analog designs). The flowrate and pressure limits are shown on a chemical resistant LED digital display. A self-flushing pump head is part of the design, which uses a secondary seal, and set of check valves in creating a steady flow. This aids the continuous washing away of any salt precipitate in the piston to avoid any form of abrasion of the high-pressure seal which could result in seal failure, leakage or possible pump damage.

### 3.2.2 **Coreholder**

The coreholder used for this study was designed and fabricated in the Engineering Workshop of the Robert Gordon University. The coreholder body is constructed of aluminium metal, the choice of material is mainly due to the lightweight of aluminium at 2.7 g/cm$^3$, and its thermal conductivity of 205 W/m-K coupled with the corrosion resistant nature of the metal. The dimensions are 7 cm external diameter, 5.1 cm internal diameter and 10 cm long (Figure 3.3). To ensure a uniform spreading of injection fluid without the formation of wormholes, the endcaps are made into two parts with a 1 mm depth hollow space and three 1 mm holes at the side interfacing with the packed sand. A depth of 1.5 mm was machined on both ends to fit into the cylindrical holder and O-rings fitted to prevent any leakage. A pair of 2.70 mesh stainless steel screens were attached to both endcaps to prevent sand particles from migrating into the flow tubing.

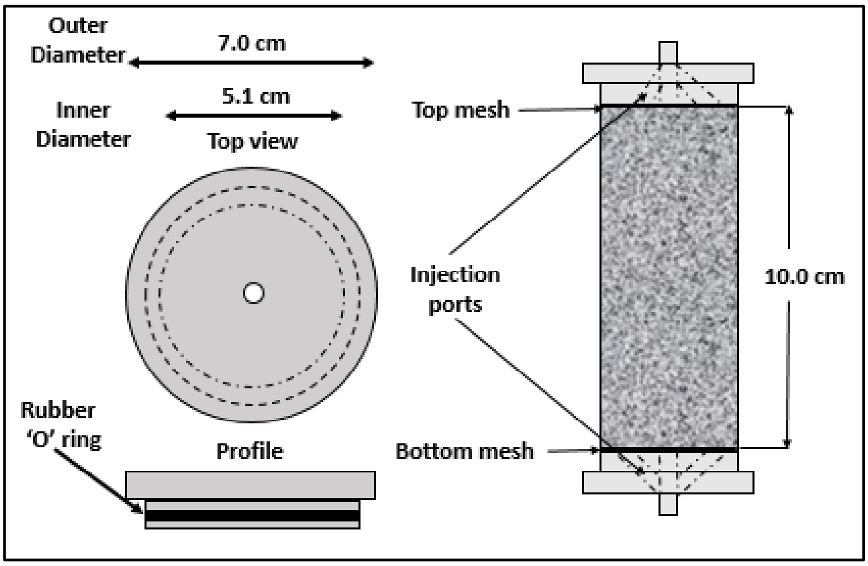

Figure 3.3: Schematic representation of the aluminium coreholder and endcap used for the experiment with dimensions

### 3.2.3 **Heating system**

The temperature system is comprised of a universal gravity convection oven, digital thermometer, and a type K thermocouple. The natural convection oven supplied by Memmert has a control cockpit aiding quick and intuitive control with simple touch. It has a twin display showing the operating parameters and allowing for graphical temperature monitoring. The oven is powered by a 230 V source and has a built-in over-temperature safety system that automatically switches it off at about 10 °C above the set temperature made possible with a 5-ft J-Type thermocouple temperature sensor. The oven can operate in a temperature range between 20 to 300 $^{o}$C with a temperature uniformity of ±2.2 $^{o}$C at 160 $^{o}$C having a control accuracy of ±0.1 $^{o}$C up to 99 $^{o}$C and 0.5 $^{o}$C above 100 $^{o}$C. The oven has a chamber of 55 cm width, 48.006 cm height and 40.005 cm depth, which is enough space for the 25 cm coreholder used for the experiments. Four 2.5 cm entry ports had to be fabricated at the back end of the oven to allow for connecting the tubing for fluid flow, pressure tapping and thermocouple probe into the coreholder for data monitoring while the experiments were running.

Since the objective is to bring the sandpack inside the coreholder to the desired temperature, the most efficient heating cycle was found through an iterative process of increasing and reducing the oven temperature during preliminary experiments. It was found that the control temperature of the oven is reached within 30 minutes with approximately another 90 minutes needed for the sandpack to reach the test temperature (Figure 3.4).

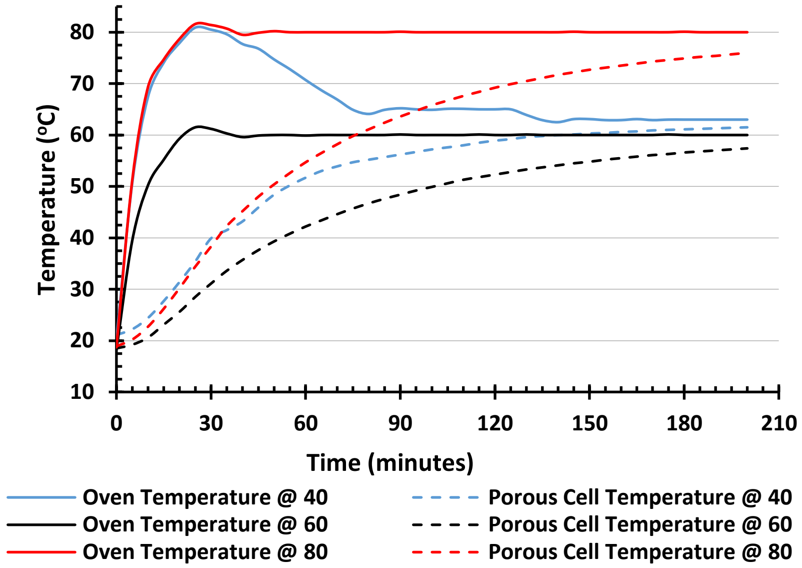

Figure 3.4: Plot of the temperature rise with respect to time for the oven and porous system for preliminary investigation of time needed for porous system to attain thermal equilibrium with set oven temperature.

### 3.2.4 **Pressure recording device**

Pressure monitoring was achieved with the use of a Micro-Machined Silicon Wet/Wet Differential Pressure Transducer and with measurements recorded electronically through the aid of a high-speed National Instruments Data Acquisition System (NIDAQ) NI 9212. The differential pressure transducer supplied by Omega had a pressure range of 0-15 PSID with an accuracy of about 0.08 % with an excitation voltage of 10 Vdc supplied by a Weir 413D power supply. The transducer can operate within a temperature range of between -45 to 121°C. After setting up the pressure measuring system, the transducers were calibrated using a DRUCK pressure calibration device to ascertain the relationship between the electric voltage and pressure readings, details of the calibration procedure is presented in Appendix I.

### 3.2.5 **Separation and collection system**

After each run, the respective fluid saturations in the core samples were measured by performing a material balance and the values recorded. This was achieved by collecting the produced fluids (effluent) in 1-inch diameter 50 mL measuring cylinders and the fluids left to be separated by means of gravity with the oil phase staying on top of the water phase owing to its lighter density (Figure 3.5). For accurate readings of produced volumes from the effluents, the measuring cylinders containing the effluents were placed in the convection oven at 40 °C for 6 hours and then allowed to separate for over 24 hours after which the respective phase volumes were recorded. This was used in computing the cumulative displaced fluid volumes.

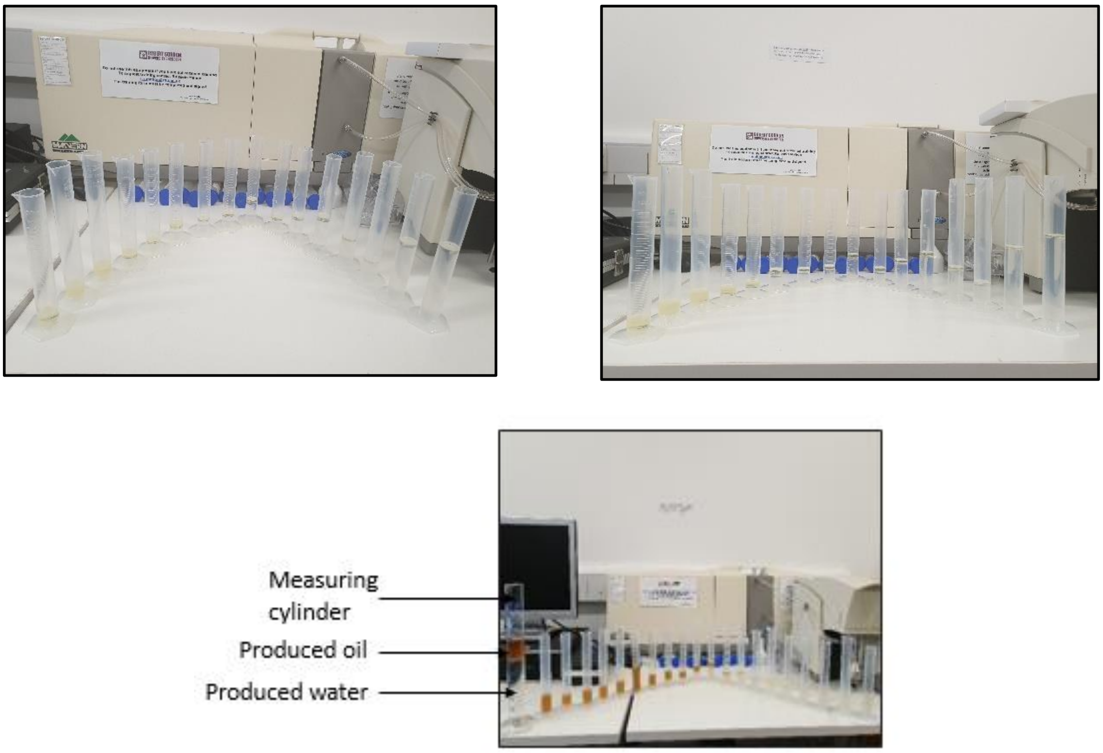

Figure 3.5: Picture of the effluents after coreflooding during material balance measurements

## 3.2.6 **Data logging and monitoring system**

Laboratory Virtual Instrument Engineering Workbench (LabVIEW) is a versatile system-design platform and the development environment by National Instruments was used to log the data and perform some transient computations. The pressure logging device was connected to the computer workstation through the appropriate electronic interfaces for data logging and monitoring in the LabVIEW program. The pressure logging/monitoring was done with time steps as short as 30 s. Continuous computations for the intrinsic permeability of the porous cell using Darcy equation was performed with the pressure data and constant parameters set in the LabVIEW program.

## 3.3 MATERIALS

The following sub-sections present the details and description of the properties and characteristics of the porous domain, brine and oil used for the experiments.

### 3.3.1 Sandpack samples

The porous systems used during this experimental work were made of commercial unconsolidated silica sand samples of varying mean grain diameters. The unconsolidated sandpack porous system had been chosen to enable experiments to be carried out with varying petrophysical properties as required; primarily the intrinsic permeability, and to also eliminate clay migration challenges. Three different grades of commercial silica sands (P230, 20/40 and 40/60 mesh sizes) were used for the experiments resulting in different permeabilities for the porous sandpack system. Characterisation of the sand samples were carried out through the following methods:

- Particle size distribution (PSD) using the mechanical sieve analysis and Malvern Mastersizer,
- Grain size identification using the optical microscopy, and
- Porosity determination using the grain weight approach and direct method.

The Malvern Mastersizer 2000 laser diffraction-testing instrument was used for PSD analysis of the different sand samples in the study. The grain samples are passed through a laser beam which results in the laser light been scattered at a wide range of angles. Detectors inside the machine measure the intensity of light scattered at that position and the system software automatically uses a mathematical model to generate the particle size distribution. More details on the procedure and results in graphical format are presented in Appendix II. As a means for cross-validation of the results, analysis of the grain size distributions was also carried out by direct mechanical sieving method of the samples.

Sieve analysis is an experimental procedure to determine the particle size distribution of a granular material. The process involves the separation of fine particles from more course particles by allowing the sample to pass through a set of sieves of varying mesh sizes on a vibrating device to aid the separation process. This makes it possible for the mass fraction of particles retained within each size range to be measured and a cumulative mass distribution computed. Establishing the size distribution of granular materials is of critical importance to the performance characteristics of the material. The results of the sieve analysis are presented in both tabular and graphical form. Details of the procedure and results from the test are reported in Appendix III. Table 3.1 shows the typical physical properties of the classes of commercial silica sand used for the study.

Table 3.1: Physical properties of the sand sample used for the study

| **Typical physical properties of the sand sample** | |
|---|---|
| Colour | White |
| Grain shape | Round |
| Hardness (Mohs) | 7 |
| Melting point (°C) | 1710 |
| Mineral | Quartz |
| Bulk density (g/cc) | 1.54 |
| Specific gravity (g/cc) | 2.65 |

Optical microscopy is a way of using visible light and a system of lenses to magnify images of small objects. The Leica DFC420 Digital Microsystems was used in this study for capturing high-resolution images of all the sands for diameter measurement and shape identification. All the sands were observed to be uncemented and unconsolidated spherically shaped grains. Figure 3.6 presents the optical micrographs and particle size distribution curves of the three sand samples used in this study.

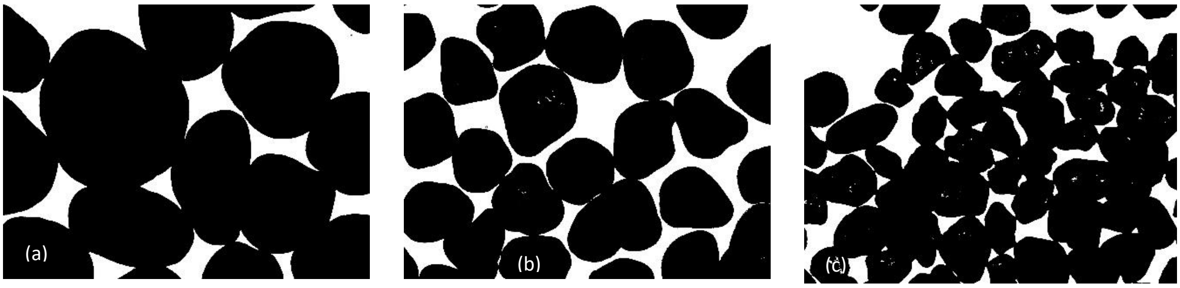

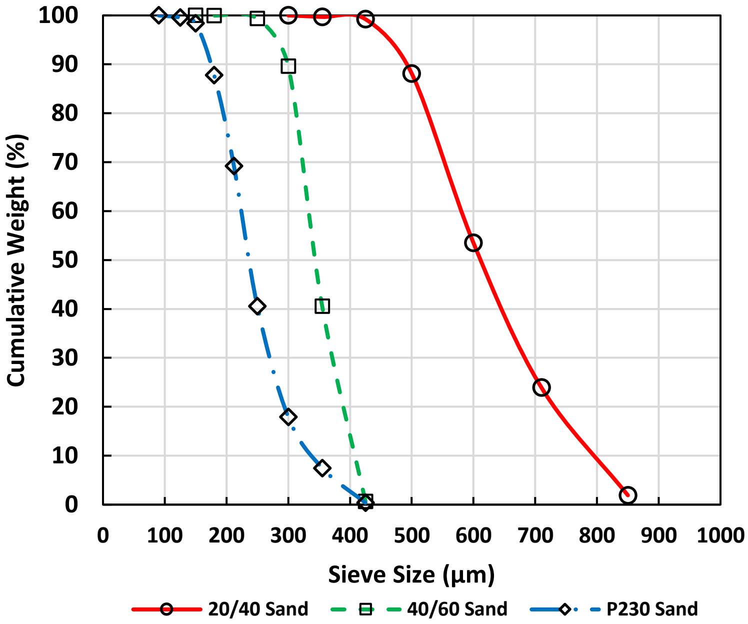

Figure 3.6: Optical micrographs and particle size distribution curves of the three sand samples used for the study; (a) 20/40, (b) 40/60 and (c) P230.

### 3.3.2 **Sand packing and porosity measurement**

Packing of the unconsolidated sand was done in such a way as to minimise preferential flow paths of fluid caused by wormholes and channels formation. A dry packing method was used which involves putting a mesh on one of the endcaps and fitting it to the coreholder which is then put to stand upright using a coreholder stand the mechanical vibrator to aid in settling of the sandpack (Figure 3.7) while the sand was being poured. From the top of the holder, the sand was poured with a funnel as the vibrator allowed it to distribute and settle uniformly in the coreholder. The sand was poured into the coreholder in batches of about 30 cc (usually 3 batches per porous cell).

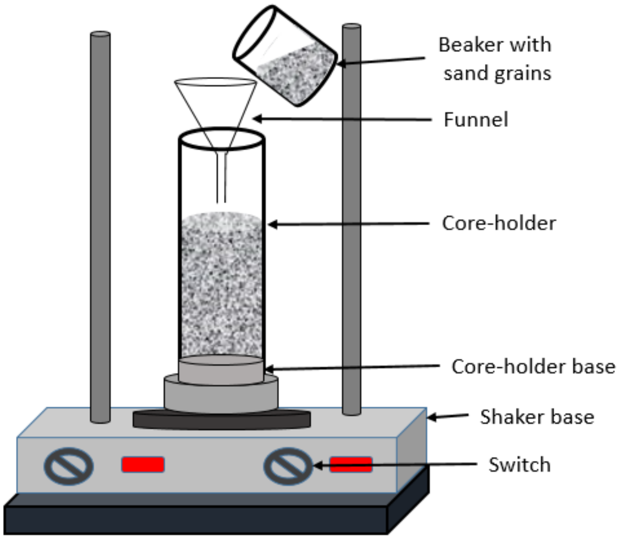

Figure 3.7: Schematic of the coreholder on the mechanical vibrator showing the sand packing process

To prevent influx of fines from the coreholder to the flow lines, 0.25-micron mesh was fixed at both ends before connecting the endcaps, as mentioned earlier. The weight method was used for the porosity measurement of the sandpack. The bulk volume ($V_b$) of the media was determined as the internal volume of the coreholder computed as the volume of a cylinder from its dimensions. The volume of the sand mass was determined by using the relationship between density, mass and volume while taking the density of 2.65 g/cc for silica sand as seen in literature (Satter, et al., 2008). The pore volume of the porous media was then computed by subtracting the grain volume determined earlier from the bulk volume. The porosity of the sandpack was subsequently calculated using the pore volume and bulk volume with Eq. 3.1.

$$Porosity\ (\emptyset) = \frac{Pore\ volume\ (V_p)}{Bulk\ volume\ (V_b)} = \frac{Bulk\ volume - Grain\ volume}{Bulk\ Volume} \qquad 3.1$$

## 3.4 TEST FLUIDS

The test fluid used for the experiments are mainly brine and oil. While the brine is divided into 2 categories; synthetic formation water and synthetic seawater; the oil sample is also in 2 categories namely Shell Rimula R4 L 15W - 40 engine oil and mineral oil. These fluids are chosen because of the high level of immiscibility, ease of handling and well-known or easily determined properties.

### 3.4.1 **Brine**

In this study, 2 different synthetic brine samples are prepared to simulate the formation water (FW) inside the porous sample before flooding, and seawater (SW) to simulate the seawater used for water injection during the waterflooding process. The brine solutions are prepared in the lab using deionised water and appropriate amounts of sodium chloride (NaCl), anhydrous calcium chloride ($CaCl_2$), potassium chloride (KCl), sodium hydrogen carbonate ($NaHCO_3$) and magnesium chloride hexahydrate ($MgCl_2.6H_2O$), all analytical grade salts. The concentration of each salt in the synthesised brine is adapted from Oluyemi (2014) and Rostami et al. (2019) and shown in Table 3.2 with the dissolved salt concentration expressed in parts per million on a mass basis (ppm). Preceding the usage of the synthetic brine, the solution was filtered with 0.22 μm filter paper. This was done to ensure that no extraneous fines are introduced into the system which can interfere with the pump piston seals and check valves and prevent undue pore blockage in the respective sandpacks. The densities and viscosities of the different brine samples were measured in the lab at ambient condition and shown in the

Table 3.3.

Table 3.2: Chemical composition of the synthetic brine samples

| Salt (ppm) | Formation water (FW) | Salt (ppm) | Seawater (SW) |
|---|---|---|---|
| NaCl | 140316 | NaCl | 26400 |
| $CaCo_3$ | 1628 | $CaCl_2$ | 1180 |
| $MgCl_2$ | 2856 | KCl | 400 |
| $CaCl_2$ | 40287 | $NaHCo_3$ | 7340 |
| $Na_2SO_4$ | 2588 | $MgCl_2.6H_2O$ | 5270 |
| $NaHCO_3$ | 2016 | | |

Table 3.3: Physical properties of the fluid samples used for the experiments at ambient condition

| Fluid | Density (kg/m$^3$) | Viscosity (cP) |
|---|---|---|
| Brine (SW) | 1000 | 1.003 |
| Brine (FW) | 1020 | 1.005 |
| Oil | 850 | 147 |

### 3.4.2 **Oil**

The viscosity of the oil sample was measured using a Fann Model 35 viscometer which is a typical Couette rotational viscometer capable of measuring the rheological properties of fluids, both Newtonian and non-Newtonian. The viscometer measures the viscosity as a function of shear rate. Fluid viscosities were measured at varying temperature ranges from 20 to 80 ºC. The Fann 35 viscometer used is a direct-reading instrument in a 12-speed design. With this viscometer, the oil sample is contained in the annular space between an outer rotating cylinder and the bob (inner cylinder).

To generate the specific temperature condition for the viscosity measurements, a stainless-steel cup with another annular space was used in this set of experiments and connected to an additional laboratory apparatus, the RW-2025G heating bath circulator (Figure 3.8a).

(a) (b)

Figure 3.8: Apparatus for viscosity measurements (a) circulating water bath and (b) Fann35 viscometer

The heating bath circulator can produce accurate and stable temperature control ranging from -25 to 150 °C and has a powerful pump for both external and internal circulation. In the setup, water is contained in the bath reservoir and connected to the sample cup of the viscometer for the water to circulate in and out of the bath and annulus of the sample cup in a closed loop system. The heating bath was set to a specified temperature and allowed to heat up the circulating water, which in turn heats up the sample cup from the outer annulus and the oil sample within the inner annulus to the required temperature (Figure 3.8b). A thermometer was connected to confirm the rise in temperature of the sample fluid to the desired temperature after which the viscosity measurement commenced. The values from the viscosity experiments are in close match to the values from the technical data sheet of the engine oil (Shell, 2018) having a viscosity of 93.27 cP at 40 $^{o}$C and 12.3 cP at 100 $^{o}$C.

### 3.4.2.1 **Sequence and procedure for viscosity measurement**

The outer circulating cylinder (rotor) and bob (inner cylinder) were both attached to the spring and the sample cup connected to the heating circulating bath to form a closed loop circulatory system. The test oil sample was then poured into the sample-heating cup and then fixed on the base of the Fann 35 making sure it sits properly on the base. The last step is to fix the spindle inside the oil sample up to the marked point by lifting the base.

With the test sample and equipment all put together, the heating bath was turned on, set at the required temperature and allowed to heat up the water and the reservoir which circulates, and heats up the fluid in the sample cup. A thermometer was connected to the test fluid for continuous temperature monitoring. The gearbox is then set to the low mode and then the motor was started at the lowest RPM. When the fluid temperature is at the desired temperature and the readings had stabilised, the dial reading was recorded. The process continued for the remaining low mode RPMs. After taking the readings for all the low mode RPMs, the motor was switched off and the gearbox set to high mode. The motor was started, and procedure repeated for all the high mode RPMs with the dial readings being recorded. The temperature of the heating bath was changed, and the entire procedure repeated. As recommended by the instrument manual, dial readings at rotor – R1, bob – B1, torsion soring – F1 and 300 RPM (equivalent to 510 $s^{-1}$ shear rate) were taken as these viscosity values were for a Newtonian fluid.

### 3.4.2.2 **Rheological behaviour of samples**

Figure 3.9 shows the shear stress and viscosity of the 3 oil samples with shear rates at the different temperatures. As seen in the figure, the shear stress varies linearly with the shear rate at the different temperatures. This demonstrates a Newtonian characteristic. With regards to the viscosity and shear rate, while there seems to be slight variation at low shear rate, at high shear rates it is constant confirming the Newtonian behaviour of the oil sample.

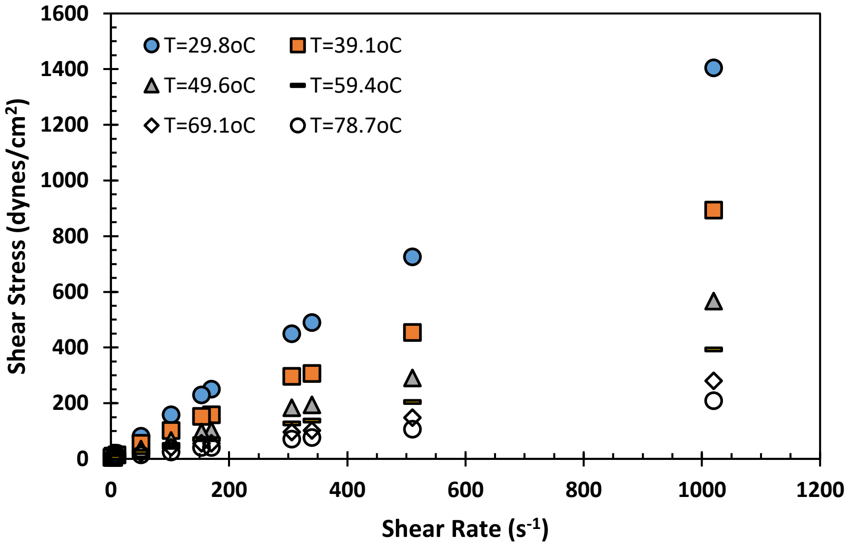

(a)

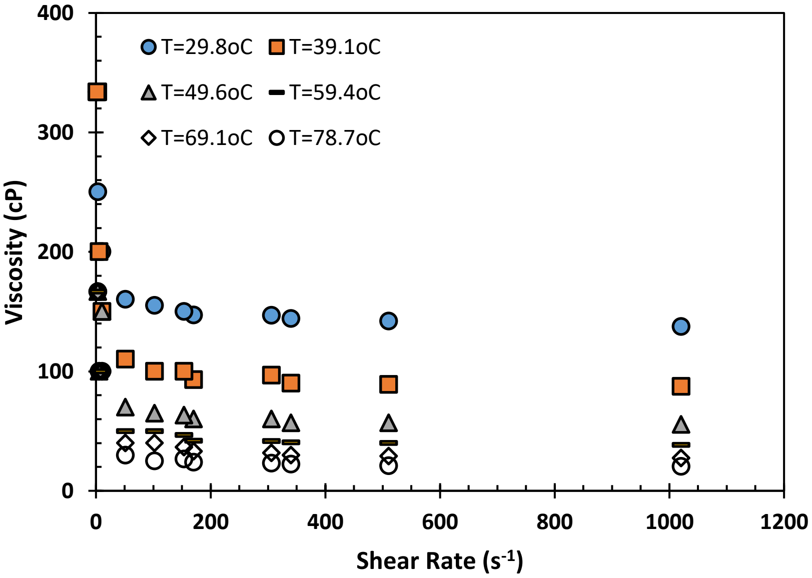

(b)

Figure 3.9: Rheological properties of the motor oil at different temperatures (a) shear stress versus shear rate (b) viscosity versus shear rate (complete data in Appendix IV)

### 3.4.2.3 **Oil density measurement**

Two measuring devices were used to measure the oil density: the mud balance and a hand-held Anton Paar density meter. The mud balance is comprised of a fixed graduated beam, sample cup and a counterweight on the other end. Density of the specific fluid sample is read at the point where the slider-weight sits on the beam at the level point. To measure the density at different temperatures, a handheld density meter; DMA 35 supplied by Anton Paar was used. The density meter takes a 2 mL volume sample for measurement and has an accuracy of ± 0.001 g/cm³. Figure 3.10 summarises the density and viscosity variation different temperature conditions. While both properties reduce with temperature, the density shows very minimal variation for all the fluid samples and the oil viscosity shows a power-law relationship.

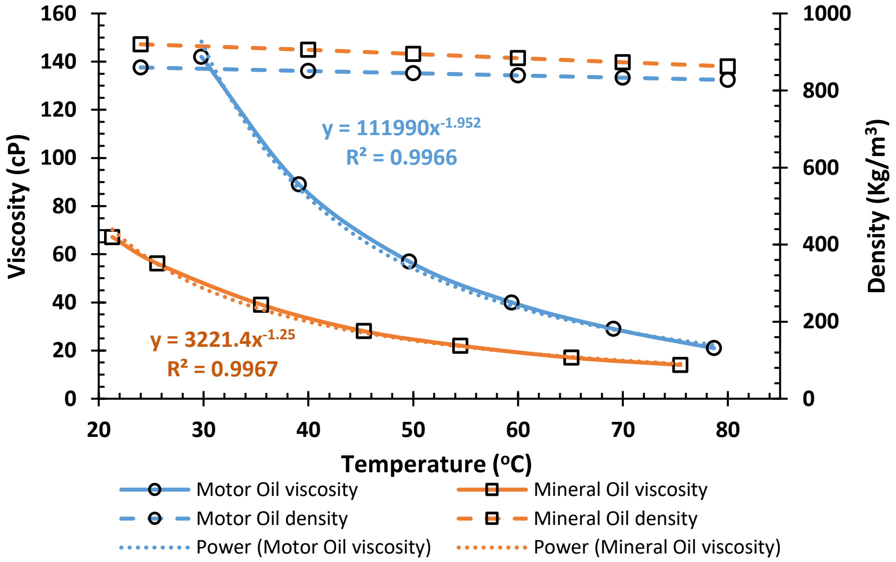

Figure 3.10: Plot of viscosity and density of the oil samples against temperature at a shear rate of 510 $s^{-1}$

### 3.4.2.4 **Sequence and procedure for density measurement**

The sample cup was filled with the test sample and covered with the cup lid firmly seated and rotated making some oil squeeze out through the vent hole. The excess oil was cleared from the exterior of the mud balance and the balance was seated with its knife-edge on the stand and levelled by adjusting the rider. The oil density was read from the edge of the slider as indicated by the marker on the rider.

## 3.5 **EXPERIMENTAL SEQUENCE AND PROCEDURE**

Prior to the main coreflooding experiments, a series of experiments were conducted to determine the porous media absolute or intrinsic permeability to brine. To achieve this, sand grains was packed into the coreholder with mesh screens placed on the endcap to prevent the sand grains from entering the tubing during the experimental run. The packing was done with some space left at the top end for the endcap to be able to fit after which another mesh was placed to aid uniform fluid distribution. Brine was poured slowly to saturate the porous system through the opening of the mesh after which the second endcap was fitted to close the cell and the coreholder was mounted on the stand and connected to the tubing.

After mounting and connecting the system, a continuous flow of brine at a low flowrate of 0.5 mL/min with the HPLC pump was carried out to ensure that the porous medium was 100 % saturated with brine and that all the air was completely flushed out of the system. It is essential to flow at a low rate for three main reasons; firstly, to prevent separation or redistribution of the sand particles as much as possible, second, to avoid the creation of fractures or easy pathways, and thirdly because the classic Darcy equation is not applicable at high flowrates. The flow was continued until about 5 pore volumes had been injected after which the differential pressure readings were taken when the system reached a SS condition (i.e. a constant flowrate was attained at the inlet and outlet with minimal pressure variations). Absolute permeability to brine was then calculated using the classic Darcy's equation, pressure differential and other parameters of the test cell.

### 3.5.1 **The coreflooding experiments**

Coreflooding at elevated temperatures is the focus of this experimental research. These experiments represent the secondary oil recovery process (waterflooding) where water is pumped into the reservoir to pressurise the reservoir while also displacing the oil to the producer well. While the general concept and procedure of a standard USS coreflooding experiment remain the same, necessary modifications were made to the existing test rig for this planned research. To achieve the objectives of this research, over 30 different sets of flooding experiments were carried out and 18 reported, 12 results were discarded due to experimental inconsistencies and errors. The main difference between the various sets of experiments would be the changing of the various parameters and investigating their resulting effects on the recorded measurements.

The steps described as follows occur after the intrinsic media permeability measurements. The drainage process was carried out by pumping oil from the inlet to displace the brine until the porous media reaches irreducible water saturation ($S_{wi}$), where the remaining water cannot be displaced from the system, with both saturations being recorded. After irreducible water saturation was reached, oil flow was continued and monitored until a SS condition was attained. After reaching irreducible water saturation, a reverse process was carried out for the imbibition process where water was pumped at specified flowrates (0.5, 0.75, 1.0 mL/min) and varying media injection temperatures (40, 60, 80 $^{o}$C) used to displace the oil in the sandpack. The waterflood continued until oil production ceased and the pressure drop across the sample became stable. After the main fluid flow was initiated, measurements of temperature, pressures and flowrate were made continuously. The procedure for the imbibition experiments is summarised in the schematic of Figure 3.11. The produced effluent was measured in graduated measuring cylinders to account for the cumulative fluid produced at the outlet at different time interval. To reduce error in measurements and calculations, the dead volumes in the flow lines were quantified and factored into the experimental data processing.

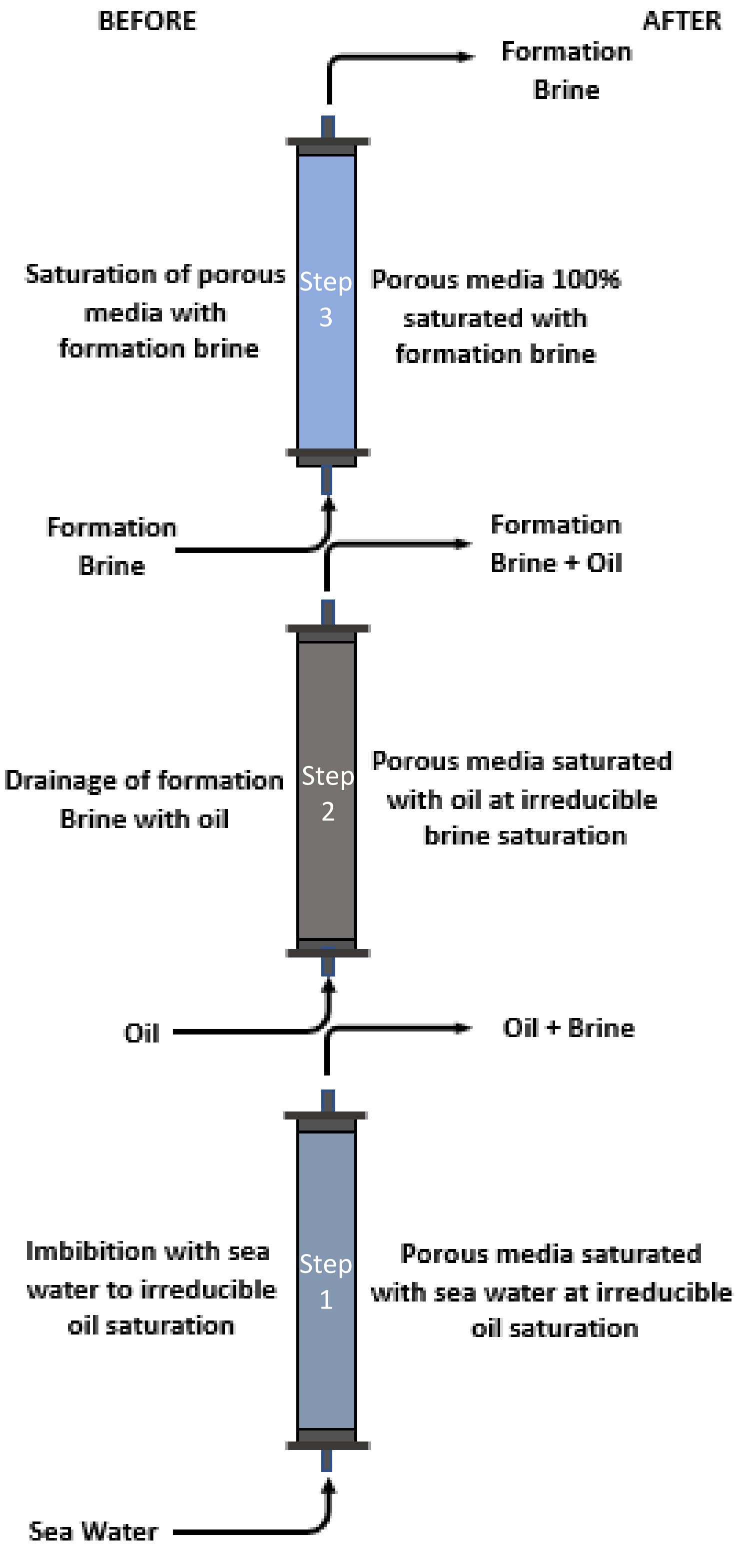

Figure 3.11: Schematic representation of the sandpack column process

## 3.6 HISTORY MATCHING METHOD AND RELATIVE PERMEABILITY CORRELATIONS USED

Relative permeability calculations from USS or displacement experimental data is achieved through either explicit methods or implicit method. The explicit techniques are mainly the JBN method by Johnson et al. (1959) and its modified version by Jones and Roszelle (1978).

Hypothetical coreflooding data was generated by Akin et al. (1998) at varying temperatures with the use of a numerical simulator for assumed relative permeability. The JBN method was used with the production data generated via simulation to calculate the relative permeability and they reported that the JBN and similar techniques can lead to erroneous results. This finding agrees with reports by Ashrafi (2013) stating that the JBN method shows a false temperature dependant behaviour of relative permeability in heavy oil systems mainly due to instabilities and viscous fingering.

Due to the inherent deficiencies of explicit methods, the implicit method has been adopted for relative permeability calculations in this study. The implicit method, otherwise referred to as the history matching approach is based on numerical computation where the different relative permeability model parameters are adjusted to match the coreflood experimental data, mainly the cumulative production and differential pressure, Wang et al. (2006). In this study, the history matching was carried out using the coreflooding numerical simulator, Sendra 2012. The Sendra software is a fully implicit two-phase one dimensional black-oil simulator for analysing data from special core analysis experiments. It can be implemented for all common experimental techniques either the SS or USS flow experiments, single- and multispeed centrifuge, as well as porous plate experiments. The software can be applied for either oil-water experiments, gas-oil or gas-water flow, during both imbibition and drainage processes. A third immobile fluid phase may also be presented in domain.

Sendra can be used both as a coreflooding simulator or for history-matching the experimental data with simulated data for generation of the relative permeability curves. The procedure involves selecting an appropriate relative permeability model in the simulator and then the software varies the empirical parameters while it attempts to match the experimental data. For more information on the functionalities and estimation method used in the Sendra software, refer to the software manual (Sendra, 2012). A short review of the different relative permeability models included in the Sendra simulator is given in the following sub-sections. In all of the models implemented, the same equation is used for the normalised water saturation as presented in Eq. 3.2:

$$S_w^* = \frac{S_w - S_{wi}}{1 - S_{wi} - S_{or}} \qquad 3.2$$

All the correlations mentioned below were explored to determine the best possible history match of the experimental data for this study.

### 3.6.1 **Burdine correlation**

Burdine (1953) used pore size distribution data in the derivation of Eq. 3.3 and 3.4 for the prediction of oil and water relative permeability from basic laws of fluid flow in the porous media.

$$K_{rw} = K_{rw}^o (S_w^*)^{\frac{2+3\lambda}{\lambda}} \qquad 3.3$$

$$K_{ro} = K_{ro}^o (1 - S_w^*)^2 \left(1 - (1 - S_w^*)^{\frac{2+\lambda}{\lambda}}\right) \qquad 3.4$$

where, the superscript o is the end value in the relative permeability, $\lambda$ is the media pore size distribution index and the superscript * the value for water saturation as defined by Eq. 3.2.

### 3.6.2 **Corey correlation**

The popular and widely accepted Corey models (Eq. 3.5 and 3.6) were derived from the capillary pressure concept and has been widely applied for consolidated porous medium (Corey, et al., 1956).

$$K_{rw} = K_{rw}^o \left({S_w^*}^{N_w}\right) \qquad 3.5$$

$$K_{ro} = K_{ro}^o (1 - S_w^*)^{N_o} \qquad 3.6$$

where $N_w$ and $N_o$ are the water and oil Corey parameters respectively which shows the curvature of water and oil relative permeability plots.

### 3.6.3 **Sigmund and McCaffery correlation**

In Eq. 3.7 and 3.8, $N_w$ and $N_o$ are the same as the Corey parameters. While A and B are parameters used to linearise the curves as the relative permeability values nears zero. If the constants A and B are zero then these correlations become the same as the Corey models, Sigmund and McCaffery (1979).

$$K_{rw} = K_{rw}^{o} \frac{(S_w^*)^{N_w} + AS_w^*}{1 + A} \qquad 3.7$$

$$K_{ro} = K_{ro}^{o} \frac{(1 - S_w^*)^{N_o} + B(1 - S_w^*)}{1 + B} \qquad 3.8$$

### 3.6.4 **Chierici correlation**

Chierici (1984) implemented a nonlinear regression approach on the sets of N experimental data points in deriving empirical coefficients A, B, L and M to be applied in Eq. 3.9 to 3.11. $R_w$ is the correlations parameter in both equations.

$$K_{rw} = K_{rw}(S_{or})e^{-BR_w^{-M}} \qquad 3.9$$

$$K_{ro} = K_{ro}(S_{wi})e^{-AR_w^{L}} \qquad 3.10$$

$$R_w(S_w) = \frac{S_w - S_{wi}}{1 - S_{or} - S_w} \qquad 3.11$$

### 3.6.5 **LET correlation**

In Eq. 3.12 and 3.13, the parameters L, E and T are empirical constants. While L describes the shape of the curve in the lower parts, E describes the slope of the curve and the parameter T alters the top of the curves, Lomeland et al. (2005).

$$K_{rw} = K_{rw}^{o} \frac{(S_w^*)^{L_w}}{(S_w^*)^{L_w} + E_w(1 - S_w^*)^{T_w}} \qquad 3.12$$

$$K_{ro} = K_{ro}^{o} \frac{(1 - S_w^*)^{L_o}}{(1 - S_w^*)^{L_o} + E_o(S_w^*)^{T_o}} \qquad 3.13$$

## 3.7 **TECHNICAL ISSUES, LIMITATIONS AND UNCERTAINTIES**

As reported by McPhee (2015), an estimated 70 % of core analysis data in public domain are unfit for purpose due to their unreliability, inapplicability or inappropriateness. The discrepancy in core analysis data has resulted from a combination of factors ranging from the methodology followed, instrumentations, and personnel competency amongst other reasons. Despite the difficulties in achieving reproducible results, coreflooding experiments remain an important aspect of hydrocarbon reservoir studies. There is therefore the real need to minimise data uncertainties by standardising the experimental best practice in core analysis data acquisition, quality control and interpretation.

In order to design and run acceptable experimental coreflooding studies, there has to be a thorough understanding of the standard procedure with full acknowledgement of the uncertainties involved. Some sources of uncertainties, study limitations and encountered technical issues are highlighted below.

i. *Capillary end effect*: With two-phase flow of oil and water into a water-wet porous media under SS conditions, it is expected that both fluids exit the outlet face at the same pressure. However, this is not the case, as there exists a build-up of the water phase (higher saturation) at the outlet face due to capillarity. This non-uniform saturation profile at the outlet is called the capillary end effect. Ignoring the effect of this phenomenon has been found to give rise to erroneous results and measurements must be taken to minimise or eliminate this effect. Possible solutions are flowing at higher flowrates, but this has its own negative effect of deviating from the Darcy flow and causing some preferential flow paths in the media. To mitigate against the effect, a relatively long porous system has been used for this study and the pressure readings were taken about 15 mm away from both the inlet and outlet face.

ii. *Unstable displacement*: Another possible source of errors and uncertainties is the occurrence of unstable displacement within the porous unit. In the displacement of a viscous fluid (oil) by a less viscous fluid (water), there exists some unstable displacement front caused by unfavourable mobility ratio between the two fluids giving rise to viscous fingering as against the expected piston like displacement with a uniform front. A major cause for this occurrence is running at a high flowrate and the use of a short porous unit. For this reason, the series of experiments in this study were carried out at relatively low flowrates and with a long porous cell.

iii. *Dead volume*: While carrying out material balance calculations for the different fluid saturations, a major source of error is the volume of fluid retained in the tubing at the inlet and outlet end of the porous system that are unaccounted for. To mitigate against this error source, the dead volume of the test trig was accounted for by measuring the length of the adjoining tubing and calculating for the volume of fluid retained within and including this value in the material balance computations for the saturation of the fluid phases.

# Chapter 4: COMPUTATIONAL FLUID DYNAMICS AND MACHINE LEARNING METHODOLOGY

**Overview**

This section presents a general introduction to the theory of CFD with specific focus on the governing equations and multiphase flow models implemented in this study. A brief overview of the SVM algorithm is also presented in this chapter.

## 4.1 MULTIPHASE FLOW MODELLING METHODS

The numerical modelling of multiphase flow is more challenging than that of single-phase flow. However, with the advances in computational fluid mechanics and higher computing power, more robust modelling techniques have been developed ensuring better understanding of the dynamics of multiphase flow. The 2 main approaches for the numerical modelling of multiphase flows are the Euler-Lagrange approach and the Euler-Euler approach (ANSYS, 2018). The detailed treatment of the various multiphase flow modelling approaches and their respective formulation can be found in Versteeg and Malalasekera (2007), Enwald and Almstedt (1996) and Tryggvason et al. (2001). The multiphase flow modelling approach implemented in this study for a liquid-liquid immiscible flow is discussed briefly in the following Section 4.1.1 and 4.1.2.

### 4.1.1 The volume of fluid model

The volume of fluid (VOF) method is a free-surface numerical modelling technique for tracking and detecting the free surface or fluid–fluid interface. In simulated 2 or more immiscible fluids flow, the VOF method is solved with a single set of momentum equations and tracks the volume fraction of each of the fluids throughout the flow domain (ANSYS, 2006). The VOF formulation works on the basis that the 2 or more fluid phases are immiscible and non-interpenetrating. Within each control volume (CV), the volume fractions of all the fluid phases are equal to 1. A volume averaged value variable and property is assigned to each of the phases if the volume fraction of each phase is known at each location. Therefore, the variables and properties within a given cell is either purely representative of a given phase, or results from a mixture of phases, depending upon the volume fraction values. Typically, the volume fraction of oil phase ($\alpha_o$)

equals to 1 if the cell is completely occupied by oil ($\alpha_o = 1$), while it equals 0 if the cell is completely occupied by water ($\alpha_o = 0$). If the cell contains the oil-water interface, then the volume fractions of oil and water lies between 0 and 1 ($0 < \alpha_o < 1$).

In this study, the VOF method has been implemented in the ANSYS Fluent® solver to study the wettability and viscosity effect on oil recovery at the pore-scale level. Details and findings from this study are presented in Chapter 5 of this thesis.

### 4.1.2 The mixture model

The main principle of the mixture theory is that the void or pore space occupied by a mixture can be seen to be filled co-jointly by the different constituents that make up the mixtures, each considered as a continuum in its own right. Therefore, at each point within the media, which is filled by the mixture, there will be a portion belonging to each of the constituents. The conservation laws for mass, momentum, and energy consider the contributions of any of these quantities within the flow domain regarding a particular constituent due to the influence of the other constituents. The mixture model is an abridged form of the multiphase model that has the capability to model multiphase flow systems where the different phases move at individual velocities but assume local equilibrium over short spatial length scales. In the mixture model, equations solved are the mass, momentum and energy for the mixture, as well as the volume fraction for the secondary phase(s), in addition to the relative velocities in flows where the phases have different velocities. A limitation of the mixture model used in this study that it gives a pressure for the mixture and not for individual phases thereby making computations for capillary pressure impracticable.

## 4.2 TRANSPORT EQUATIONS AND CLOSURE MODELS

This section describes the averaged governing equations implemented and the closure equations in the multiphase model framework as implemented in the present study. The detailed information of the derivation coupled with the various averaging procedures of the governing equations can be found in Versteeg and Malalasekera (2007). The governing equations solved in the different multiphase models include the standard mass, momentum and energy conservation equations with inclusion of the volume fraction equation, Eq. 4.1 – 4.3.

*Mass conservation equation:*

$$\frac{\partial \rho}{\partial t} + \nabla \cdot (\rho \vec{u}) = 0 \qquad 4.1$$

*Momentum conservation equation:*

$$\frac{\partial (\rho \vec{u})}{\partial t} + \nabla \cdot (\rho \vec{u} \vec{u}) = -\nabla p = \nabla \cdot [\mu(\nabla \vec{u} + \nabla \vec{u}^T )] + \vec{F} \qquad 4.2$$

*Energy conservation equation:*

$$\frac{\partial (\rho \mathrm{T})}{\partial t} + \nabla \cdot (\rho \vec{u} \mathrm{T}) = \nabla \cdot (\frac{k}{c_p} \nabla \mathrm{T}) \qquad 4.3$$

where $\vec{\mathrm{u}} = (\mathrm{u}, \mathrm{v})$ is the velocity vector $\rho$ is the volume-averaged density and p is the pressure, μ is the coefficient of kinetic viscosity, $\vec{\mathrm{F}}$ is the surface tension force per unit volume, T is the temperature, k is the thermal conductivity and $c_p$ is the specific heat capacity.

## 4.2.1 **Material property and volume fraction**

The volume fraction equation is expressed in Eq. 4.4:

$$\frac{\partial \alpha_w}{\partial t} + \vec{u} \cdot \nabla \alpha_w = 0 \qquad 4.4$$

When a computational cell or CV is completely filled by a single phase, only the properties of that phase are applied in the equations, whereas when a fluid interface lies within the CV, the mixture properties of the two phases are used in a volume fraction weighted average. For example, in a two-phase oil-water system, denoted the by the subscripts *o* and *w*, if the volume fraction of the water is being tracked, the density in each cell is given Eq. 4.5:

$$\rho = \alpha_w \rho_w + (1 - \alpha_o) \rho_o \qquad 4.5$$

All other fluid properties are computed in a similar manner and are stated in Eq. 4.6 for the viscosity as:

$$\mu = \alpha_w \mu_w + (1 - \alpha_o) \mu_o \qquad 4.6$$

## 4.2.2 **Surface tension and wall adhesion**

In a two-phase immiscible fluid flow at microscale, surface tension plays a dominant role. The continuum surface force (CSF) model by Brackbill et al. (1992)

for surface tension was implemented in the ANSYS Fluent® model by the inclusion of a source term in the momentum equation. Equation 4.7 the surface tension force per unit volume $\vec{F}$ in the momentum equation.

$$\vec{F} = \sigma \frac{\rho k_w \nabla \alpha_w}{\frac{1}{2}\left(\rho_w + \rho_o\right)} \qquad 4.7$$

where $\sigma$ is the surface tension coefficient and k is the interface curvature computed using Eq. 4.8.:

$$k = -(\nabla \cdot \hat{n}) \qquad 4.8$$

where $\hat{n}$ is the unit normal vector of the interface. The surface normal at the cell next to the wall is:

$$\hat{n} = \hat{n}_w cos\theta_w + \hat{t}_w sin\theta_w \qquad 4.9$$

where $\hat{n}_w$ and $\hat{t}_w$ are the unit vectors normal and tangential to the wall, respectively.

### 4.2.3 **Solution method**

From the previous step, the governing equations or mathematically models have been discretised into a set of linear algebraic equations. The difficulty and size of the set of equations to be solved are determined by dimensionality and the number of grid nodes (Versteeg & Malalasekera, 2007). Two solution techniques for linear algebraic equations are the direct and indirect or iterative methods. The solution approach for this study uses the iterative solver based on the repeated application of a specified algorithm resulting in the final convergence after the number of iterations.

## 4.3 **DISCRETISATION APPROACHES**

As stated earlier, since the ANSYS Fluent® CFD solver used in this study implements the finite volume discretisation method, only the finite volume method (FVM) will be discussed in this section.

### 4.3.1 **Finite volume method**

In the FVM, the integral form of the governing equation is implemented as its starting point after the computational domain has been partitioned into a finite number of contiguous CVs with the governing equations applied to each CV. The parameters of interest are computed at the computational node at the centroid of each CV. The finite volume discretisation method is notable as a highly successful numerical approach in solving problems of fluid mechanics, meteorology and many other engineering areas (Abobaker & Bambang, 2014). The generalised form of the transport equations, written the form of Eq. 4.10 for mass, momentum and energy are solved on this set of control volumes.

$$\frac{\partial}{\partial t}\int_{V} \rho\phi dV + \oint_{A} \rho\phi V \cdot dA = \oint_{A} \Gamma\nabla\phi \cdot dA + \int_{V} S_{\phi} dV \qquad 4.10$$

The first term on the left-hand side is the unsteady term and the next is the convection term. On the right-hand side, the first is the diffusion term while the generation term is next. In Eq. 4.1, $\rho$ is the density, t is the time factor, $\emptyset$ is the scalar variable, A is the area, V is volume and S is the source term.

The procedure for the CFD numerical implementation used in this study is summarised in Figure 4.1.

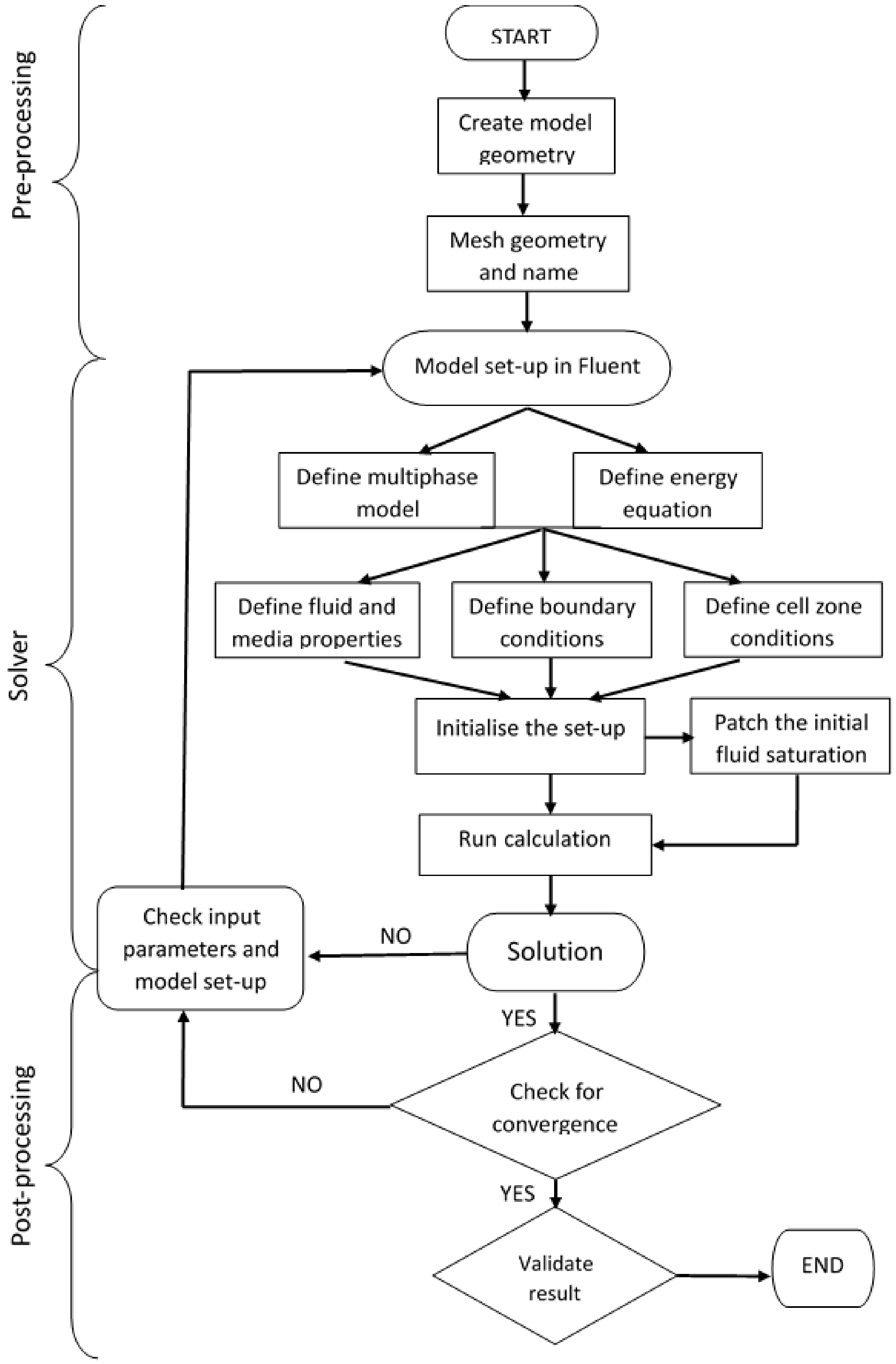

Figure 4.1: Process flow diagram for the CFD modelling and experimental validation

## 4.4 SUPPORT VECTOR REGRESSION

Considering a simple linear regression problem with the training data set $\{(x_1, y_1), \dots, (x_l y_l)\} \subset \mathcal{X} \times \mathbb{R}^d$, where $\mathcal{X}$ denotes the space of input patterns (e.g. $\mathcal{X} \times \mathbb{R}^d$). According to Vapnik (1995), a function f(x) needs to be found with the most ε deviation from the predicted target variable $y_i$ for the entire training data, while being as flat as possible. That is, there can be errors as far as it is less than ε, any deviation larger than this is unacceptable. The function f(x) takes the form:

$$f(x) = (w, x) + b \; with \; w \in \mathcal{X}, b \in \mathbb{R} \tag{4.11}$$

where (.,.) is the dot product in $\mathcal{X}$. The flatness in Eq. 4.11 above means *w* needs to be small (Smola & Bernhard, 2004). A possible approach is to minimise the norm, i.e. $\|w\|^2 (w, w)$. This problem can thus be written as a convex optimisation problem:

$$\begin{aligned} & minimise \; \frac{1}{2}\|w\|^2 \\ & subject\ to \begin{cases} y_i - (w, x_i) - b \le \varepsilon \\ (w, x_i) + b - y_i \le \varepsilon \end{cases} \end{aligned} \tag{4.12}$$

It is generally assumed in Eq. 4.12 above that there exists such a function f which approximates all pairs *($x_i$, $y_i$)* with ε precision, i.e., that the convex optimisation problem is achievable. This however may not be possible sometimes and thus the need to introduce slack variables analogous to the ”soft margin” loss function. Introducing the slack variables, $\xi_i$, $\xi_i$* to cope with the otherwise infeasible constraints of the optimisation problem results in the Vapnik (1995) formulation:

$$\begin{aligned} & minimise \quad \frac{1}{1}\|w\|^2 + C\sum_{i=1}^{l}(\xi_i + \xi_i^*) \\ & subject\ to \begin{cases} y_i - (w, x_i) - b \le \varepsilon + \xi_i \\ (w, x_i) + b - y_i \le \varepsilon + \xi_i^* \\ \xi_i, \xi_i^* \qquad\qquad \ge 0 \end{cases} \end{aligned} \tag{4.13}$$

The trade-off between the flatness of *f* and the tolerance for deviations larger than ε is decided by the constant, C > 0. This relates to treating the ε-insensitive loss function $|\xi|_\varepsilon$ represented in Eq. 4.14. Cherkassky and Mulier (1998) gives a detailed selection procedure for C and ε.

$$|\xi|_{\varepsilon} := \begin{cases} 0 & if|\xi| \leq \varepsilon \\ |\xi| - \varepsilon & otherwise. \end{cases} \tag{4.14}$$

The relationship between oil-water relative permeability and saturation is nonlinear, making linear function approximation impracticable. Figure 4.2 shows a schematic of the concept of nonlinear SVR, corresponding to Eq. 4.14. More details on the fundamentals of the SVR can be found in Lahiri and Ghanta (2008) and Smola and Bernhard (2004).

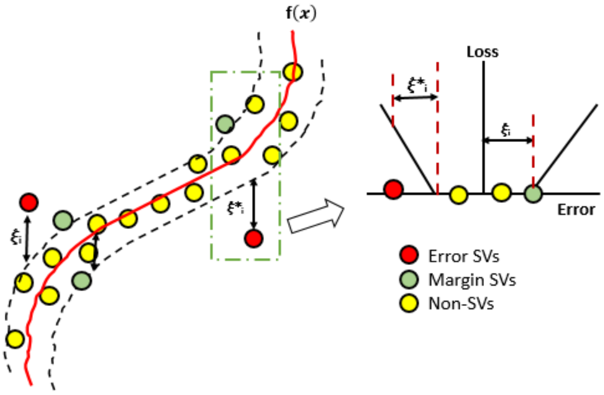

Figure 4.2: The soft margin loss setting for a linear SVM (adapted after Pao-Shan et al. (2006))

The SVR algorithms were implemented using the Sklearn (or Scikit-learn) library in Python. Sklearn is a Python library offering different features for data processing applied for classification, clustering and model selection. The process involves training the model with a particular dataset and testing against another dataset. Achieving this typically involves splitting the dataset into a train and test datasets in various proportions using the Sklearn train_test_split function. A few considerations in the data splitting process are the test_size or train_size which determine the size of the dataset used for training and testing the developed model. Another consideration is the random state acting as the seed for the generation of random numbers during the split. The procedure for the model implementation is presented in the Figure 4.3.

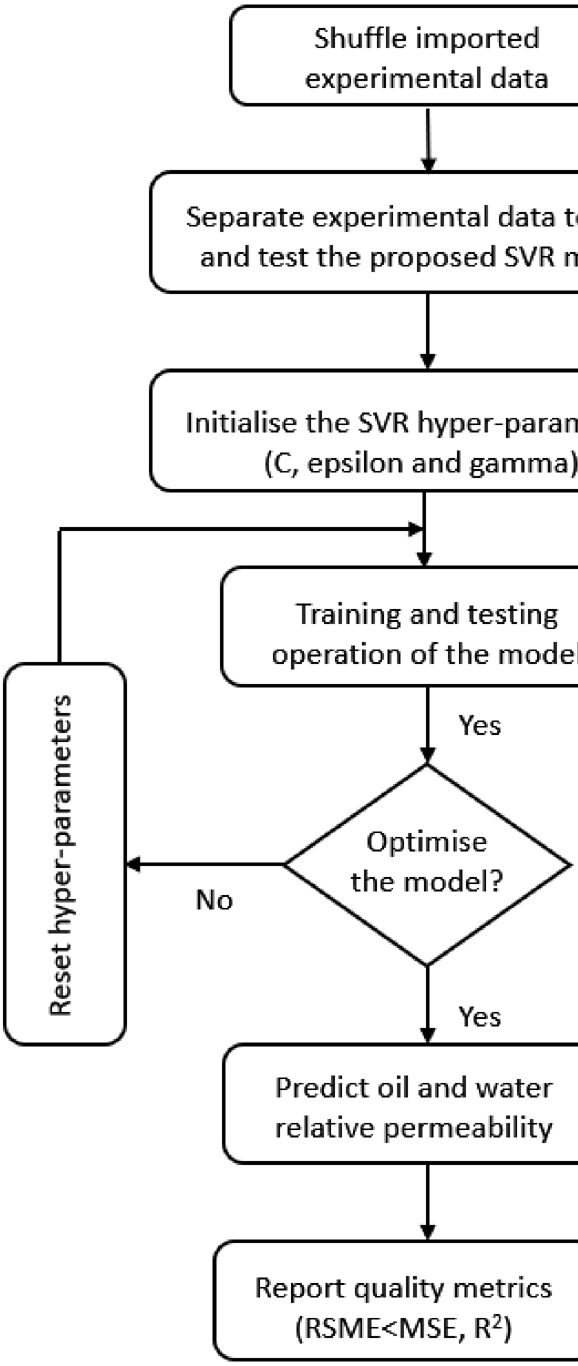

Figure 4.3: Flow chart of the machine learning procedure followed for the model implementation

# Chapter 5: COMPUTATIONAL FLUID DYNAMICS MODELLING OF WETTABILITY, INTERFACIAL TENSION AND TEMPERATURE EFFECT ON OIL RECOVERY AT PORE-SCALE LEVEL

**Overview**

This chapter discusses the effects of wettability on oil recovery with hot-water injection at varying temperature conditions using a 2-D pore-scale structure by applying a CFD approach. A 2-D geometry comprising of pore spaces of varying sizes and interconnected pore-throats was utilised; 18 different scenarios were simulated in this study. The VOF method was implemented in the CFD software ANSYS Fluent® 18.1 to develop a two-phase flow and heat transfer model.

## 5.1 COMPUTATIONAL MODEL FORMULATION

For a multiphase flow simulation at pore-scale, capturing the interface between the immiscible fluids is usually a matter of interest. In this study, the VOF multiphase flow model for interface tracking has been implemented to track the oil-water interface. Three different temperature scenarios were simulated in this study under varying wettability conditions for the matrix wall. Water was injected at different temperatures of 20, 40 and 60 °C into the computational domain with an initial temperature of 60 °C, initial oil saturation of 80 % and irreducible water saturation of 20 % at 0.025 N/m and 0.045 N/m IFT levels.

### 5.1.1 Model geometry

The 2-D pore scale geometry used in this study is a 22 mm by 10 mm rectangle block shown in Figure 5.2. The micromodel in this study is made of polydisperse solid grains having two different diameters of 1 and 2 mm which is representative of commercial grade silica grade silica sand 8/16. Pore-bodies and pore throats of varying dimensions characterise the model. While some studies (Mingming & Shuzhong, 2015; Zhao & Dongsheng, 2017) utilise a homogenous porous medium with the same diameter for all the grains, it is obvious that that is not a realistic representation of a natural porous media. The different diameter sizes for the sand grains have been used to mimic the true nature of a natural porous system with varying grain sizes and thus heterogeneous flow characteristics. The pore throat width was varied between 0.10 mm and 0.35 mm to mimic a low and high permeability zone as representative of a natural porous media.

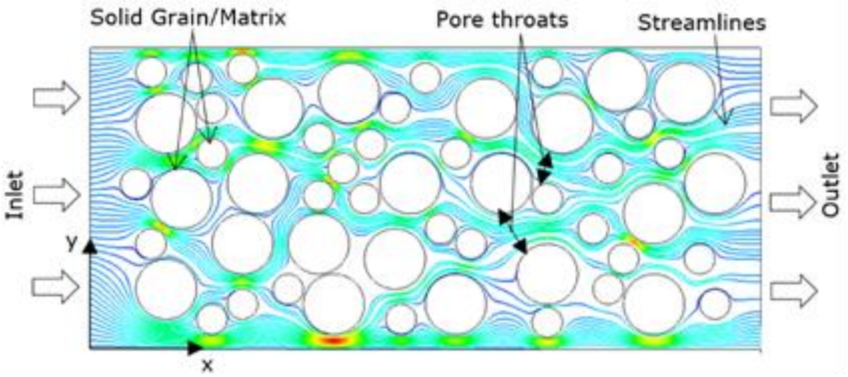

Figure 5.1: The 2-D pore-scale media configuration

For a better capture of the occurrences near the walls and for the accuracy of the results, the grid around the individual grain wall region was structured and refined with fine meshes. Care was taken to refine the mesh by conducting a number of sensitivity studies to determine the optimum inflation layers, mesh sizes and number of CVs needed to ensure that the computed profiles of the oil/water interface are grid independent. The final mesh used for the simulations has a total CV of 39817 (Figure 5.2). The time step sizes used for the simulation is 0.0005 and the PISO scheme was adopted for the pressure-velocity coupling, PRESTO for the pressure discretisation and Geo-Reconstruct for the volume fraction.

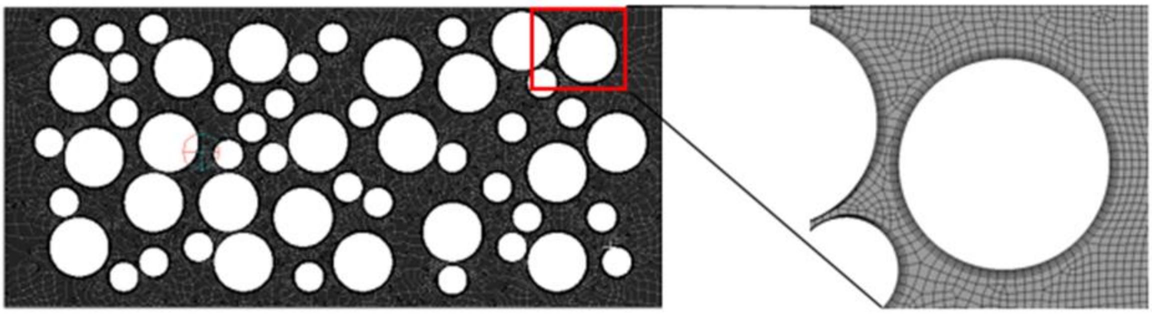

Figure 5.2: Grid used for the study showing the refined inflation layers.

The pore volume of the sample is 1.28 × $10^{-4}$ $m^3$, which gives a porosity of approximately 58 %. Single-phase flow simulation with water indicates an absolute permeability of $8.6 \times 10^{-9}$ $m^2$. At the inlet and outlet face, a gap of approximately 1 mm was allowed before the first set of grains. Although a natural rock-2-D slide would have a spatially periodic matrix at these faces, the gaps imposed here would allow the flow to develop before meeting the first set of obstructions in the solid grain matrix. While an idealised geometry as this does not reflect the 3-D connectivity of real porous media, it can be adopted as a computationally affordable alternatives to 3-D pore-scale models that allows for more detailed visualisation of the intricate physics in a much clearer way than the 3-D models. Another advantage for the application of micromodels is the prospect of designing, fabricating and studying different shapes and patterns.

A no-slip boundary condition was imposed on the grain walls and on all the lateral sides. The flow domain is initially saturated with phase-1 (oil) at 80 % and phase-2 (water) at 20 % and water was injected at a constant velocity of 0.005 m/s from the inlet and 0 Pa pressure was specified as the outlet boundary condition. A velocity inlet condition has been used in the model as a standard practice in situations where the injection flowrate or velocity is known without information of the pressure at the inlet. In this set of simulations, the numerical model computes the pressure at the inlet from the imposed velocity condition and other flow parameters. Based upon the injection velocity, pore diameters and velocity of fluids the flow is mainly in the laminar flow regime and as such no turbulence model has been solved in the numerical model.

## 5.2 PROPERTIES OF FLUID AND POROUS MEDIA

Simulations were conducted with constant fluid properties, except for the viscosity of the oil phase owing to the heat transfer between the fluids and solid matrix walls. The water phase has a viscosity of 0.001 kg/m-s, while the oil has a varying viscosity with respect to operating temperature. The oil phase was simulated with a temperature dependent viscosity while the water phase viscosity was kept constant, since the experimental observation of water viscosity change with temperature is minimal, and as such has a negligible effect in flooding a highly viscous oil phase. The viscosity ratio ($\mu_w/\mu_o$) for the simulations was found to be between 0.007 – 0.081 which is less than $1\times10^3$ as recommended by ANSYS Fluent® to avoid convergence difficulties. In addition, the effect of temperature on the fluid thermal conductivity and specific heat capacity were not considered. A survey of the literature showed a near linear decrease in the oil/water IFT, $\sigma_{ow}$ with an increase in temperature, and a 1 $^{o}$C increase in temperature resulting in a 0.05 mN/m decrease in oil/water IFT using a reference value of 47 mN/m at 60 $^{o}$C.

The viscosity of the primary phase (oil) as a function of local temperature was incorporated through a user defined function (UDF). The experimental viscosity data was used to determine a function for corresponding oil phase viscosity for temperatures ranging from 20 to 100 °C. The model for the viscosity with corresponding temperature is given in Eq. 5.1. As seen in the function, at temperatures above 100 °C, the oil viscosity is 12.3 cP, when the temperature is below 20 °C the oil viscosity is 142 cP while for temperatures between the range of 20 to 100 °C, the function in Eq. 5.1 was used to calculate the viscosity of the oil phase. This function has been derived from the experimental data generated for viscosity measurement and presented in Appendix IV.

$$\mu = f(T) = \begin{cases} 0.0123\ (kg/ms), & T > 373\ K \\ 4504.7e^{-0.035T}\ (kg/ms), & 293k \leq T \leq 373\ K \\ 0.142\ (kg/ms), & T < 293\ K \end{cases} \qquad 5.1$$

## 5.3 RESULTS AND DISCUSSION

The results of the hot waterflooding process involving the different wettability and IFT scenarios are presented and analysed in this section. The results are in the form of volume recovery factors (RF) which is defined as the volume fraction of oil that was displaced from the porous media and was computed using Eq. 5.2.

$$RF = \frac{V_{displaced}}{V_{initial}} = \frac{V_{initial} - V_{residual}}{V_{initial}} \times 100 \qquad 5.2$$

where $\mathrm{V_{initial}}$ is the initial volume of oil in the domain, $\mathrm{V_{displaced}}$ is the volume of oil displaced, and $\mathrm{V_{residual}}$ is the residual volume of oil left in the domain after the waterflooding process.

The respective pressure drops across the computational domain at different injection temperatures under the 3 wettability conditions considered are shown in Figure 5.3. It was observed that the entire wettability scenario shows a reduction in the pressure with an increase in temperature but become almost insignificant with the water-wet scenario. However, under a low injection temperature, the pressure drops for the intermediate-wet and oil-wet cases show a higher value in comparison to the water-wet media. This could be attributed to the fact that the oil phase adheres to the solid grain walls and thus resulting in a resistance to flow causing an increase the pressure drop. With an increase in temperature from 20 to 60 °C, it can be observed that the pressure drop reduces and having almost the same magnitude with that of the water-wet media. This may be due to the reduction in the oil viscosity and pressure drop with the increase in temperature.

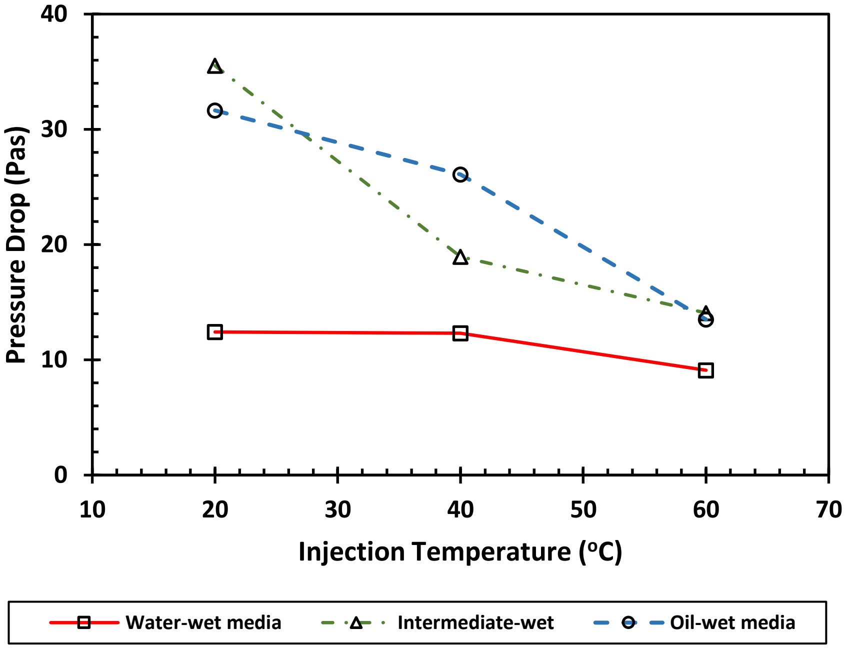

Figure 5.3: Pressure drops across the domain at different temperature

### 5.3.1 **Combined effect of wettability and temperature on the recovery factor**

The effect of porous media wettability on recovery factor at different injection temperature is presented in Figure 5.4. The result of the wettability cases presented were conducted using three different water contact angles – 45°, 90° and 150°. As shown in the plot, the recovery factor in the water-wet or hydrophilic (i.e. media with a greater affinity for water than for oil) is the highest with values above 70 % and the recovery factor decreases with increasing contact angle with values around 40 % for the intermediate-wet system and less than 20 % of the oil-wet media.

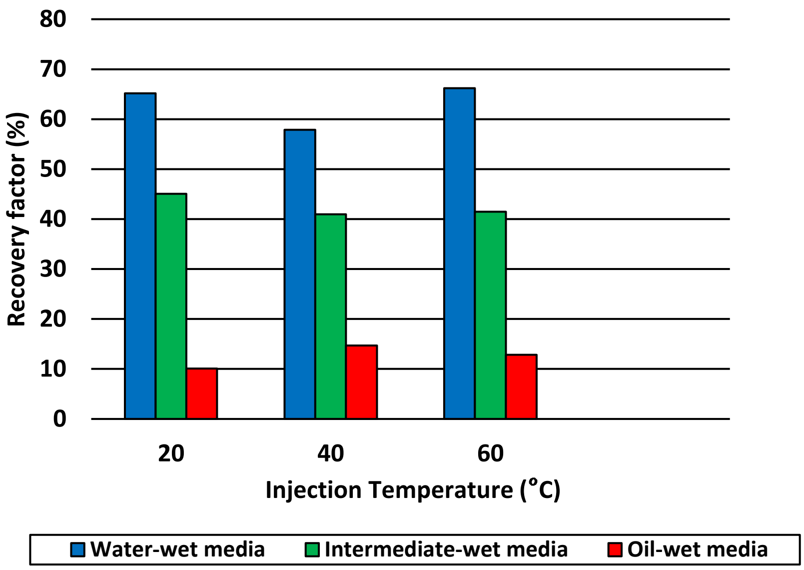

Figure 5.4: Recovery factor for different media wettability with respect to temperature at high IFT

A similar result is observed in the contour plots in Figure 5.6, with the oil phase sticking to the spherical solid grains for all the oil-wet scenarios. It can also be seen that with the transient evolution of the fluid-fluid interface, the water phase shows a convex orientation to the left in the water-wet media with the water filling up the small pore spaces while the oil forms globules of varying sizes in the central part of the large pores. The oil phase has no direct contact with the matrix wall but is covered with a thin water film and serves as a form of slippery surface for the oil to be displaced and recovered. In this case, the water breakthrough time is relatively delayed because the displacement process favours the outward flow of the oil phase more than the water.

However, in the case of hydrophobic rock, the reverse of the above process is seen on the rock surface with the oil phase creates a form of lubricating lining for the easy passage of the invading water, this results in a faster water breakthrough time. In addition, the effect of oil-wetness can also be seen in the pressure profile shown in Figure 5.3 where at 20 $^{o}$C, the pressure drop in the water-wet media is about 12 Pa when compared to the 35 Pa for the oil-wet media. It is evident that higher pressure is required to mobilise the oil from the inner small pores of the media and to detach the oil phase from the walls of the porous media. The effect of temperature is found to be more slightly higher in the water-wet media. For the water-wet case and temperature between 20 and 60 $^{o}$C, a variation of about 17 % is observed in the recovery factor, while a 13 % variation is observed in the oil-wet case. It can be explained that water-wetness makes it relatively easier for the oil to be displaced by the invading water while the oil-wet case requires more thermal energy in the system to reduce the oil viscosity; thereby releasing the oil stuck onto the matrix wall to displace as much oil as possible.

For the low temperature (20 $^oC$) injection case, the recovery factor of the water-wet media is observed to be about 72 %, while that of the oil-wet media is a little above 10 %. However, with increasing temperature, there seems to be a slight reversal in the profile with higher recovery favouring the oil-wet case. This observation agrees with the findings of Mingming and Shuzhong (2015) that reported an increase in the oil recovery with an increment in temperature for the oil-wet media. A possible explanation for this occurrence is that a reduction in the viscosity of a fluid under the same IFT results in a reduction in the capillary number, which can be observed in the water-wet system displayed in Figure 5.5. Furthermore, an injection temperature of 20 $^oC$ leads to a recovery of 72 % and reducing the viscosity of the oil phase (by increasing the temperature to 60 $^oC$) under the same IFT condition and water-wetness leads to a reduction in the capillary number, which hinders the recovery of the oil phase (60 %).

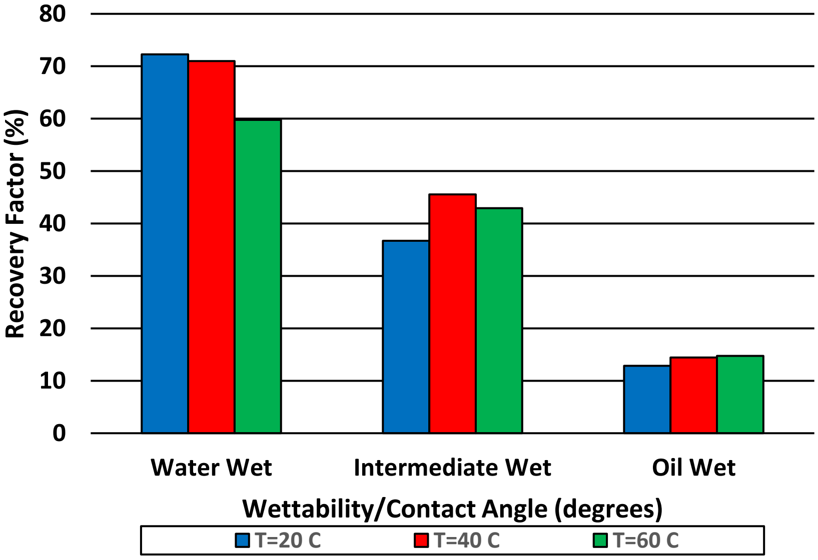

Figure 5.5: Combined effect of wettability and temperature on recovery factor at low IFT

The wettability condition of a reservoir rocks affects the effectiveness of any oil recovery method in use. At the commencement of oil production through primary recovery, the displacement of the oil phase is mainly under the influence of a pressure drop with the oil phase having a relatively high mobility and relative permeability due to its high saturation, making it easy to move in the direction of the wellbore. With the decline in relative permeability of the oil via the reduction in its saturation as seen in Figure 5.6, water saturation increases by the invading water filling the pore spaces which was earlier occupied by oil and then leaves the remaining oil in the form of isolated globules sandwiched in-between the water. This makes it difficult to extract the oil singularly by the effect of a pressure difference.

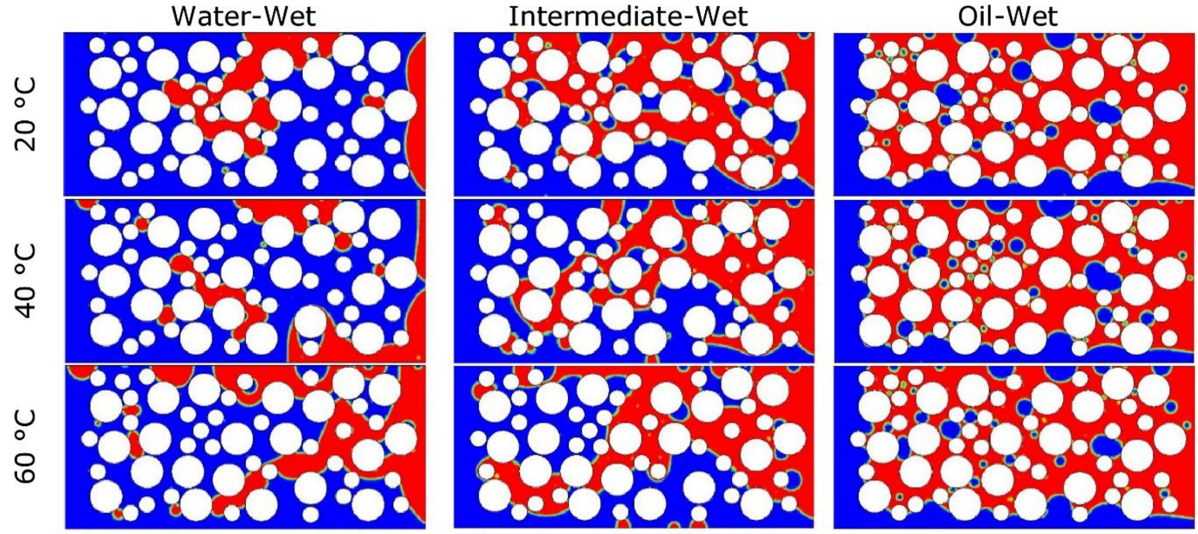

(a) Simulations under low interfacial tension of 0.025N/m

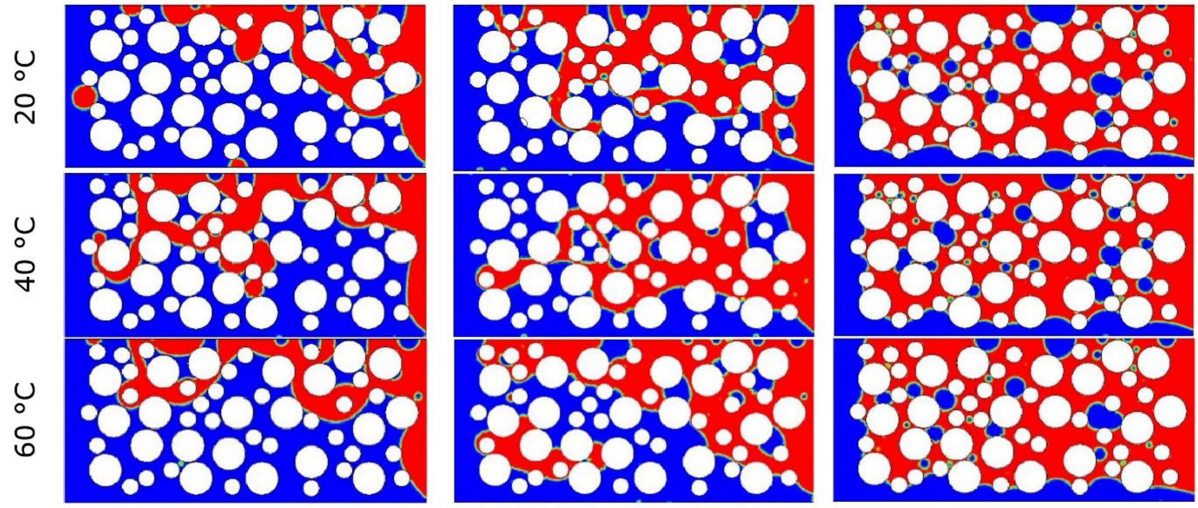

(b) Simulations under high interfacial tension of 0.045N/m

Figure 5.6: Fluid distribution of the different cases (the red and blue colour is oil and water respectively) (a) low IFT and (b) high IFT

With an increase in temperature of the injection water (thermal recovery method), more oil is recovered (mainly in the oil-wet media) as shown in Figure 5.5 and Figure 5.6. As the oil viscosity reduces due to temperature increase, the capillary pressure reduces. This results in the coming together of the oil globules into larger droplets (coalescence). This coalesced oil phase forms a zone or chain-like network of connected oil (oil bank) that easily migrates to the outlet. Besides the reduction in the oil viscosity, other studies have reported that temperature aids in the oil recovery by changing the media wettability in the hydrophilic direction.

As reported by Dangerfield and Brown (1985), at high temperatures, ionic compounds separate from the wall of the media resulting in a change of the wettability to become more hydrophilic. Donaldson and Alam (2008) reported a similar increase in recovery with an increase in temperature due to the relative permeability increase of oil with increasing temperature. A comparison of the significance of temperature variation and wettability condition to recovery factor shows that the changes in wettability affects the recovery more. While the change in injection temperature from 20 – 60 °C results in recovery factor variation of 9 – 31 %, changing the media wettability between water-, intermediate- and oil-wet results in recovery factor changes between 75 – 85 %. It can thus be stated that a proper understanding of the wettability conditions in the reservoir is needed in selection of any recovery strategy as different recovery methods selected would result in a corresponding effect on the rock matrix.

### 5.3.2 **Effect of interfacial tension**

The effect of IFT on the displacement process under different wettability conditions are presented in Figure 5.7 (a-c). The relative trend shows that the percentage recovery of oil from the flooding is higher in the cases of lower IFT. The displacement process was simulated under the water-wet (45°), intermediate-wet (90°) and oil-wet (150°) states, at varying injection temperatures. In practice, in the primary oil recovery, approximately 20 % of the original oil in place (OOIP) is recovered depending on the type of reservoir, with a secondary recovery mechanism adding another 15 to 20 %. The quest to recover the unswept oil is the aim of every enhanced oil recovery mechanism.

As stated by Carcoana (1992), the 2 main factors that determine the recovery of residual oil are the capillary number and mobility ratio. It is evident from the results in Figure 5.7 that a reduction of the IFT leads to better recovery. This could be explained with the capillary number ($Ca = \frac{\mu V}{\sigma}$), representing the ratio of viscous to capillary forces. A reduction in the IFT for the same media constriction (pore geometry) resulted in an increase in capillary number which is a significant parameter in oil recovery. In essence, a lower capillary number suggests that capillary forces dominate the flow, while a larger capillary number indicates that the flow is dominated by viscous forces. In practice, enhanced oil recovery mechanism benefit from an increase in the capillary number in order to reduce trapping. In this regard, Thomas (2007) pointed out that capillary number needs to be increased by three orders of magnitude to recover about 50 % of the residual oil saturation.

The benefit of combining IFT and wettability is apparent from this study. For an injection temperature of 20 $^{o}$C under high IFT of 0.045 N/m, a recovery of about 10 % was observed. Reducing only the IFT to 0.025 N/m improves the recovery minimally to about 13 %. On the other hand, reducing the wettability for the oil-wet case of 150$^{o}$ to intermediate-wet of 90$^{o}$ results in a recovery factor between 35 – 45 %, and a further reduction of the wettability to water-wet (45$^{o}$) results in recovery factor of between 60 – 75 %. This clearly shows that, though a low IFT is enough to resist the capillary effects, an improved oil recovery factor cannot be achieved at relatively high contact angles due to the adherence of the oil to the walls caused by the wettability condition of the porous media.

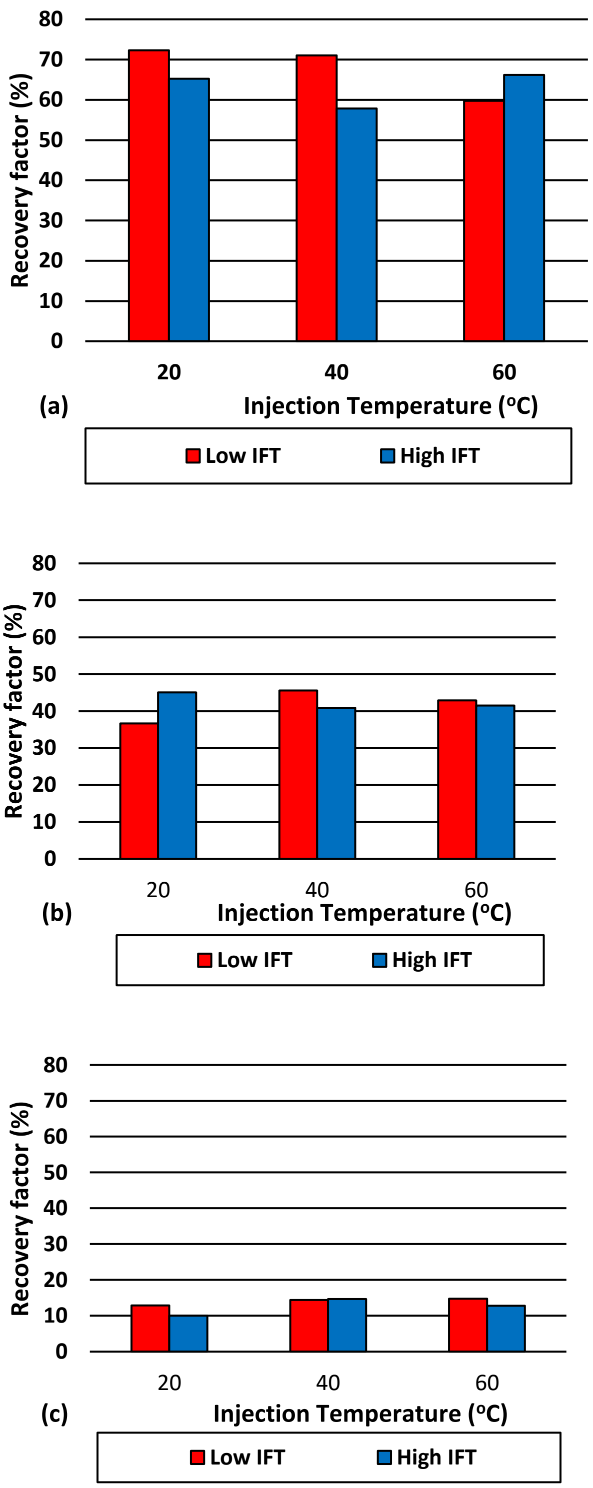

Figure 5.7: Combined effect of interfacial tension and temperature on recovery factor for oil-wet media (a) water-wet (b) intermediate-wet (c) oil-wet.

# Chapter 6: EXPERIMENTAL RESULTS AND DISCUSSION

**Overview**

This chapter presents the results from the coreflooding experiments conducted at varying operating temperatures, injection flowrates and oil viscosities. The experiments have been conducted to investigate the effect of injection flowrate and oil viscosity on oil-water relative permeability as well as the effect of temperature on relative permeability. All the experiments involved a displacement flow performed at varying temperature of 40, 60, and 80 °C with varying injection flowrates of 0.5, 0.75 and 1.0 mL/min. Two different oil samples of varying viscosities and densities were used. A relatively low flowrate was chosen to mimic the flow in a typical petroleum reservoir and all injection fluids were at ambient temperature conditions.

## 6.1 EXPERIMENTAL CONDITIONS

In this study, 18 different sets of experiments were conducted to investigate the effect of temperature, injection flowrate and oil viscosity on relative permeability and endpoint saturations. The experiments were subdivided based on flowrate, oil viscosity and temperature. Table 6.1 and Table 6.2 summarise the experimental conditions considered for the study and correlation parameters used for the history matching of experimental data. Since the porous media is highly permeable, capillary pressure was not considered in the models. All the experimental runs were carried out with the porous media at a specified constant temperature. The oil production has been presented as a percentage of the OOIP plotted against the injected pore volume of water derived from the Eq. 6.1 below:

$$NPV = \frac{q_t t}{A\varphi L} \qquad 6.1$$

where, NPV is the number of pore volume injected, $q_t$ is the rate of injection, and t time of injection. The media pore volume is the AφL where A is the flow surface area, φ media porosity and L the axial length of the media.

Table 6.1: Specification of porous media properties and injection flowrates considered in the series of experiments and Corey exponents used for the history matching (Mo-motor oil and Mi-mineral oil); SP1 – SP6 are at 40 °C.

| S/N | Media permeability (K) | Pore volume (cc) | Initial water saturation ($S_{wi}$) | Injection rate (mL/min) | Corey exponents | |
|---|---|---|---|---|---|---|
| | | | | | $N_w$ | $N_o$ |
| SP1_Mo | 7.01 | 59.75 | 0.23 | 1.0 | 3.83 | 6.00 |
| SP2_Mo | 5.03 | 61.26 | 0.25 | 0.75 | 6.88 | 3.56 |
| SP3_Mo | 6.01 | 58.09 | 0.17 | 0.5 | 2.64 | 12.78 |
| SP4_Mi | 6.50 | 60.02 | 0.17 | 1.0 | 3.81 | 2.98 |
| SP5_Mi | 5.02 | 60.88 | 0.24 | 0.75 | 7.02 | 7.99 |
| SP6_Mi | 4.59 | 59.75 | 0.19 | 0.5 | 5.77 | 3.94 |

Table 6.2: Specification of porous media properties and injection flowrates considered in the series of experiments and LET correlation parameters used for the history matching (Mo-motor oil and Mi-mineral oil); SP7–SP12 are at 60 °C while SP13–SP18 are at 80 °C.

| S/No | Media permeability (K) | Pore volume (cc) | Initial water saturation ($S_{wi}$) | Injection rate (mL/min) | LET Parameters | | | | | |
|---|---|---|---|---|---|---|---|---|---|---|
| | | | | | $L_w$ | $E_w$ | $T_w$ | $L_o$ | $E_o$ | $T_o$ |
| SP7_Mo | 6.95 | 59.75 | 0.28 | 1.0 | 1.52 | 2.28 | 0.8 | 4.26 | 6.29 | 0.82 |
| SP8_Mo | 5.23 | 61.26 | 0.25 | 0.75 | 5.38 | 0.55 | 0.8 | 3.8 | 4.37 | 0.78 |
| SP9_Mo | 7.12 | 58.09 | 0.26 | 0.5 | 1.96 | 2.63 | 0.8 | 5.43 | 7.91 | 0.87 |
| SP10_Mi | 4.86 | 60.88 | 0.11 | 1.0 | 1.89 | 2.39 | 0.8 | 4.26 | 7.74 | 0.87 |
| SP11_Mi | 5.25 | 61.56 | 0.25 | 0.75 | 1.89 | 2.39 | 0.8 | 4.26 | 7.74 | 0.87 |
| SP12_Mi | 5.17 | 61.87 | 0.24 | 0.5 | 3.05 | 1.15 | 0.8 | 4.77 | 13.85 | 0.58 |
| SP13_Mo | 5.32 | 61.64 | 0.12 | 1.0 | 5.00 | 3.99 | 0.8 | 5.00 | 1.49 | 0.98 |
| SP14_Mo | 5.07 | 62.39 | 0.26 | 0.75 | 3.05 | 3.69 | 1.34 | 3.85 | 29.8 | 1.66 |
| SP15_Mo | 5.63 | 60.50 | 0.21 | 0.5 | 2.39 | 3.42 | 0.95 | 2.31 | 45.9 | 1.59 |
| SP16_Mi | 5.02 | 60.50 | 0.11 | 1.0 | 7.20 | 1.12 | 0.8 | 2.47 | 5.54 | 0.63 |
| SP17_Mi | 5.03 | 60.50 | 0.24 | 0.75 | 5.00 | 1.77 | 0.8 | 6.50 | 1.40 | 0.65 |
| SP18_Mi | 5.01 | 60.50 | 0.21 | 0.5 | 7.49 | 0.37 | 0.89 | 3.96 | 8.00 | 0.59 |

The initial water saturation ($S_{wi}$) for the entire set of experiments is between 0.11 – 0.28 with a mean value of 0.23 while the intrinsic permeability and pore volume have a range of 4.86 – 7.12 D and 58.09 – 61.87 cc, respectively. This shows that the properties of the sandpacks for the entire sets of experiment are essentially very close.

### 6.1.1 **Comparison of different production pressure schemes and residual saturations**

The relative permeability was calculated by history matching the cumulative production data and pressure differential data using the Sendra simulator. Figure

6.1 shows the history matched and experimental results for differential pressure and corresponding cumulative oil production as a percentage of OOIP against the number of pore volume injected. As seen from the figures, a good match was achieved between the experimental and simulated data in all the tests conducted in this study.

In the history matching process, different relative permeability correlations were used allowing the optimisation parameters to be estimated by the software to get the best possible match. While it is possible to optimise all the operating parameters in the history matching process, it is sufficient to optimise only the uncertain variables. Thus, the irreducible water saturation ($S_{wi}$) and oil relative permeability ($K_{ro}$) at irreducible water saturation has not been optimised as it is assumed that the $K_{ro}$ is 1 at $S_{wi}$.

The results show that the production pressure depletion scheme for both the motor and mineral oil at different injection flowrates. For the test cases with motor oil at 1 mL/min and 0.5 mL/min, the highest pressure from the experiment is approximately 2 psi while the mineral oil reaches a high of about 1.4 psi. While the production pressure depleted uniformly from about 2 psi to 1 psi for the motor oil after flowing more than 5 PV through the media, the differential pressure of the core saturated with mineral oil reduces to approximately 0.6 psi after injecting the same pore volume of water. This can be attributed to the higher viscosity of the motor oil, which requires higher pressure to flow through the constricted pore throats of the media.

Several phenomena can be observed as the experimental floods progress. At the inception of the flood, the injection pressure increases slowly with time as the pressure is transmitted to the entire flow domain of the sandpack. During this period, a small volume of oil was produced with no water. As the pressure diffused through the entire flow domain, more fluid was produced. After several minutes of continuous oil production, the peak of the oil production was reached accompanied by water breakthrough. At the later stages of the tests, the cumulative total production remained stable and approximately same.

Mineral oil @ 0.5 cc/min

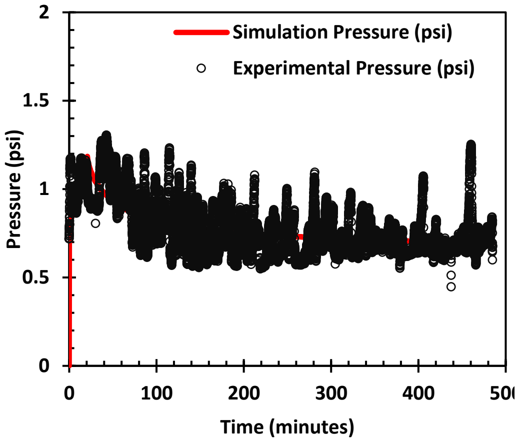

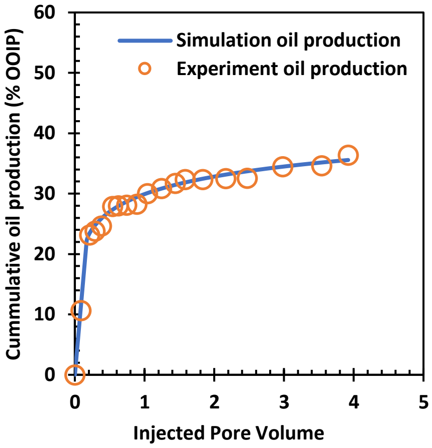

Mineral oil @ 0.75 cc/min

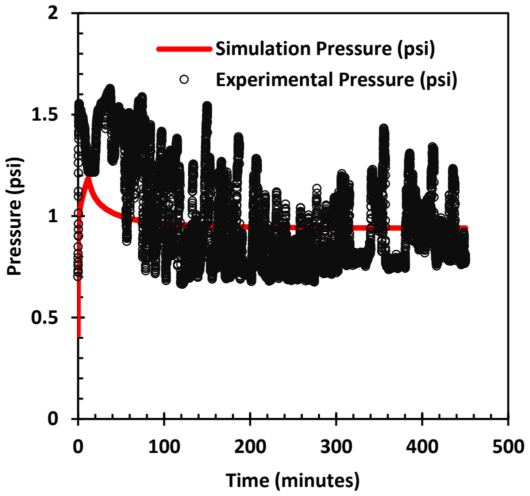

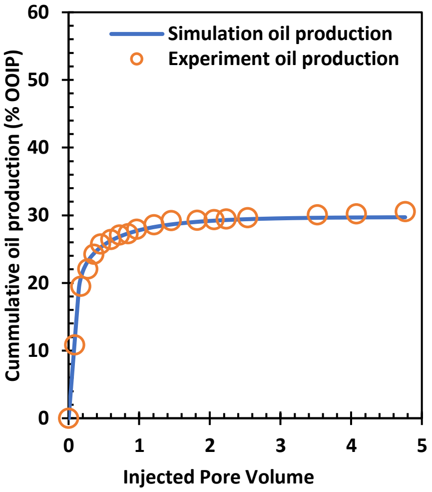

Mineral oil @ 1.0 cc/min

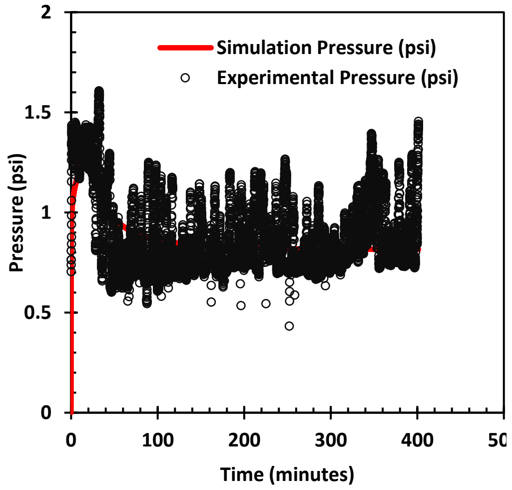

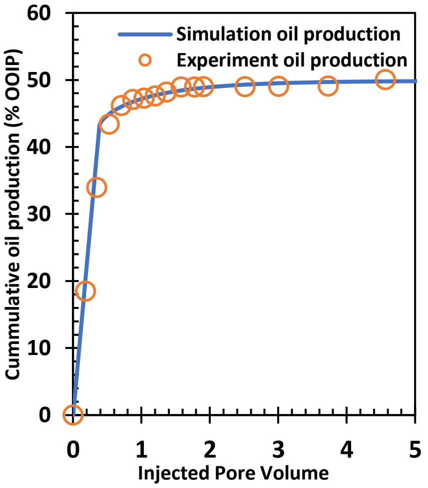

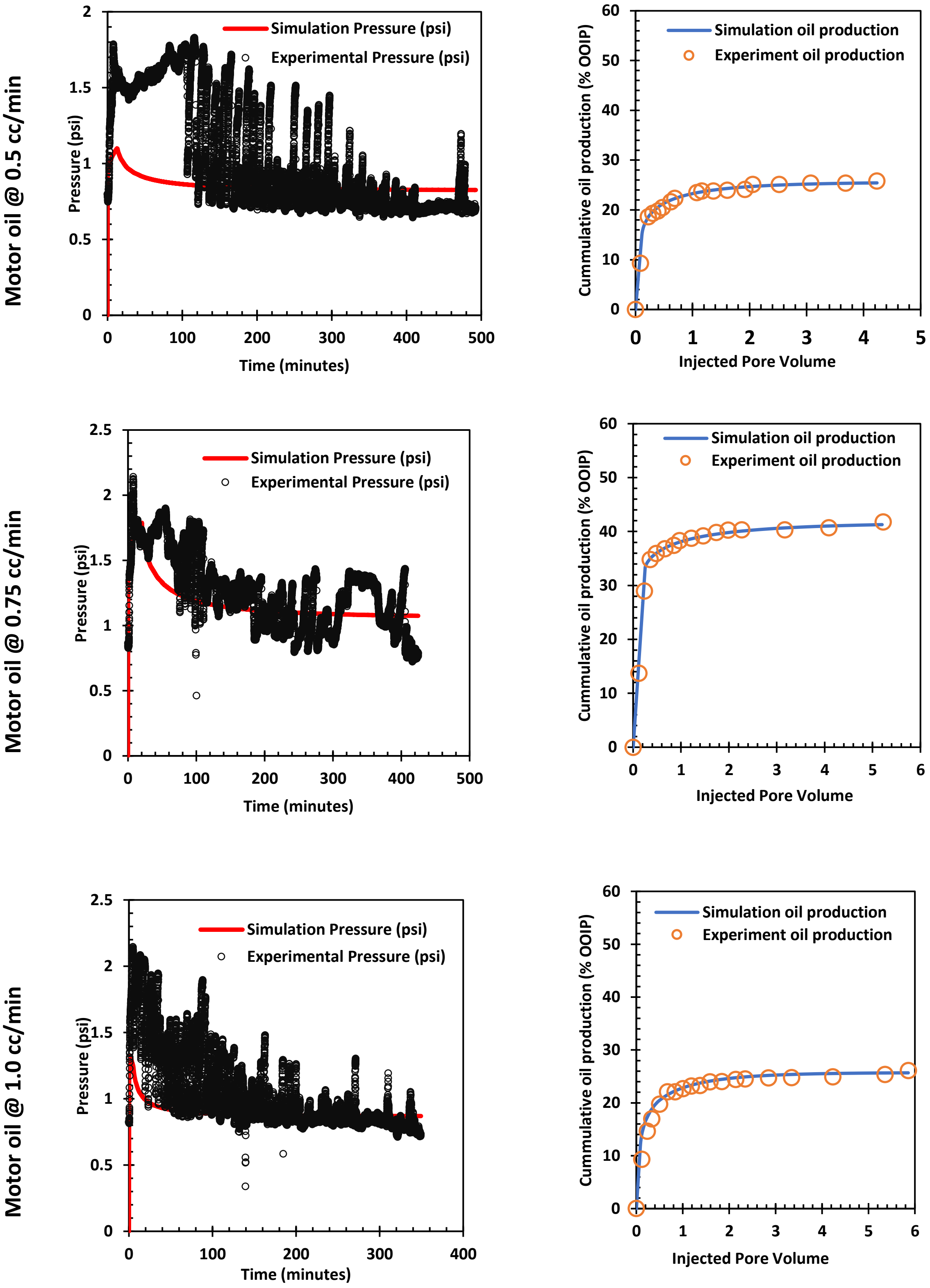

Figure 6.1: Imbibition experimental pressure data compared with history matched pressure from simulations for mineral and motor oil at 0.5, 0.75, and 1 mL/min at 60 °C (column 1). Experimental cumulative oil produced as a percentage of the OOIP against number of injected pore volume of water, compared with the production from history matched simulations corresponding to the pressure curve conditions under same condition as the pressure profiles (column 2).

## 6.2 EFFECT OF TEMPERATURE ON IRREDUCIBLE WATER SATURATION AND RESIDUAL OIL SATURATION

Initialisation of the sandpack is typically a favourable displacement process involving the displacement of a less viscous phase (brine) by a more viscous phase (oil). With a rise in temperature however, the oil viscosity reduces much more than that of water, decreasing the oil/water viscosity ratio (Figure 6.2) and correspondingly resulting in an expected rise in the irreducible water saturation with temperature. A similar scenario plays out for the residual oil saturation ($S_{or}$) during the waterflooding process in the oil-saturated system. With an increase in temperature, there is a corresponding increase in water/oil viscosity ratio, due to the decrease in oil viscosity relative to water. This occurrence results in a more favourable displacement process and thus a reduction in the residual oil saturation. While these behaviours were expected, some of the experimental results showed a different result and it is believed to be caused by some inherent viscous instabilities and possible occurrences of viscous fingering or experimental error in the coreflooding process.

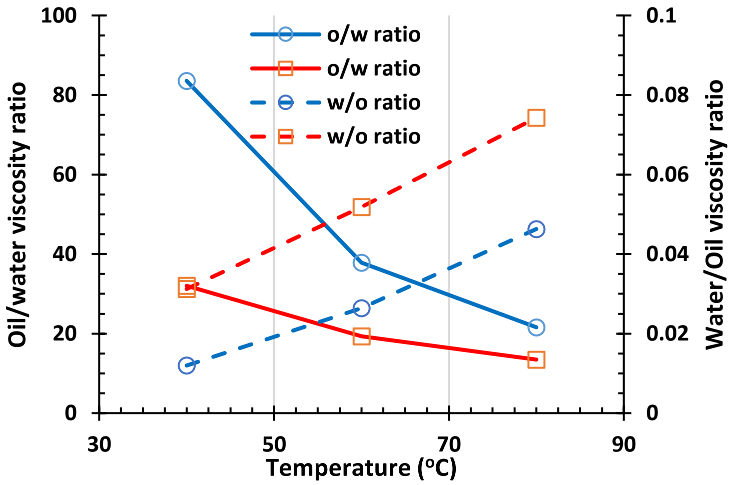

Figure 6.2: Plot of viscosity ratio and temperature (blue for motor oil and red for mineral oil)

Plots of irreducible water and residual oil saturation with temperature are presented in Figure 6.3 (a-b). In some experimental runs, a minor increase with temperature appears particularly from 40 to 60 °C. The low irreducible water saturation at low temperature is the result of the piston-like displacement scenario when a less viscous phase (water) is displaced by a more viscous phase (oil). With a rise in temperature, the viscosity of the oil reduces while the rock expands which reduces the micro-pores and blocks the pore throats making it difficult to displace the fluid filling the small pores. In addition, the reduction in viscosity at high temperature resulted in less efficient displacement at a given number of pore volumes injected. With a decrease in the oil viscosity, the viscosity ratio of oil to water decreases with an increase in the mobility ratio, leading to an increased flowability of the oil phase as a displacing phase thereby increasing the irreducible water saturation. A similar phenomenon is reported by Qin et at. (2018) who reported a linear increase in irreducible water saturation from 31.34 % at 45 °C to 39.31 % at 200 °C with an average increase of 2.66 % per 50 °C. However, the observations from the set of experiments conducted did not fully establish the trend of the irreducible water saturation increase with temperature as some fluctuations occurred when the temperature increases to 80 °C. The fluctuations in the results reflect the complex interplay of both the fluid viscosity ratio and the injection flowrate at varying temperature conditions.

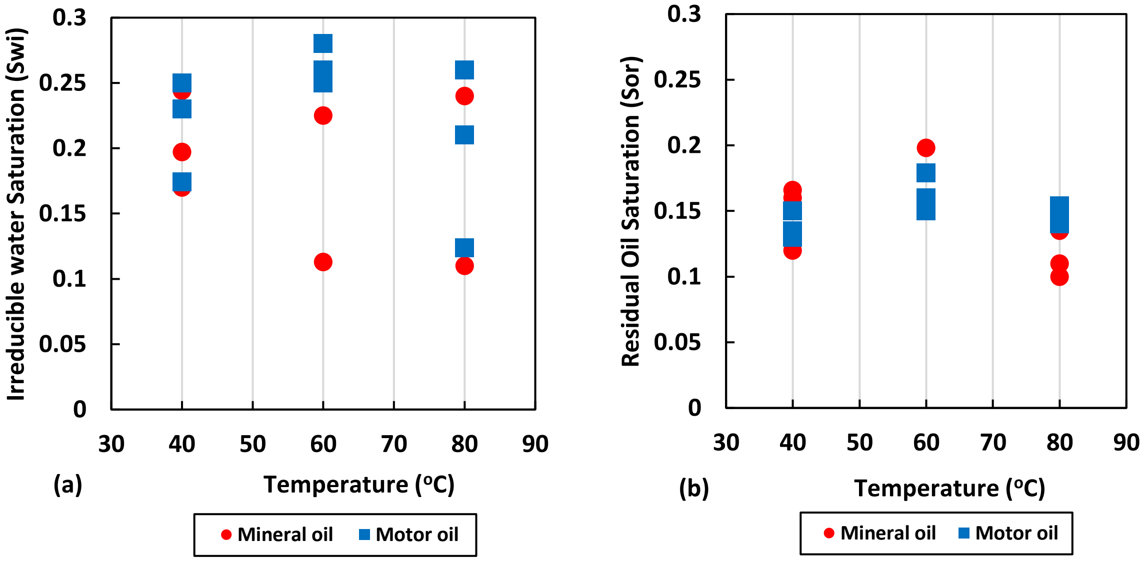

Figure 6.3: Plot of irreducible (a) water saturation and (b) residual oil saturation for all the experiments conducted.

As shown in Figure 6.3, there exists some changes in the residual oil saturation with no definite trend established. In most of the experimental runs, there is a reduction in the residual oil saturation as the operating temperature is increased. A major reason for the observation could be attributed to the occurrence of viscous fingering at low temperature as the water struggles to displace the more viscous oil phase. This phenomenon also accounts for the reason why the water cut increases rapidly after breakthrough. Under the present mobility ratio, it is apparent that viscous fingering seems to be inevitable. Droplets of oil occupying small pores within the porous matrix cannot be displaced, resulting in higher residual oil saturation. With a rise in temperature, the viscosity of the oil phase decreases, thereby decreasing the mobility ratio of water to oil. This occurrence reduces the effect of viscous fingering and results in a corresponding increase in the sweep area of water, thereby producing more oil at the outlets. The saturation profiles along the core length at varying time-steps are presented in Appendix VI.

In order to establish a relationship between the injection flowrate and residual oil saturation, the set of experiments at 60 °C shown in Figure 6.4 are used. The experimental result suggests that the residual oil saturation is affected by the injection flowrate for both oil samples tested. While the motor oil with a higher viscosity shows a reducing residual oil saturation with flowrate, the reverse was observed with the mineral oil of a lower viscosity. At an injection rate of 0.5 mL/min, the residual oil saturation of the mineral oil is lower than that of the motor oil, which indicates that a higher recovery was obtained under the same flowrate for the lighter oil. At 0.75 mL/min, the residual oil saturation is about the same while at 1 mL/min the motor oil has a lower residual oil saturation. This result at 0.5 mL/min agrees with that presented by Wang et al. (2006) that residual oil saturation decreases with increasing oil viscosity. A possible explanation for this phenomenon could be the effect of viscosity ratio resulting in the invading water bypassing the oil in the smaller pore spaces. It is noteworthy however that the variation of residual oil saturation for all the tests is very negligible, between 0.15 – 0.18.

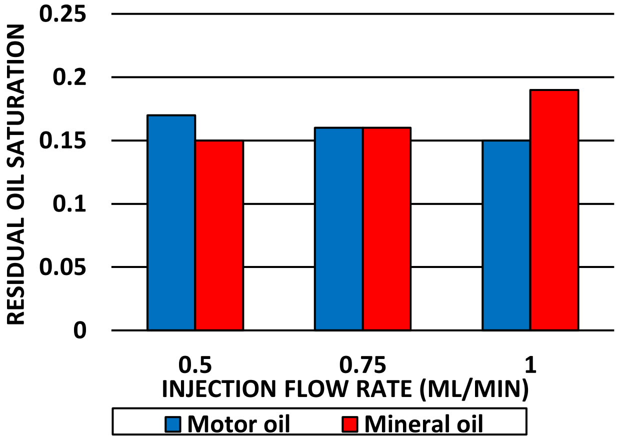

Figure 6.4: Residual oil saturation plotted against water injection flowrate for the two oil samples tested at a temperature of 60 °C.

## 6.3 EFFECT OF TEMPERATURE AND FLOWRATE ON PRODUCTION PROFILE

Experimental data plots of cumulative oil production against number of injected pore volumes of water are shown in Figure 6.5. The data represents 6 separate experiments with the motor oil under injection flowrates of 0.5 and 0.75 cc/min and temperatures of 40, 60 and 80 °C while plots for the full range of experiments are presented in Appendix V. In general, the curve begins to plateau after about one pore volume injected indicating the time of water breakthrough is approximately 1 hour. As shown in the figures, some disparity in the total production curves exist because the volume of injected water tends to vary with time along with small variations in the permeability of the sandpack. Due to the time constraint for each experimental flood, the residual oil saturation ($S_{or}$) was not attained. Therefore, $S_{or}$ was included as one of the matching parameters in the Sendra software. The simulator in the history matching process could adjust the parameter freely. From the values obtained from the simulator, it is obvious that further water injection will not increase the ultimate recoveries significantly.

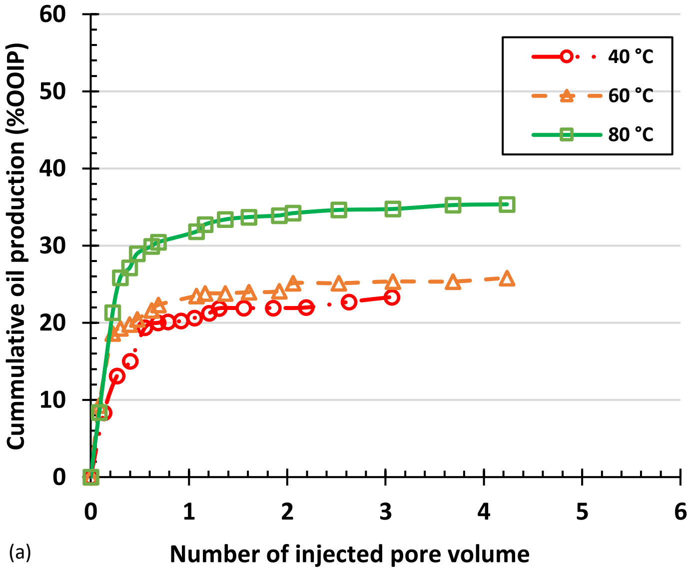

(a)

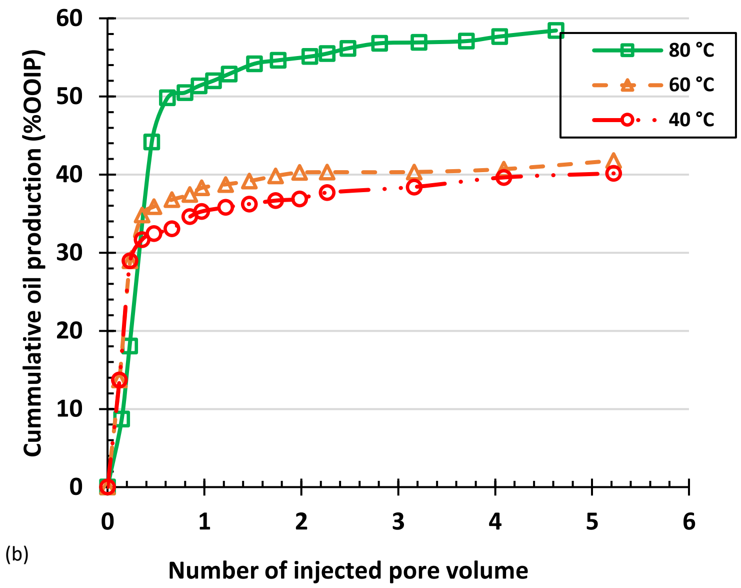

Figure 6.5: Cumulative oil production vs pore volumes injection for experimental runs on Motor oil at (a) 0.5, and (b) 0.75 under varying temperatures

The initial water saturation ($S_{wi}$) for the range of experiments has an average of 0.21 with an average permeability of 5.55 mD. The flooding of the motor oil saturated sandpacks at 0.5 cc/min recovered approximately 20 – 35 % of OOIP for the different temperatures considered. As expected, the highest waterflood recovery was attained at the highest temperature of 80 °C with a higher water/oil viscosity ratio. Observations show that a change in the operating temperature has a significant difference in the recovery profile at 80 °C. This is apparently due to the favourable displacement owing to the fact that the oil viscosity reduces with temperature, water/oil viscosity ratio increases and thereby favours the displacement of the oil by injected water. Although the temperature varies by 20 °C, the recovery profile between 40 to 60 °C shows an increase of about 14 % compared to the 40 % increase from 60 to 80 °C. This is indicative of the fact that at 60 °C, an optimum flow condition has not been reached making it necessary to increase the temperature for increased recovery.

In the experiment at 0.75 cc/min, a similar trend was observed with respect to the increase in recovery factor as temperature increases. As shown in Figure 6.5b, with an increase in the operating temperature, the recovery increases by a factor of 58, 42 and 38 % at temperatures of 80, 60 and 40 °C respectively after 5 pore volumes were injected.

# 6.4 EXPERIMENTS AT CONSTANT TEMPERATURE OF 60 $^{o}$C

## 6.4.1 Effect of water injection flowrate on oil-water relative permeability

Relative permeability curves showing the effect of injection flowrate are presented in Figure 6.6. In the figures presented, it is seen that for the motor oil with relatively higher viscosity, the oil relative permeability curve increases (shifts to the right) with an increase in the injection flowrate from 0.5 mL/min to 1 mL/min. On the other hand, Figure 6.6b shows the curves for the mineral oil where the effect of injection flowrate on oil relative permeability shows an opposite trend. For the water phase, it is seen from the two figures that the same trend was observed with the highest flowrate having the highest relative permeability. These sets of results show that there exists a relationship between relative permeability and injection flowrate for both oil samples tested.

The observed phenomena could be explained in terms of fundamental multiphase flow concepts involving wettability and contact angles. According to Tarek (2019) there exists 2 main distinguishing features between oil-wet and water-wet relative permeability curves. Firstly, if the cross-over saturation, that is the water saturation at which oil and water relative permeability curves are equal or intersects is greater than 50 %, the media is a water-wet system. On the other hand, if it is less than 50 % it is an oil-wet system. Secondly, the water relative permeability at maximum water saturation is lower than 0.3 for water-wet and higher than 0.5 for oil-wet media. As shown in the results presented, saturation at which oil and water relative permeability intersects is always lesser than 50 %, showing an oil-wet condition for the entire set of experiments. The oil-wetness could be explained from the findings of Wang and Gupta (1995) and Rao (1996) stating that sandstones generally become more oil-wet with temperature increase, while most carbonates show water-wet behaviour under similar scenario. While the temperature of 60 $^{o}$C could have influenced the wettability, other factors such as the brine and mineral composition of the system have an equally important contribution to the oil-wetness of the media (Alotaibi, et al., 2011; Lu, et al., 2017).

Furthermore, the relative permeability sensitivity to oil viscosity can be elucidated according to Keller et al. (2007) that with highly viscous oils, contact angle increases with flowrate. Similarly, Nguyen et al. (2005) reported a comparable conclusion that an increment in contact angle and/or in flowrate signifies a higher imbibition relative permeability. As expected, higher oil relative permeability is desirable because it guarantees an easier displacement of the oil over the water. From the set of experiments conducted, higher flowrates are desirable for motor oil which has a higher viscosity, while for the less-viscous mineral oil, low flowrates are better as it gives extra time for the injected fluid to imbibe inside the smaller pores and displace the oil phase. Flooding at high flowrates tend to result in the bypassing of smaller pores containing oil as the injected water flows at a relatively higher velocity through the larger pores instead of entering small pores preferentially by capillary forces.

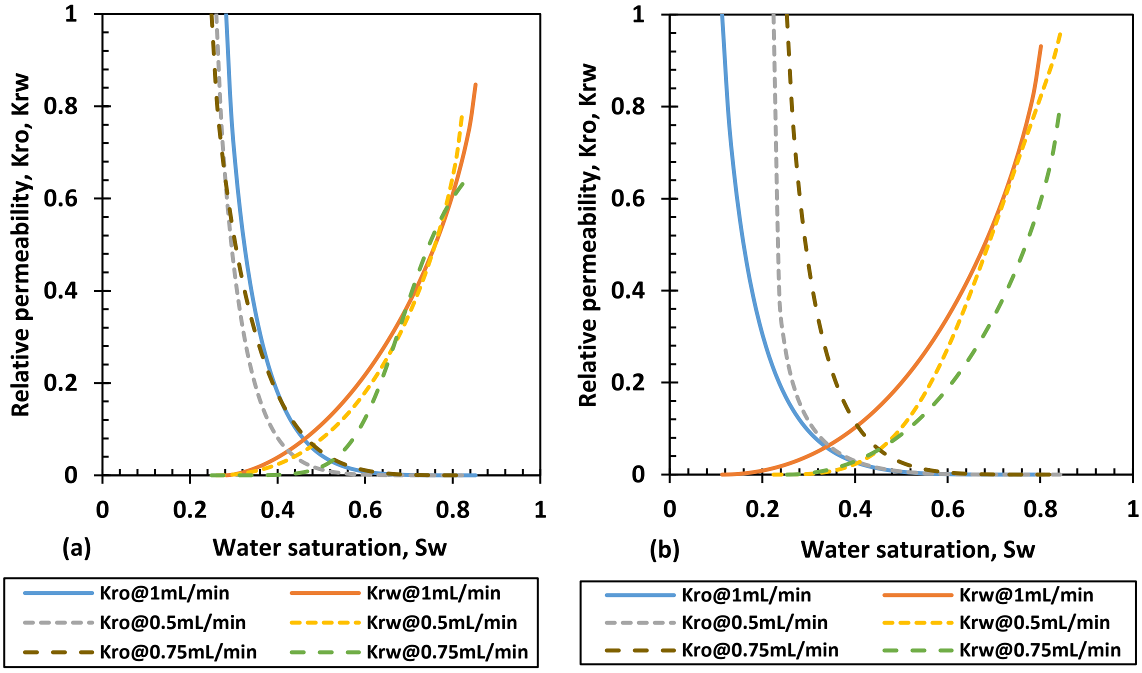

Figure 6.6: The oil–water relative permeability curves at varying water injection flowrate for (a) motor oil and (b) mineral oil

### 6.4.2 **Effect of oil viscosity on oil-water relative permeability**

Figure 6.7 shows the relationship between oil and water relative permeability and the water saturation of both the motor oil and mineral oil under varying injection flowrates. The results show that under the same injection flowrate, the relative permeability to oil is far lower for the more viscous oil while the water relative permeability is higher for the same oil. In other words, the higher the oil viscosity, the lower the oil relative permeability under the same injection flowrate. The general trend of the results presented in the Figure 6.7 (a-c) is similar to other published results in literature, which showed that the relative permeability curves for oil shifts rightwards with a decrease of oil viscosity under a similar wetting condition.

Another notable observation from the results is that with an increase in the oil viscosity, there exists a corresponding increase in the residual oil saturations signalling the relative difficulty in displacing all the oil phase in the porous media under that same injection flowrate. For the 3 flowrates considered 0.5, 0.75 and 1.0 mL/min, the same trend is seen though with varying magnitude. The viscosity of the motor oil is more than that of the mineral oil resulting in a higher resistance to flow within the porous media. Consequently, the oil relative permeability decreases with an increase in viscosity.

Furthermore, as the oil viscosity increases, the oil-water viscosity ratio ($\mu_o/\mu_w$) correspondingly increases while the oil-water relative permeability ratio ($K_{ro}/K_{rw}$) decreases. Since the water cut is strongly affected by the viscosity under the same water saturation, the water cut of the motor oil is greater than that of the mineral oil under the same water saturation. Consequently, the water breakthrough time for the motor oil of relatively higher viscosity is comparatively short, resulting in a low sweep efficiency and a brief oil production without water. This phenomenon explains the relatively higher residual oil saturation for the motor oil compared to the mineral oil as some volume of residual oil is trapped within the pore spaces.

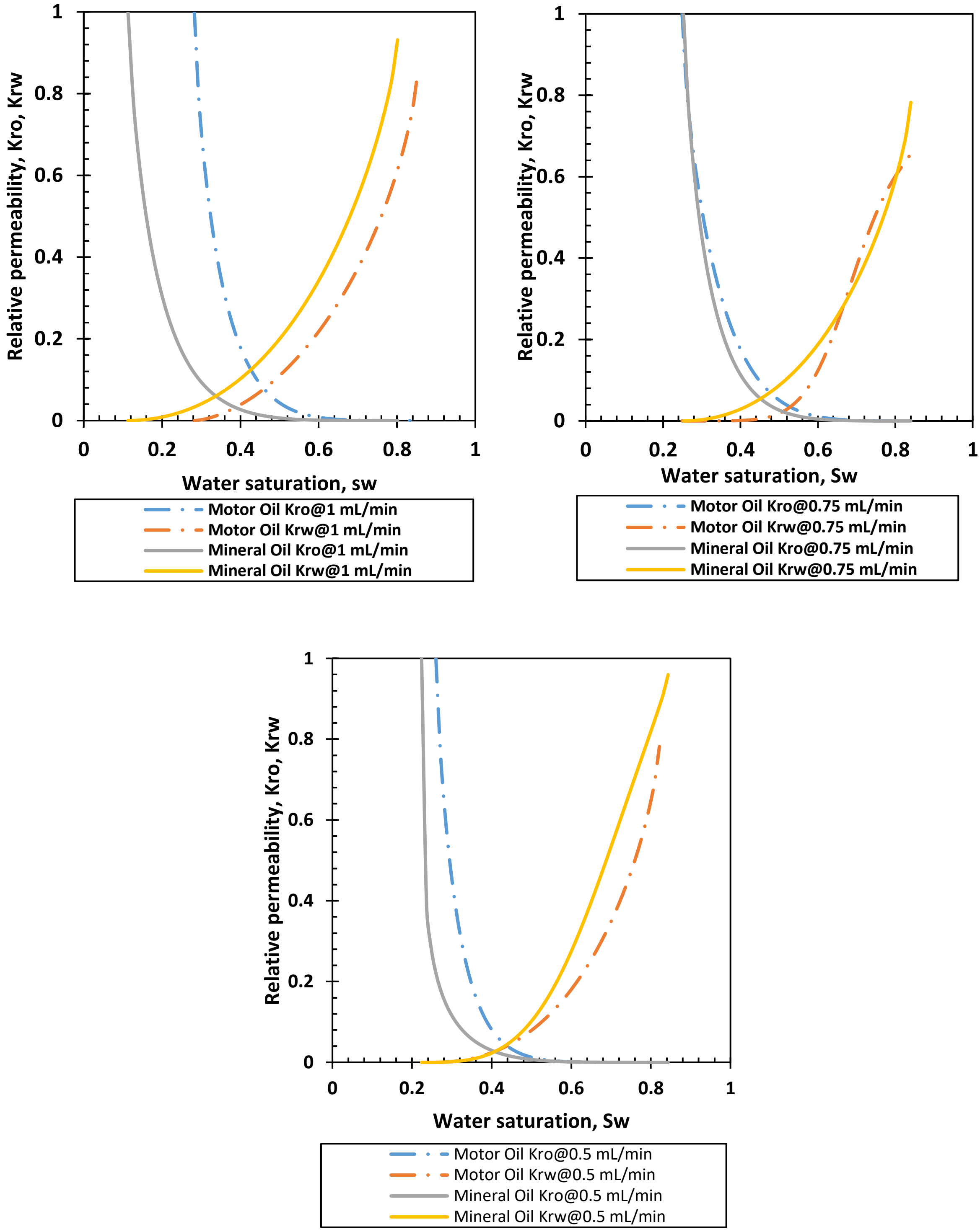

Figure 6.7: Comparison of the oil–water relative permeability of motor oil and mineral oil at different water injection flowrates, (a) 1 mL/min, (b) 0.75 mL/min, and (c) 0.5 mL/min

To explain the viscosity effect with the governing mechanism of the flow system, fractional flow curves plotted against the water saturation are presented in Figure 6.8. In the result shown, the fractional flow of the motor and mineral oil at a flowrate of 1 mL/min shows that a higher fractional flow is as a consequent of a less viscous oil. It is understood that the efficiency of a waterflood is dependent greatly on the mobility ratio of the displacing fluid (water) to the displaced fluid (motor or mineral oil). A lower mobility ratio gives a more efficient displacement with the curve shifted to the right. The effect of oil viscosity on the fractional flow curves and corresponding influence on the drive mechanism is more pronounced under the highest flowrate considered in this study.

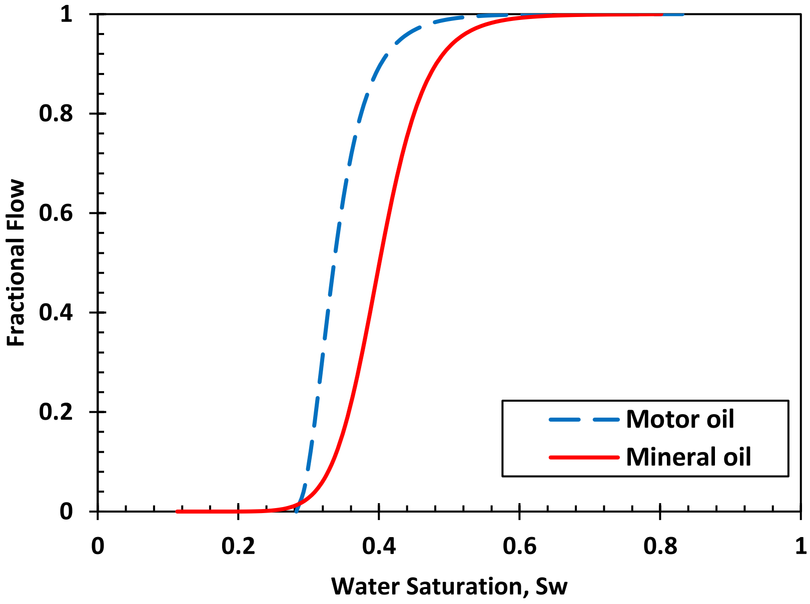

Figure 6.8: Effect of oil viscosity on fractional flow curve under the same injection flowrate

## 6.5 EFFECT OF VARYING TEMPERATURE ON OIL-WATER RELATIVE PERMEABILITY CURVES

This set of experiments have been conducted to investigate the sensitivity of oil and water relative permeability curves to temperature. Temperatures of 40, 60, and 80 °C have been investigated by varying water injection flowrates of 0.5, 0.75, and 1.0 cc/min. The relative permeability curves for the experiments performed on the unconsolidated sandpacks using mineral oil are shown in

Figure *6.9*. The correlation that gives the best matching of the data is the LET for 60- and 80 °C while the Corey model was used for the 40 °C set of experiments. Table 3.3 presents the model parameters taken for the relative permeability history matching process in the Sendra software.

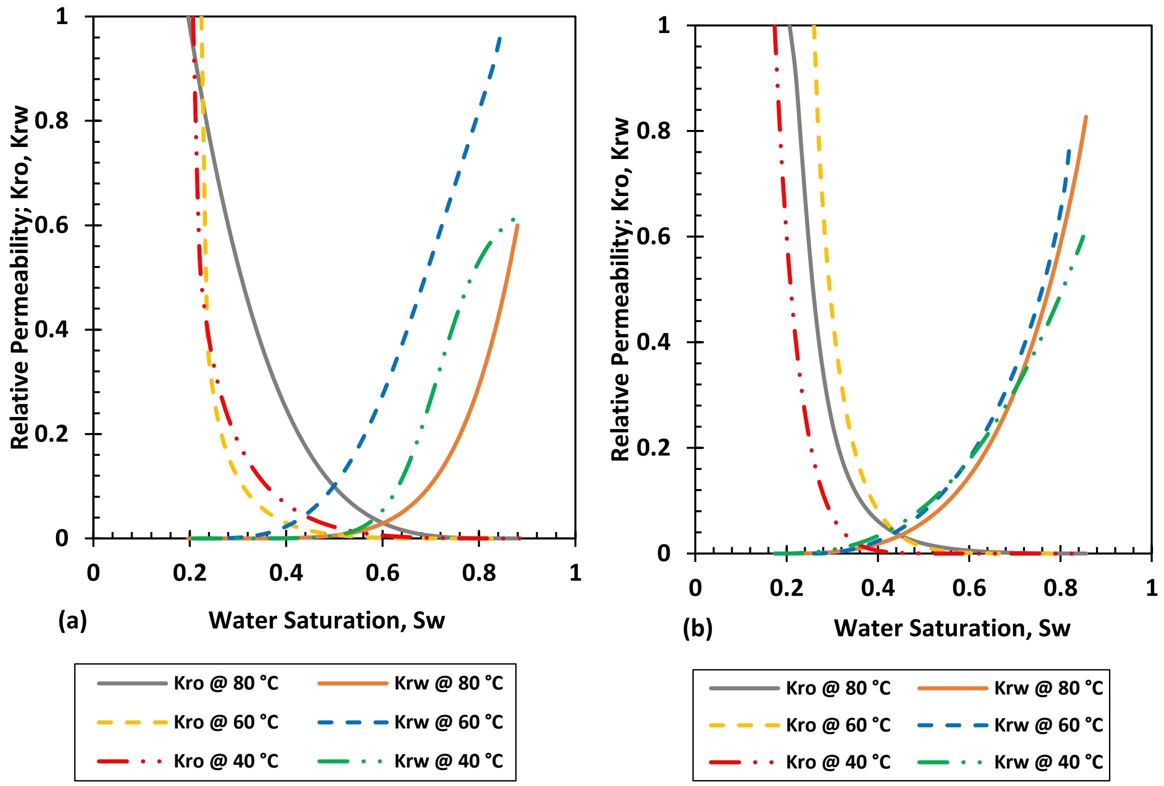

Figure 6.9: Relative permeability curves for the experiments done on sandpacks at 0.5 cc/min for (a) mineral oil, and (b) motor oil

The figures show that there is a definite temperature dependency of both the oil and water relative permeability curves, though with varying magnitude. The difference in the oil-water relative permeability curves is noticeably larger for the mineral oil when compared to the motor oil under the same flowrate and operating temperature. This suggests that relative permeability sensitivity is significant to the mineral oil but very small for the water phase when the invading fluid phase was injected at 0.5 cc/min. As seen for the mineral oil results, the effect of temperature on both the oil and water phase is very noticeable with a shift to right as temperature increases. However, with an increase of the oil phase viscosity to a more viscous oil, a similar result of temperature sensitivity is observed for the oil phase, the water shows insignificant variation making it apparent that the viscosity of the displaced fluid equally affects the curve.

Generally, oil and water relative permeability sensitivity to temperature is governed by 3 mechanisms, which are change in fluid viscosity, thermal expansion of porous matrix and fluid, coupled with the possible adsorption and desorption of fluid molecules. As the operating temperature increases, the oil viscosity decreases thereby enhancing the flow capability of oil. Furthermore, as the temperature increases, the adsorption of water molecules becomes stronger resulting in a decline of the mobility of water. Consequently, the oil phase has a higher relative increase in relative permeability when compared to the water phase. In addition, the thermal expansion of the rock matrix and fluid triggered by the increase in temperature creates an expansion pressure that acts as a drive mechanism and supports the production of fluid. This pressure results in a corresponding increase in the oil-water relative permeability.

As mentioned earlier, an increase in temperature reduces oil viscosity which in-turn aids the mobility of the oil, consequently increasing the oil relative permeability due to an increase in oil velocity. As shown in the Figure 6.10 for both mineral and motor oil, the oil relative permeability is higher in water-wet media compared to the oil-wet systems under the same injection flowrate. In a typical oil-wet porous system, small pore spaces are filled with oil with correspondingly high capillary pressure retaining the oil phase and causing a reduced oil relative permeability. An increase in the temperature for a oil-wet system tends to aid the oil relative permeability by reducing the oil viscosity and shifting the media wettability to water-wetness. For the different sand grains considered in this study, the media permeability ranges between 4.8 – 7.3 mD with relatively large pore throats making the effect of capillary pressure less significant.

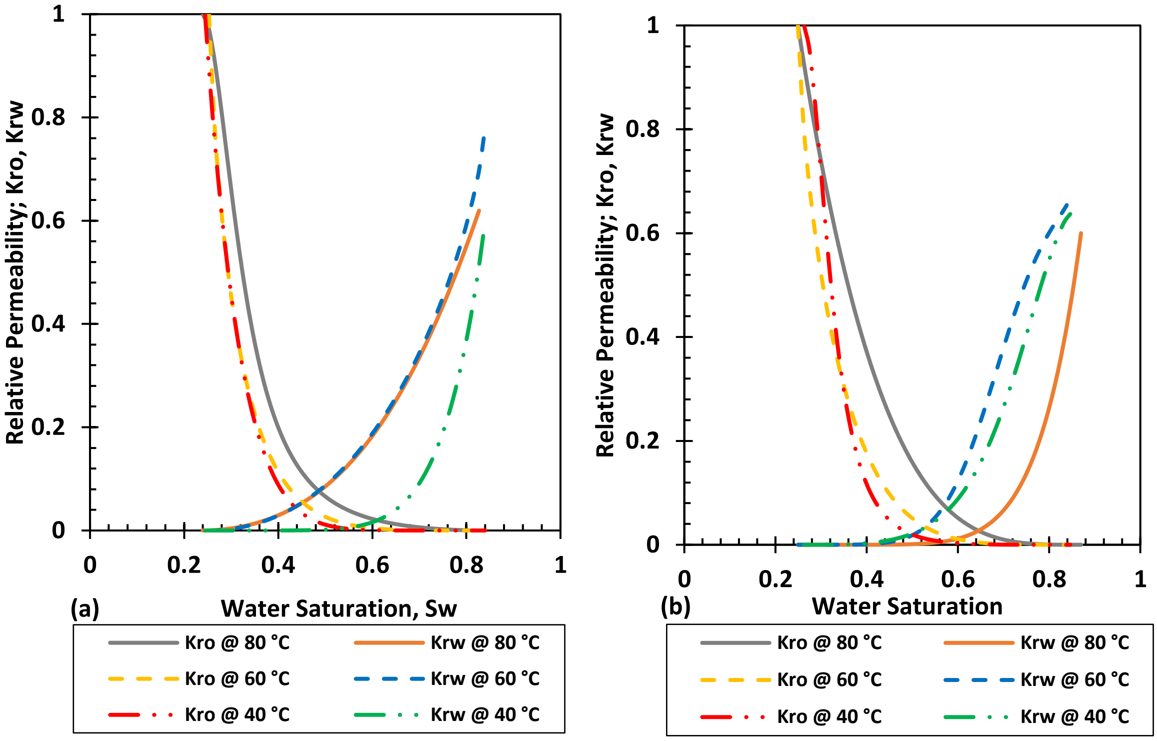

Figure 6.10: Relative permeability curves for the experiments done on sandpacks at 0.75 cc/min for mineral oil and motor oil

The relative permeability curves shown in Figure 6.11 shows the relationship between water saturation and relative permeability for both mineral and motor oil under varying temperatures. The presented relative permeability curves show that with an increase in temperature, the water saturation at the crossover points increase nonlinearly, particularly at the temperature of 80 °C. At 40 °C, with an injection flowrate of 0.75 cc/min, the water saturation at the crossover point is about 44.45%, and it reaches 65.20 % at 80 °C (Figure 6.10b). A similar trend is observed at a flowrate of 1.0 cc/min at 80 °C with the crossover saturation being 58.5 % and 53.55 % for mineral and motor oil, respectively (Figure 6.11). It is apparent that the water-wetness of the media is supported at high temperature for some of the systems. The change of wettability shows that elevated temperature results in the adsorption of fluid molecules which alters the rock properties. The water saturation at crossover or equal-permeability points shows a gradual increase as the temperature increases. This is reflected in the variations in residual oil saturations and endpoint permeability as discussed earlier in the thesis. The experimental results presented has been able to demonstrate the effect of temperature on relative permeability curves. The relative permeability curves sometimes show a rise with operating temperature and a reversal with continuous temperature increase while also showing no effect in some cases. This suggests that experimental artefacts in the flooding process can cause the observed differences in some of the cases.

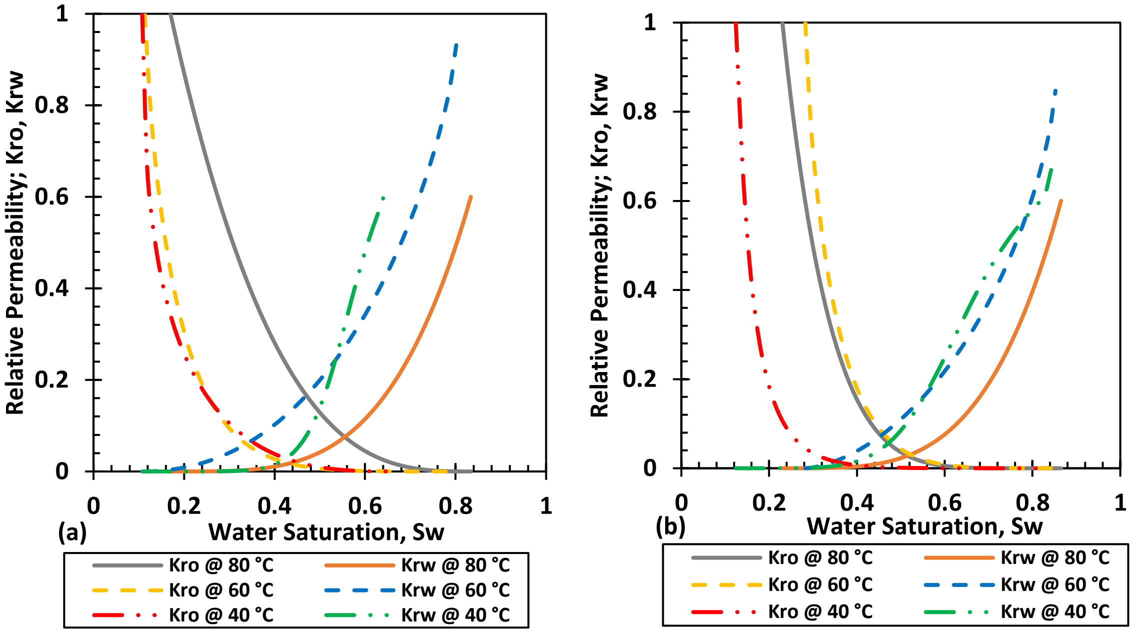

Figure 6.11: Relative permeability curves for the experiments done on sandpacks at 1 cc/min for (a) mineral oil, and (b) motor oil

## 6.6 COMPARATIVE ANALYSIS OF RELATIVE PERMEABILITY BY EXPERIMENTAL AND COMPUTATIONAL FLUID DYNAMICS (CFD) APPROACH

In this section, results from the experimentally derived relative permeability for both oil and water are compared with results from using the commercial CFD software. Out of the eighteen cases reported in the physical experimental section, only two scenarios have been replicated using the CFD approach for comparison. The numerical model for simulation of water injection into an oil saturated core sample was designed in the ANSYS Fluent® software. The modelling approach is based on the Eulerian-Mixture model, with a 3D cylindrical core sample of same dimensions used in the experiment while the absolute permeability and porosity is taken for the specific cases for the motor oil. As typical for a macroscopic representation of fluid flow in the subsurface, the flow is described as a continuum process using averaged or "continuous" parameters for the bulk system rather than describing the shape and orientation of each solid matrix within the porous body. Inputting the bulk properties into the classic Darcy's equation (Eq. 6.2) gives an average flow rate for the total volume.

$$\begin{cases} v_w = -\dfrac{Kk_{rw}}{\mu_w}(\nabla P_w - \rho_w g) \\ v_o = -\dfrac{Kk_{ro}}{\mu_o}(\nabla P_o - \rho_o g) \end{cases} \tag{6.2}$$

where v is the velocity in m/s, K is the media permeability in mD, Kr is the dimensionless relative permeability, ρ density in kg/m$^3$ and g is gravity in m/s$^2$.

Considering the fact that both phases are incompressible, the fluid densities $\rho_w$ and $\rho_o$ are constant in the flow domain and the porosity and permeability are independent of the pressure and temperature. The fluid saturations must fulfil the following relation that $S_w + S_o = 1$ where $S_{wi} \leq S_w \leq 1 - S_{or}$ and $S_{or} \leq S_o \leq 1 - S_{wi}$.

The sampled average saturation for each fluid phase, pressure drop, and flow rates are continuously recorded at stimulated time steps during the transient flow simulation. The quantitative values were gotten after each simulation from the surface integral reports for the different parameters of interest and put into the equations in excel for calculations. The Eq. 6.2 have been used to estimate the relative permeability in the two-phase porous flow under study. In these simulations, a strong of dependency of the oil viscosity on the temperature was considered and this was achieved by writing a user defined function (UDF) for the oil viscosity using values from the experimental data for viscosity. The UDF has be presented in the Appendix VII.

### 6.6.1 **Operating/Boundary conditions and key assumptions**

The simulated flow involved the injection of water at a flow rate of 0.5 cc/min (imposed as a velocity inlet where Q=VA) and temperature of 20 °C into a porous media of temperature 60 and 80 °C as carried out in the physical experiments. The outlet boundary was set as pressure outlet and the local thermal equilibrium (LTE) assumption is considered to be valid between the fluids and the porous body.

In addition, the following assumptions have been made in the setting up of the model:

- The porous media is assumed to be both homogenous and isotropic with the flow same in all three directions.
- The flow is laminar and no turbulence model has been solved.
- The viscosity of water is constant while that of oil varies with temperature with the input done through the UDF.
- The fluids are incompressible with density remaining constant at different pressure and temperature value.
- The porosity and permeability are assumed to be constant and do not vary with pressure and temperature.

To simulate a porous media in Fluent, the major parameters are the porosity, inertial resistance, and viscous resistance. Since a laminar flow has been assumed, the inertial resistance formulation is not used in the Fluent model while the viscous resistance is taken as the inverse of the absolute permeability.

### 6.6.2 **Oil-water saturation profiles**

The oil volume fraction contour along the length of the core sample for the 60 $^{o}$C case at varying time intervals have been shown in the Figure 6.12. At the injection point from the left, the oil volume fraction is zero, and the water has a volume fraction of 1. This frontal advance profile is in line with the expected trend as the blue colour for the water from the left stretches to the right in all the cases. This is representative of the initial water saturation fixed in the model signifying a core sample containing both oil and water before the commencement of the injection process. Since oil and water are two immiscible fluids owing to the difference in physical properties, the frontal profile at 5 minutes appears to be very dispersed which is typical of the inception of the flow process. As the flow proceeds and gets steady with time, a more stable frontal advance is observed in the contours and the water continuously displaced the oil from the porous domain.

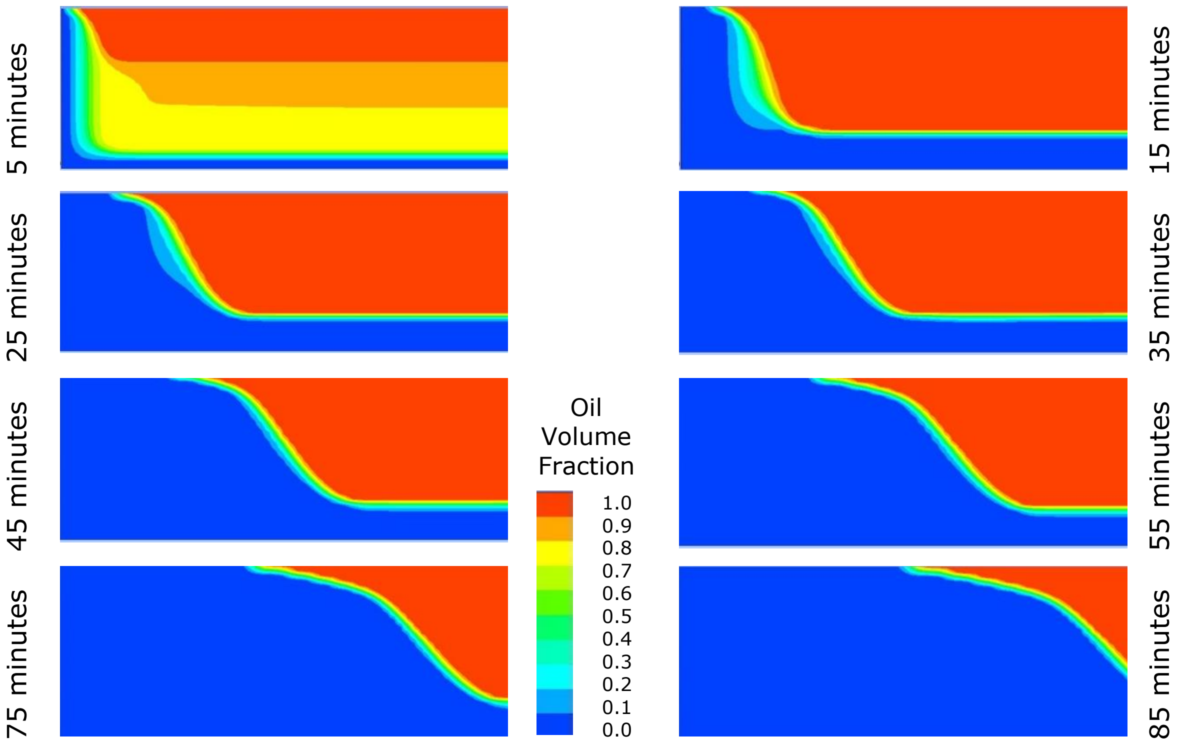

Figure 6.12: Oil volume fraction contour at varying time steps

### 6.6.3 **Comparison of relative permeability results**

As the base case for validation, plot for oil and water relative permeability against the water saturation at injection temperature of 60 and 80 °C and inlet rate of 0.5 cc/min is presented in Figure 6.13. The aim is to evaluate the applicability of the CFD approach for relative permeability calculations. The final results of matching measured data from the core flooding experiments with those obtained from the numerical simulator as presented in Figure 6.13. The results show a relatively good match for the water relative permeabilities for both temperature conditions compared to the oil phase. The variation of the simulation results from the experiment shows that while the simulation results for water are within 10% error margin, the oil phase has a variation of over 20%. Additional numerical error data is presented in *Table 6.3* showing lowest values of the mean square error for the water phase indicating lesser error margin.

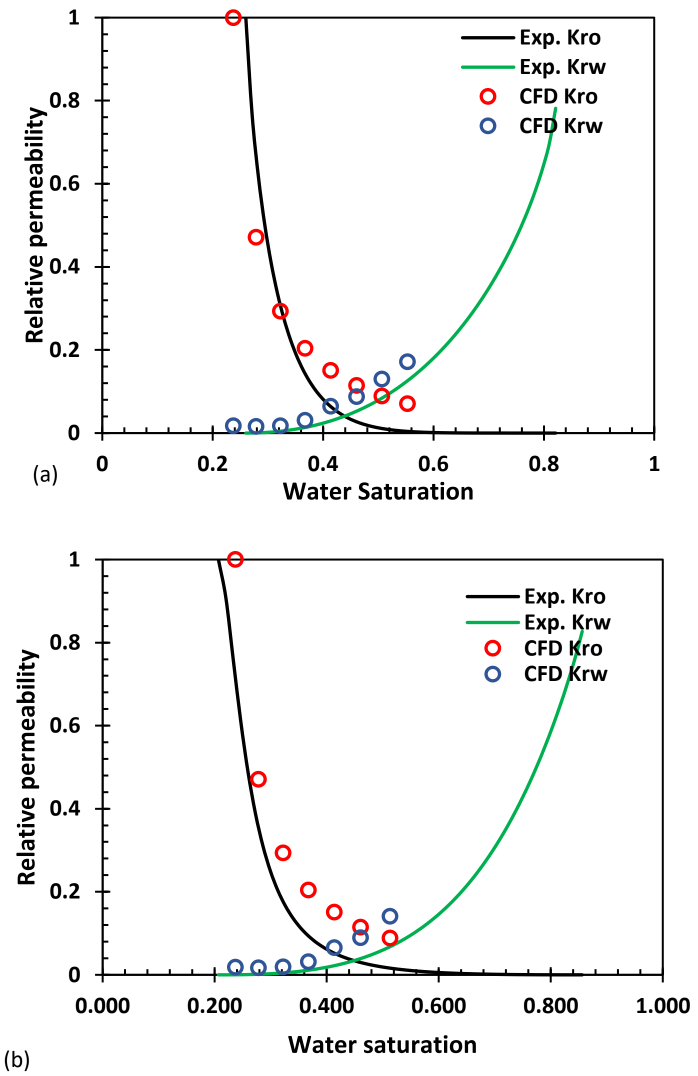

Figure 6.13:Relative permeability curves for the experimental and CFD calculations at water injection rate of 0.5 cc/min (a) temperature of 60 °C and (b) temperature of 80 °C

Table 6.3: Quantitative error metrics for comparison of the experimental derived relative permeability and CFD

| | Error metrics | 60 °C | 80 °C |
|---|---|---|---|
| Relative permeability for oil | MSE | 0.0062 | 0.0172 |
| | RMSE | 0.0790 | 0.1310 |
| Relative permeability for water | MSE | 0.0011 | 0.0110 |
| | RMSE | 0.0327 | 0.1049 |

The CFD approach has been used with considerable success to simulate a displacement of oil by water under varying temperatures to mimic a laboratory core flood experiment. In view of the results found in the present study, it has been shown that CFD approach can be used to derive macroscopic properties of porous media such as relative permeability. A limitation of this approach however is the time taken to run transient computations with high accuracy. As observed in the Figure 6.12, the total flow time for the CFD simulations is less than that of the physical experiments and this also contributes to the wide disparity in the presented result. The disparity in the two approaches is in consonance with the conclusion of Maini et al. (1990) after a comparative study of different methods for relative permeability. The study reported that results gotten from different methods have showed inconsistencies and it has been suggested that the primary fundamentals of each method are valid under different flow conditions.

## 6.7 EMPIRICAL MODEL DEVELOPMENT

Relative permeability values evaluated under typical reservoir temperature and pressure is deemed reliable and representative of the real-world situation. However, this approach is fundamentally time expending, complex and expensive. Consequently, empirical correlations and mathematical models have been formulated from the abundance of experimental data to compute oil-water relative permeability. Relative permeability values generated from empirical models have been found to have agreeable comparison with experimental data, however, these mathematical models do not consider the effect of temperature (Xiao, et al., 2012; Xu, et al., 2013). In recent years, several empirical models have been developed with the temperature effect included but among the several models, that of Zhang (2017) is the most reliable (Esmaeili, et al., 2019; Nait, et al., 2019). The Zhang model has therefore been adopted and appropriately adapted for this study.

The authors formulated the model from experimental data gathered from temperature dependent oil-water relative permeability. The USS experimental technique was carried out using tight sandstone with light oil of viscosity range of $4 \leq \mu_o \leq 48\, cP$ and a temperature range of $25 \leq T \leq 100\, ^oC$. In developing the model, the authors used a combination of JBN and Corey correlation with a set of empirical constants that can be adopted to fit experimental data generated under real reservoir conditions.

While empirical models are simple and easy to use, they are not capable of making accurate predictions under conditions different from those under which they have been formulated (Fan, et al., 2019). Since the operating conditions under which the model was formulated falls outside the range of parameters for this study, modifications have to be made to adopt the model. For this purpose, a nonlinear least squares regression has been implemented to fit the Zhang model to our experimental dataset. This approach was chosen as it can be used with a large and more general class of functions. The basic form of a nonlinear model is written in Eq. 6.3 as:

$$y = f(\vec{x};\vec{\beta}) + \varepsilon, \tag{6.3}$$

where the functional part of the model is not linear with respect to the unknown parameters, $\beta_0$, $\beta_1$,…, and the unknown parameters are estimated by the method of least squares.

While a nonlinear least square regression has the advantage of producing reliable results with limited datasets, a major challenge is the need to supply an initial guess value for the unknown parameters prior to the optimisation process. It is expected that the initial values be moderately close to that of the unknown parameter for the optimisation procedure to converge (NIST, 2013).

The Zhang model has been presented in its original form as Eq. 6.4 and 6.5 shows while the empirical constants have been optimised using the nonlinear least square method for application with unconsolidated porous media; sandpacks or glass beads, similar temperature range and oil viscosity.

$$k_{rw} = k_{rw}^{0-50C}(e_1 + e_2 T + \frac{e_3}{T} + \frac{e_4}{T^2})\left(\frac{S_w - S_{wi}}{1 - S_{wi} - S_{or}}\right)^{a_3 T + a_4} \tag{6.4}$$

and

$$k_{ro} = \left(\frac{1 - S_w - c_1 \ln(T) - c_2}{1 - b_1 T - b_2 - c_1 \ln(T) - c_2}\right)^{a_1 T + a_2} \tag{6.5}$$

Specifically, for the unconsolidated sandpacks used in our experiments and porous media of similar nature, the optimised values of the empirical parameters in the Eq. 6.4 and 6.5 above are as follows: $a_1$=-0.00295, $a_2$=3.976, $a_3$=-9.9991E-06, $a_4$=4.176, $b_1$=0.0025, $b_2$=0.001, $c_1$=-0.1121, $c_2$=0.6711, $e_1$=20.14, $e_2$=-0.053, $e_3$=-1638.84, $e_4$=40763.24, $k_{rw-50}$=0.048.

Comparison of the experimental relative permeability and the empirical correlation is presented in Figure 6.14. The results show that the oil and water relative permeability values generated from the empirical model adopted to fit the experiment data with optimised constants compares well with the experimental values. The predicted results are in good agreement with the experimental data with a variance of 0.08175 and 0.0055 for oil and water respectively, an RMSE value of 0.01 and $R^2$ of 0.994 for the oil phase and RMSE of 0.02 and $R^2$ of 0.975 for water.

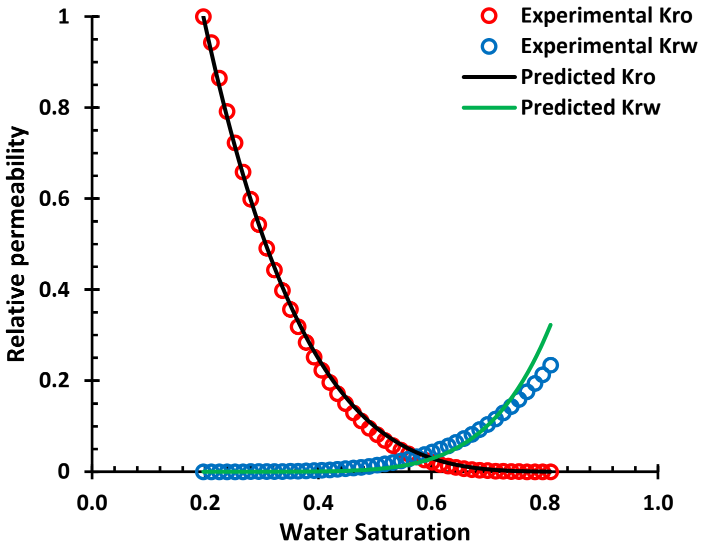

Figure 6.14:Comparison between the experimental relative permeability values and outputs predicted from the empirical model with the modified empirical constants

### 6.7.1 Model validation

Figure 6.15 is a validation plot to evaluate the reliability of the optimised parameters used with the Zhang correlations for predicting temperature dependent oil-water relative permeability in unconsolidated porous media. An experimental dataset from Ashrafi et al. (2012) using light oil and glass beads of relative high permeability at 70 °C has been compared with relative permeability values generated from the empirical model. As seen in Figure 6.15, relative permeability values generated from the empirical model compare satisfactorily with the data from the published experiment with a variance of 0.11211 and 0.00024 for oil and water respectively, establishing the reliability of the predictive capability of using the optimised constants with the Zhang model in literature.

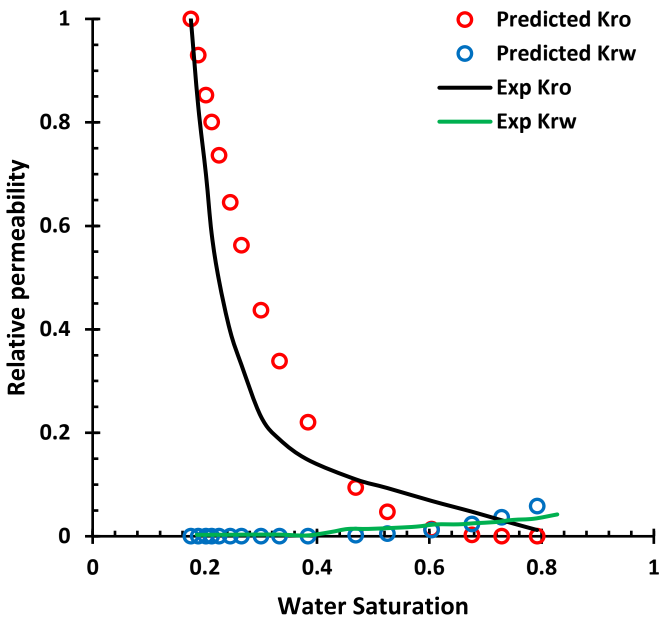

Figure 6.15: Comparison between experimental relative permeability from Ashrafi et al. (2012) and outputs generated the modified empirical constants in this study

It should be noted that the proposed empirical constants with the model for predicting a temperature dependent oil and water relative permeability needs to be used when the operating conditions fall within the range of applicability, otherwise its reliability is not guaranteed.

# Chapter 7: MACHINE LEARNING PREDICTION OF TEMPERATURE EFFECT ON OIL-WATER RELATIVE PERMEABILITY

**Overview**

This chapter presents a ML modelling approach to predict the two-phase oil-water relative permeability using the experimentally generated data in this study. The purpose of this is to develop a suitable modelling technique that can predict oil-water relative permeability with high accuracy using less time.

## 7.1 OIL-WATER RELATIVE PERMEABILITY DATA

Oil-water relative permeability data generated from the experimental work has been used for the ML model. 900 data points for experimental oil-water relative permeability was used for the model formulation. The feature inputs used to develop the model comprised of the following: water saturation ($S_w$), temperature (T), oil viscosity ($\mu_o$), absolute permeability of sandpack (K), initial water saturation and injection flowrate (cc/min). The oil viscosity is in the range of $13.46 \leqslant \mu_o \leqslant 83.55$ cP with water injection flowrate of 0.5-, 0.75-, and 1 cc/min.

Table 7.1 summarises the input features and statistical parameters. To verify the correlations developed, the dataset was split randomly into training data containing 85 % of the whole dataset, and testing data made up of the remaining 15 %. The 85 % training data was used to train the model in order to establish the best correlations or pattern, while the testing data was used to assess the correctness of the correlations with independent data.

Table 7.1: Statistical summary of the entire dataset used for both training and testing

| | **Water saturation** | **Temperature (°C)** | **Oil viscosity (cP)** | **Sandpack permeability (D)** | **Initial water saturation** | **Injection flowrate (cc/min)** |
|---|---|---|---|---|---|---|
| **Count** | 900 | 900 | 900 | 900 | 900 | 900 |
| **Mean** | 0.52 | 60.00 | 38.07 | 5.55 | 0.21 | 0.75 |
| **Std** | 0.19 | 16.34 | 25.62 | 0.79 | 0.05 | 0.20 |
| **Min** | 0.11 | 40.00 | 13.46 | 4.59 | 0.11 | 0.50 |
| **25%** | 0.36 | 40.00 | 19.29 | 5.02 | 0.17 | 0.50 |
| **50%** | 0.52 | 60.00 | 32.02 | 5.20 | 0.24 | 0.75 |
| **75%** | 0.68 | 80.00 | 37.86 | 6.01 | 0.25 | 1.00 |
| **Max** | 0.89 | 80.00 | 83.55 | 7.12 | 0.28 | 1.00 |

## 7.2 SUPPORT VECTOR REGRESSION MODEL FORMULATION

To develop the SVR model with a reliable predictive capability for temperature dependent oil-water relative permeability, a set of independent variables are chosen from the entire dataset. The water saturation is considered one of the most essential parameters that needs to be considered. Generally, two-phase oil and water relative permeability is presented as a function of the water saturation. Other factors which affect the relative permeability include oil and water viscosity, the intrinsic permeability of the porous system, water injection rate and initial water saturation as described in Eq. 7.1 and 7.2:

$$k_{ro} = f(S_w, T, \mu_o, K, S_{wi}, q) \tag{7.1}$$

$$k_{rw} = f(S_w, T, \mu_o, K, S_{wi}, q) \tag{7.2}$$

The water viscosity was kept constant for the range of temperatures in this study and hence not included as one of the independent variables in the model development. Many other variables such as the oil/water interfacial tension and wettability are believed to affect oil-water relative permeability, but these were not captured in our experiments and hence not included in the model development. The intrinsic media permeability of the porous media has been included in the model as it is indicative of the mean grain size and the specific surface area that makes up the sandpack and directly affects the residual wetting phase saturation.

The performance or estimation accuracy of the developed model depends on the tuning parameters C and ε and kernel type. Selection of the kernel type and function parameter is done based on the knowledge and distribution of the input (x) values of the training data. The parameter C defines the compromise between the model complexity (flatness) and the acceptance condition for which deviations larger than ε are tolerated in optimisation formulation (Sandip & Kartik, 2009). Parameter ε determines the width of the ε-insensitive zone that fits the training data, and it influences the number of support vectors for the regression function. The RBF kernel was used and a function written with a range of values given for which the best selection of these parameters is made and applied for the model. Table 7.2 presents the values provided for the function to loop through in obtaining optimum values for the C, epsilon and gamma parameters. The procedure for the model implementation is presented in the Chapter 4 of the thesis.

Table 7.2: SVR tuning parameters tried in the model and specific values applied

| | Set of tuning values given to the function | Used value |
|---|---|---|
| C | 0.1, 1, 100, 1000 | 1000 |
| ε | 0.0001, 0.0005, 0.001, 0.005, 0.01, 0.05, 0.1, 0.5, 1, 5, 10 | 0.0001 |
| γ | 0.0001, 0.001, 0.005, 0.1, 1, 3, 5 | 100 |

### 7.2.1 **Quality metrics**

Different methods are used to measure the accuracy of a predictive model as relying only on a single metric is problematic. While appropriate visualisations of the model fit and residual plots have been adopted to evaluate if the model is fit for purpose, other numerical parameters have been used in characterising the model's predictive capabilities. The quality metrics adopted to assess the performance of the SVR model are presented in Eq. 7.3 to Eq. 7.6. The predicted water or oil relative permeability is denoted as $\hat{f}(x_i)$ and the experimental data denoted by $\boldsymbol{y_i}$. In this section, 4 statistical parameters for evaluating model performance are introduced.

The determinate coefficient ($R^2$) which measures the closeness of the data points to the fitted regression line. In practical sense, the $R^2$ is a measure of correlation (how much of the dependent variable is predictable by the independent variable), not accuracy (Kuhn & Johnson, 2013).

$$R^2 = 1 - \frac{\sum_{i=1}^{N}\left(y_i - \widehat{f(x_i)}\right)^2}{\sum_{i=1}^{N}(y_i - \bar{y})^2} \qquad 7.3$$

where $\boldsymbol{\bar{y}}$ is the average of the experimental data and $N$ is the number of samples. The mean square error (MSE) between the model predicted oil-water relative permeability and corresponding experimental values is the average of the square of the errors. The larger the MSE the larger the error in the predictions.

$$MSE = \frac{\sum_{i=1}^{N}\left(\hat{f}(x_i) - y_i\right)^2}{n} \qquad 7.4$$

The root mean squared error (RMSE) which is the square root of the mean of the error squares within the dataset. This metric is considered a good measure of accuracy (Simon, et al., 2018).

$$RMSE = \left[\frac{1}{N}\sum_{i=1}^{N}\left(y_i - \hat{f}(x_i)\right)^2\right]^{\frac{1}{2}} \qquad 7.5$$

The mean absolute error (MAE) is the average of the absolute values of the different prediction errors for the entire dataset.

$$MAE = \frac{1}{N}\sum_{i=1}^{N}\left|\hat{f}(x_i) - y_i\right| \qquad 7.6$$

## 7.3 COMPARISON OF MACHINE LEARNING WITH EXPERIMENTAL RESULTS

Figure 7.1 (a) and (b) shows the cross plots of the experimental versus predicted relative permeabilities for the oil and water phase, respectively. In these plots, the corresponding datapoints for the training and testing-subset have been included. A cross plot consists of a plot of predicted values against the corresponding experimental values, equated with a unit slope line, which is representative of the ideal model. The nearer the datapoints are to this line, the higher the accuracy of the model. As seen in both plots, a large amount of the data points lies on the 45° line which indicates high predictive capability and accuracy of the model. A plot on the y=x line with a tight cloud of data is indicative of the accuracy of the estimations made. Deviations from the y=x line is indicative of the prediction error in the model.

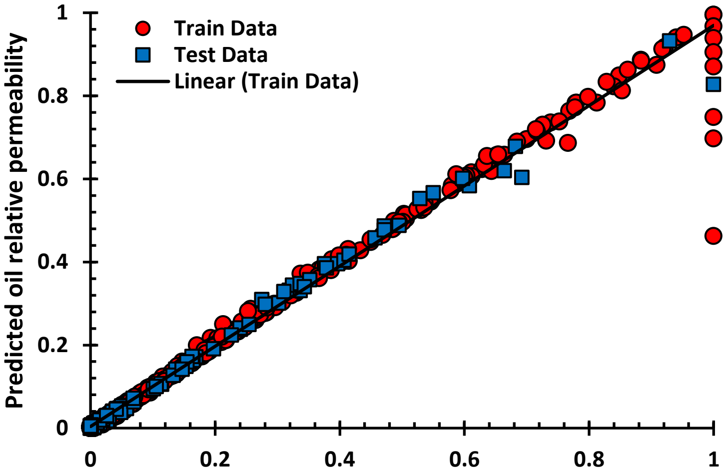

(a)

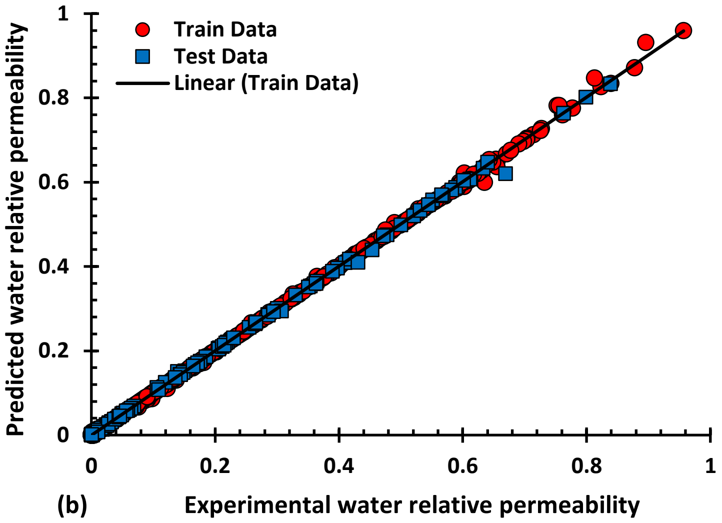

Figure 7.1: The cross plot of experimental versus predicted relative permeability (a) oil and (b) water

The percentage relative deviation of predicted values for both oil and water relative permeabilities against the experimental values are shown in the Figure 7.2 (a) and (b) for the training and testing subset. For both plots, it is seen that the $K_{ro}$ and $K_{rw}$ cases meet the acceptable deviation from the corresponding experimental values. As shown in these figures, as the relative permeability tends to zero, there is generally an increase in the relative deviation. A typical case is the percentage relative deviation of 1.94 % for oil relative permeability of 0.378 changing to 36.5 % as the relative permeability becomes 0.0085. This can be explained mathematically because with a near-zero relative permeability, ratio of absolute deviation to experimental relative permeability values has a very small denominator, resulting in high relative error. It should be noted that from these figures, the relatively high deviations occur within the range of 0 to 0.1, with the remaining dataset lying within the zero line. This indicates that over 90 % of the prediction has a very minimal deviation from the experimental data.

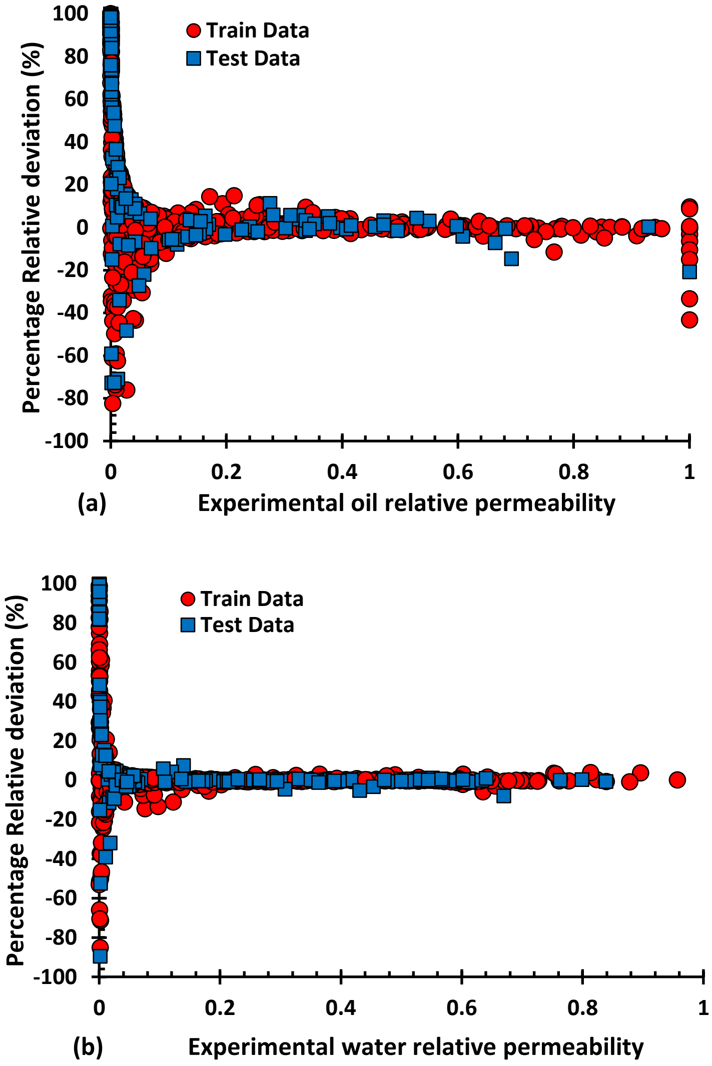

Figure 7.2: The relative deviation of predicted versus experimental relative permeability (a) oil, and (b) water

Additionally, due to the possibility of the infinite value of relative deviation as the relative permeability tends to zero and potential miss-interpretations of the data, the absolute deviation of the model estimated oil and water relative permeabilities against experimental are presented in Figure 7.3 (a) and (b). The relative advantage of presenting the error values as absolute values is that it eliminates potential exaggeration of error near zero and gives an idea of the exact non-zero values. For example, while the percentage relative deviation reaches above ± 80 % for relative permeability between 0 – 0.1 (Figure 7.2 (a) and (b)), the absolute error values are around 0.01 (Figure 7.3 (a) and (b)) which is a very small value compared to the entire dataset. Absolute error values around 0.01 indicate approximately 99 % accuracy of the predictive model as 0.01 is only 1 % of the highest relative permeability of 1. As shown in Figure 7.3, as the relative permeability values increase, the absolute errors increase correspondingly, though less than 10 % are in the highest error margin.

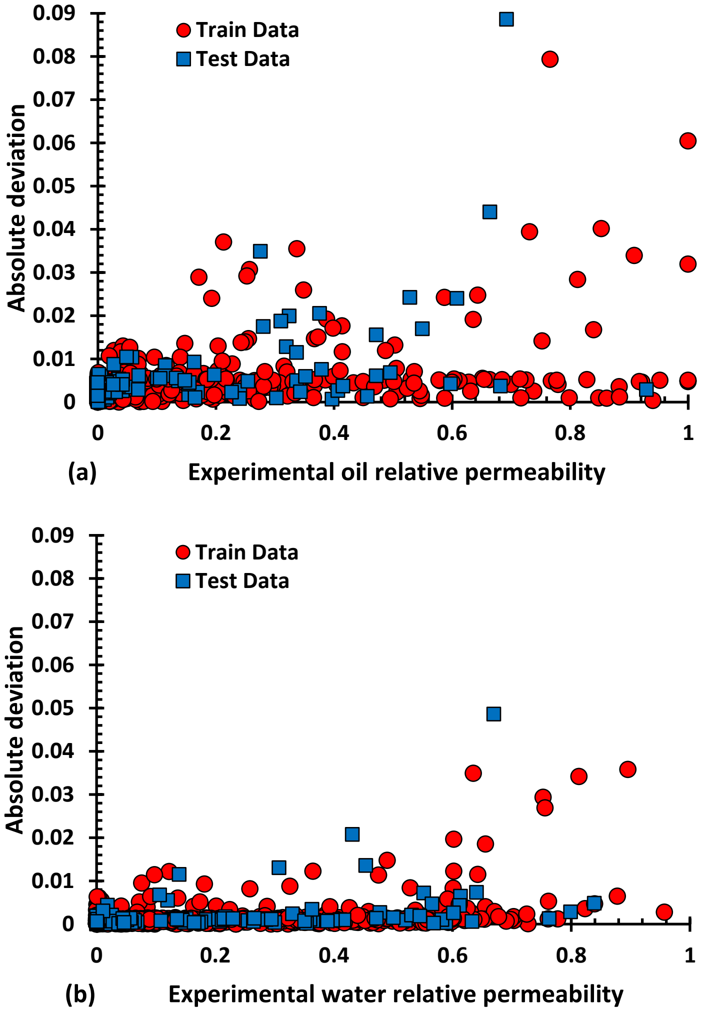

Figure 7.3: The absolute deviation of predicted versus experimental relative permeability (a) oil and (b) water

To better assess the predictive performance of the developed SVR model for water and oil relative permeability, necessary statistical quality parameters are presented in

*Table 7.3*. The determinant coefficient or $R^2$ has values lying between 0 and 1, indicative of the validity of the correlation made. While a value near 1 means a more reliable prediction, values nearer to 0 indicates a poor model.

Table 7.3: Quantitative measures of performance

| | | $R^2$ | MAE | MSE | RMSE |
|---|---|---|---|---|---|
| $K_{ro}$ | Training | 0.9858 | 0.006881878 | 0.000810109 | 0.02846241 |
| | Testing | 0.9826 | 0.007012088 | 0.000343168 | 0.018524796 |
| $K_{rw}$ | Training | 0.9878 | 0.001564707 | 0.000013649 | 0.003694537 |
| | Testing | 0.9846 | 0.002031303 | 0.000027686 | 0.005261768 |

As seen in the summary table, the $R^2$ value is approximately 0.99 for all the implementations for the model for both oil and water training and testing dataset. The recorded values of MAE, MSE and RMSE also confirm that the developed model is capable of predicting the water and oil relative permeabilities in the sandpack systems. The developed predictive model for a temperature-based oil–water relative permeability has a RMSE value between of 0.004 and 0.02 for the entire range with a corresponding MAE of between 0.002 and 0.007.

To demonstrate the reliability of the SVR predictions, the predicted relative permeabilities and their corresponding  experimental values are plotted against their corresponding indexes in Figure 7.4 and Figure 7.5 for oil and water respectively. As these figures show, the predicted results from the model very close to actual values of oil and water relative permeabilities for both the training and testing datasets. As the quality metrics and presented graphs suggest, employing the developed model on the temperature dependent oil and water relative permeability data in the training and testing subsets generates accurate results.

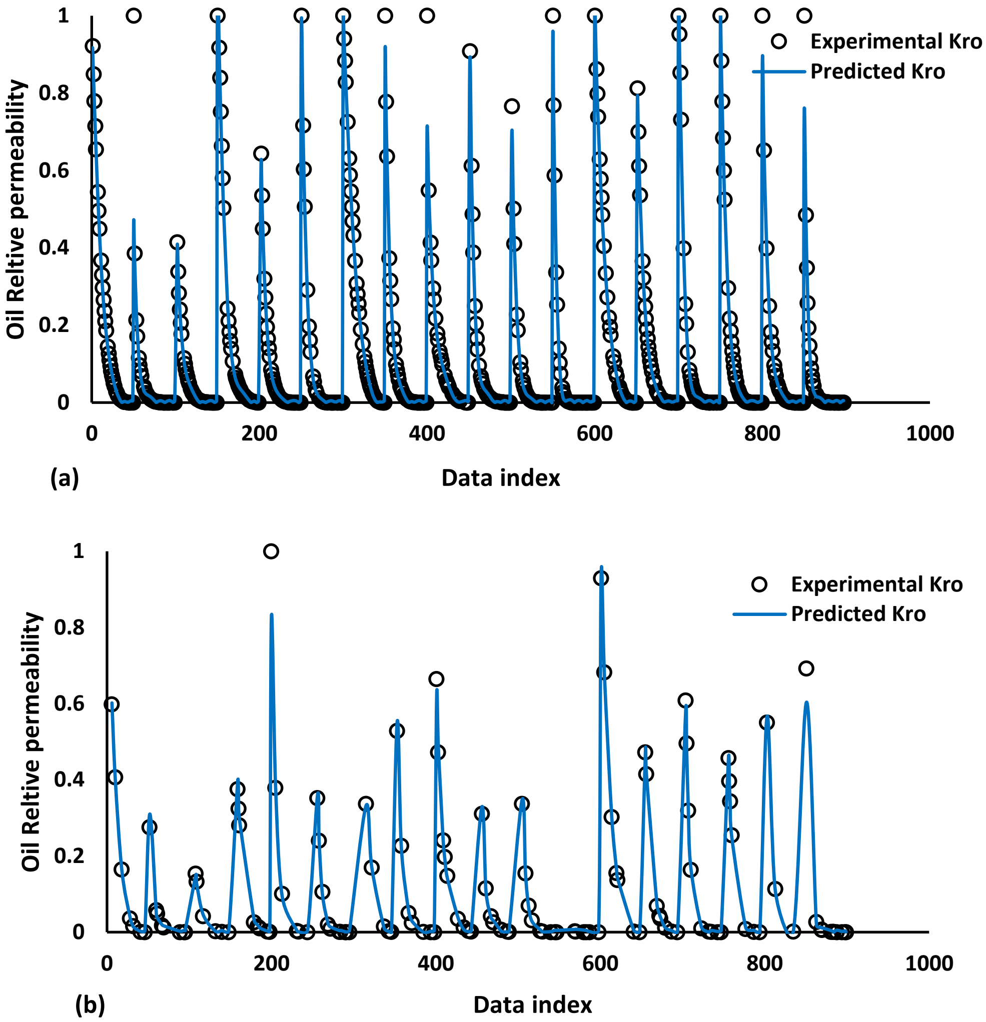

Figure 7.4: The comparison between the predicted $K_{ro}$ values by the SVR model and the experimental values: (a) training data and (b) testing data

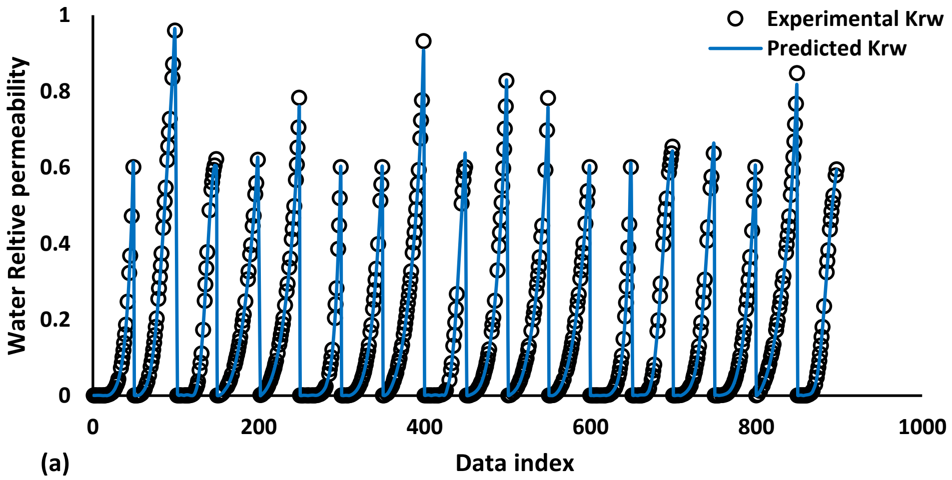

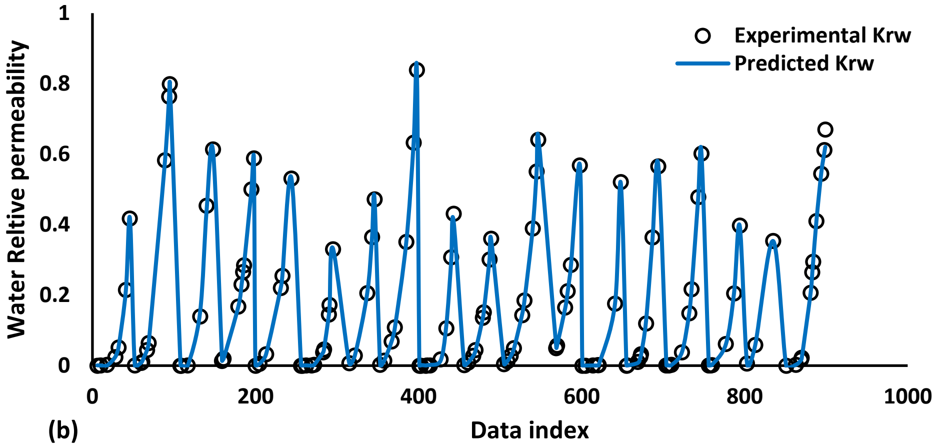

Figure 7.5: The comparison between the predicted $K_{rw}$ values by the SVR model and the experimental values: (a) training data and (b) testing data

While the ML and empirical model developed have been shown to be reliable and an efficient way for relative permeability measurements, they are not intended to replace standard laboratory measurements. Instead, the use of the models can serve as reference for laboratory experiments and can be applied for preliminary measurements and design of experiments.

# Chapter 8: CONCLUSION AND RECOMMENDATION FOR FUTURE WORK

## 8.1 CONCLUSION

A range of factors including temperature, viscosity, flowrate, IFT, amongst others are likely to affect oil-water relative permeability. To explore the influences of these factors qualitatively and quantitatively, a series of specially designed high temperature coreflooding experiments (accompanied by some other adjoining laboratory experiments) were carried out. In this study, the effect of temperature, oil viscosity and water injection flowrate on oil-water relative permeability curves and residual oil saturation has been investigated for a set of predominantly water-wet porous systems. The USS waterflood method was adopted and numerical computation with history matching implemented for the analysis of experimental data and generation of relative permeability curves. Generated experimental data was curated and used in implementing a ML model for predicting a temperature dependent two-phase oil-water relative permeability. For this purpose, supervised machine learning has been employed using the SVR algorithm. 900 data points for both oil and water relative permeability have been used for the training and testing of the model. Independent variables considered were water saturation, temperature, oil viscosity, initial water saturation, absolute permeability and injection flowrate for the prediction of the phase relative permeability.

Based on the results and discussion presented, the following conclusions can be drawn on the effect of temperature, viscosity, and flowrate on oil-water relative permeability of porous sandpacks.

- The CFD results showed that the displacement behaviour of water and oil-wet systems is strongly affected by the contact angle with a profound effect on the oil recovery factor. In the water-wet case, relatively more oil is displaced from the domain thereby improving the oil recovery factor. The water-wet system resulted in about 35 – 45 % oil recovery than the oil-wet system, with the unrecovered oil mainly adhering to the wall region of the pore bodies for the oil-wet system. For the intermediate wet case, initial fluid distribution is seen to have a more significant effect on the displacement behaviour than the contact angles. The results from this study are consistent with published experimental and numerical studies.

- A general trend for the series of experiments conducted shows an increase in the oil and water relative permeabilities occasioned by a rightward shift of the curves with rising temperature. In addition, the irreducible water saturation increased with a rise in temperature, coupled with a decrease in the residual oil saturation in most of the experimental runs.
- Also, with a rise in temperature there was a rightward shift of the crossover saturation beyond 0.5 of the water saturations which is indicative of a shift to water-wetness with temperature rise. The influence by viscous fingering and unstable displacement front due to the adverse mobility ratio condition is apparent in the results owing to the viscosity ratio and media properties.
- The shape of oil relative permeability curves for the sandpack system with a highly viscous oil increased with a rise in the injection flowrate. An opposite trend was observed for the less viscous oil as an increase in the injection flowrate does not favour the displacement process. In other words, with increasing flowrate the relative permeability curves increases for more viscous oils and decreases for less viscous oils. A factor believed to cause the variation under different flowrate is the contact angle increase with oil viscosity.
- The residual oil saturation is observed to be sensitive to the injection flowrate for both oil systems. The flooded sandpack with highly viscous oil showed a reducing value for the residual oil saturation with increasing flowrate. At an intermediate flowrate, the residual oil saturation is unaffected, but a higher residual oil saturation was observed in the lighter oil under the same flowrate. With regards to the water relative permeability curves, the effect is minimal in most of the cases. With the general trend showing the highest water relative permeability curve under the highest flowing rate.
- The endpoint water relative permeability varies slightly for the set of experiments with the values being higher for the less viscous oil under the same flowrate. The effect of oil viscosity on fractional flow and consequently on the oil recovery was observed to be more predominant in the tests under higher flowrate and shows a higher fractional flow for the lighter oil.
- The results presented for both the ML and empirical optimisation shows that the approaches are reliable, robust and accurate for relative permeability prediction within the range of applicability. Furthermore, empirical model

developed by Zhang et al. (2017) was optimised to fit the experimental data and empirical constants generated through nonlinear least square minimisation approach. The generated parameters compare very well with the experimental data and was validated against published data in literature, which also show satisfactory performance.

In summary, the results presented in this study demonstrate that relative permeability curves are affected by the operating temperature, injection flowrate and fluid viscosity. Consequently, the temperature factor is a very vital parameter to be considered when incorporating relative permeability data into reservoir simulators for effective reservoir production modelling. The ML and empirical modelling would serve as valuable data benchmark tools for future high temperature relative permeability laboratory experiments while equally being used for preliminary evaluation purposes.

## 8.2 RECOMMENDATIONS FOR FUTURE WORK

A few of the factors affecting oil-water relative permeability have been examined in this research would require additional investigation as follows:

- The coreflooding experiments in this study covered intrinsic permeability specific to unconsolidated sandpacks in the range of 10 – 100 mD. Further investigation on consolidated core samples with smaller permeability range could be used and the formulated model updated to enlarge the range applicability.
- It has been established that relative permeability is affected by several influencing parameters such as temperature, interfacial tension, flowrate, wettability, fluid viscosity, pore shape and pore size distribution. However, only a few of these contributing parameters have been investigated in this study, it would be necessary for more research to be conducted to explore the complex interrelationships between the contributing parameters on relative permeability.
- Several other experimental techniques such as gas chromatograph/mass spectrometer (GC/MS) could be used to further analyse the fluid samples and X-ray CT scanning, Scanning Electron Microscope (SEM) imaging, thin-

section studies incorporated to further improve the insights to the intricate pore-scale phenomenon taking place during the coreflooding experiments.

- The samples used in this study are mainly commercial grade silica sand. Considering the possibility of more intricate interaction between carbonate cores and the fluids, more tests need to be conducted using carbonate core to expand the understanding further.
- At appropriate temperature and pressure, a three-phase flow scenario occurs in the petroleum reservoir. Thus, there is the need for three-phase coreflooding, which could potentially generate more robust results.
- More datasets need to be generated for a wider range of contributing parameters and the curated databank used to strengthen the predictive capacity of the developed ML model which will result in a wider range of applicability.

# REFERENCES

Abdussamie, N., 2009. *Flow and Transport Problems in Porous Media Using CFD (Doctoral dissertation),* Egypt: Arab Academy, Mechanical Eng.

Abdus, S. & Iqbal, G. M., 2016. Reservoir rock properties. In: *Reservoir Engineering.* s.l.:Gulf Professional Publishing, pp. 29-79.

Abobaker, M. A. & Bambang, B., 2014. Comparison between Structured and Unstructured Grid Generation on Two Dimensional Flows Based on Finite Volume Method (FVM). *International Journal of Mining, Metallurgy & Mechanical Engineering (IJMMME) ,* 2(2), pp. 97-103.

Ahmadi, M., Ebadi, M., Shokrollahi, A. & Majidi, S., 2013. Evolving artificial neural network and imperialist competitive algorithm for prediction oil flow rate of the reservoir. *Appl Soft Comput ,* 13(2), p. 1085–98.

Akhlaghinia, M., Torabi, F. & Chan, C., 2014. Experimental investigation of temperature effect on three-phase relative permeability isoperms in heavy oil systems. *Fuel,* Volume 118, pp. 281-290.

Akin, S., Castanier, L. & Brigham, W., 1998. *Effect of temperature on heavy-oil/water relative permeabilities.* New Orleans, Louisiana, Society of Petroleum Engineers.

Akin, S. & Demiral, M. R. B., 1997. *Effect of flow rate on imbibition three-phase relative permeabilities and capillary pressure.* San Antonio, Texas, Society of Petroleum Engineers.

Alhammadi, A. M. et al., 2019. *Pore-scale imaging and determination of relative permeability and capillary pressure in a mixed-wet carbonate reservoir rock at subsurface conditions.* s.l., Society of core analysts, pp. 1-11.

Ali, J., 1997. *Developments in measurement and interpretation techniques in coreflood tests to determine relative permeabilities.* Rio de Janeiro, Brazil, s.n.

Alizadeh, A. H., Keshavarz, A. & Haghighi, M., 2007. *Flow rate effect on two-phase relative permeability in iranian carbonate rocks.* Kingdom of Bahrain, Society of Petroleum Engineers.

Alizadeh, A. H. & Piri, M., 2014. The effect of saturation history on three-phase relative permeability: An experimental study. *Water Rersources Research.*

Alotaibi, M. B., Nasralla, R. A. & Nasr-El-Din, H. A., 2011. Wettability Studies Using Low-Salinity Water in Sandstone Reservoirs. *Society of Petroleum Engineers,* 16(06).

Al-Wahaibi, Y. G. C. & Muggeridge, A., 2006. Drainage and imbibition relative permeabilities at near miscible conditions. *Journal of Petroleum Science and Engineering,* 53(3-4), pp. 239-253.

Amirian, E. et al., 2018. Artificial neural network modeling and forecasting of oil reservoir performance. *In Applications of data management and analysis,* pp. 43-67.

Amir, J. H. S. & Mehran, S., 2016. Gas/Oil relative permeability normalization: Effects of permeability, wettability, and intercaila tesnion. *SPE Reservoir Evaluation & Engineering,* pp. 673-682.

Anifowose, F., Jane, L. & Abdulazeez, A., 2015. Improving the prediction of petroleum reservoir characterization with a stacked generalization ensemble model of support vector machines. *Applied Soft Computing,* Volume 2015, pp. 483-496.

ANSYS, F., 2006. *Overview and Limitations of the VOF Model,* s.l.: Fluent Inc..

ANSYS, F., 2018. *Fluent 18.0 Documentation,* Lebanon: ANSYS Inc.

Apostolos, K., Bryan, J. & Taheri, S., 2016. *Fundamentals of fluid flow in porous media,* Alberta: University of Calgary.

Arabloo, M., Shokrollahi, A., Gharagheizi, F. & Mohammadi, A., 2013. Toward a predictive model for estimating dew point pressure in gas condensate systems. *Fuel Process Technology,* Volume 116, pp. 317-24.

Archer, J. & Wong, S., 1973. Use of a reservoir simulator to interpret laboratory waterflood data. *Society of Petroleum Engineers Journal,* Volume 13, pp. 343-347.

Arigbe, O. D., Oyeneyin, M. B., Arana, I. & Ghazi, M. D., 2019. Real-time relative permeability prediction using deep learning. *Journal of Petroleum Exploration and Production Technology,* Volume 9, pp. 1271-1284.

Arthur, J. A., 2015. *Thermal Conductivity Measurements of Bitumen Bearing Reservoir Rocks.* s.l., s.n.

Asar, H. & Handy, L. L., 1988. Influence of Interfacial Tension on Gas/Oil Relative Permeability in a Gas-Condensate System. *Society of Petroleum Engineers Reservoir Engineering,* 3(01), pp. 257-264.

Ashrafi, M., 2013. *Experimental Investigation of Temperature Dependency of Relative Permeability Data in Heavy Oil Systems with Applications to Thermal Recovery,* Trondheim: PhD Thesis, Norwegian University of Science and Technology.

Ashrafi, M., Souraki, Y. & Torsaeter, O., 2014. Investigating the Temperature Dependency of Oil and Water Relative Permeabilities for Heavy Oil Systems. *Transport in porous Media,* pp. 517-537.

Ashrafi, M., Yaser, S. & Ole, T., 2012. Effect of Temperature on Athabasca Type Heavy Oil – Water Relative Permeability Curves in Glass Bead Packs. *Energy and Environment Research,* 2(2), pp. 113-126.

Bagci, S., M. V. K. & Ulas, T., 2001 . Effect of Brine Composition on Oil Recovery by Waterflooding. *Petroleum Science and Technology,* pp. 359-372.

Baker, L. E., 1988. *Three-phase relative permeability correlations.* Tulsa, Oklahoma, Society of Petroleum Engineers.

Bastian, P., 1999. *Numerical computation of multiphase flow in porous media,* Kiel: s.n.

Bennion, D. B., Thomas, F. B., Schulmeister, B. & Ma, T., 2006. *A Correlation of the Low and High Temperature Water-Oil Relative Permeability Characteristics of Typical Western Canadian Unconsolidated Bitumen Producing Formations.* Calgary, Alberta, Petroleum Society of Canada.

Blom, S., Jacques, H. & Soetekouw, D., 2000. Relative Permeability at Near-Critical Conditions. *SPE Journal,* 5(2), pp. 172-181.

Blunt, J. M., Jackson, D. M., Piri, M. & Valvatne, H. P., 2002. Detailed physics, predictive capabilities and macroscopic consequences for pore-network models of multiphase flow. *Advances in Water Resources,* Issue 25, pp. 1069-1089.

Blunt, M. J., 1999. *An empirical model for three-phase relative permeability.* Houston, Texas, Society of Petroleum Engineers.

Blunt, M. J., 2001. Flow in porous media: Pore-network models and multiphase flow. *Curr. Opin. Colloid Interface Sci., ,* p. 197– 207.

Brackbill, J. U., Kothe, D. B. & Zemach, C., 1992. A Continuum Method for Modeling Surface Tension. *Journal of Computational Physics,* Volume 100, pp. 335-354.

Buckley, J., Liu, Y. & Monsterleet, S., 1998. Mechanisms of Wetting Alteration by Crude Oils. *SPE Journal,* Issue 37230, pp. 54-61.

Buckley, S. E. & Leverett, M. C., 1942. Mechanism of Fluid Displacement in Sands. *Society of Petroleum Engineers.*

Burdine, N. T., 1953. Relative Permeability Calculations From Pore Size Distribution Data. *Society of Petroleum Engineers.*

Burges, C., 1998. A tutorial on support vector machines for pattern recognition. In: *Data Mining and Knowledge Discovery.* s.l.:s.n., pp. 121-167.

Cao, L., Shenglai, Y., Xiangrong, N. & Sanchuan, L., 2016. The Effect of Temperature and Rock Permeability on Oil-Water Relative Permeability Curves of Waxy Crude Oil. *Int. Journal of Engineering Research and Applications,* pp. 16-21.

Carcoana, A., 1992. *Applied Enhanced Oil Recovery.* s.l.:Prentice Hall.

Ccoicca, Y., 2013. Applications of support vector machines in the exploratory phase of petroleum and natural gas: a survey. *International Journal of Engineering and Technology,* 2(2), pp. 113-125.

Chaki, S. et al., 2014. Well tops guided prediction of reservoir properties using modular neural network concept: a case study from western onshore, India. *Journal of Petroleum Science Engineering ,* Volume 123, pp. 155-163.

Chen, A. & Wood, A., 2001. *Rate effects on water-oil relative permeability.* Edinburgh, Scotland, s.n.

Chen, X. K. A. & DiCarlo, A., 2016. An extended JBN method of determining unsteady-state two-phase relative permeability. *Water Resources Research,* 52(10), pp. 8374-8383.

Cherkassky, V. & Mulier, F., 1998. *Learning from Data: Concepts Theory and Methods.* New York: Wiley.

Chierici, G., 1984. Novel Relations for Drainage and Imbibition Relative Permeabilities. *Society of Petroleum Engineers,* pp. 275-276.

Chinedu, A., Abhijit, Y. D., Santanu, K. & James, R. H., 2008. The Effect of Wettability on Oil Recovery: A Review. *Society opf Petroleum Engineers ,* Issue 114496.

Chiroma, H., Sameem, A., Adamu, I. A. & Tutut, H., 2014. Kernel Functions for the Support Vector Machine: Comparing Performances on Crude Oil Price Data. *Recent Advances on Soft Computing and Data Mining,* pp. 273-282.

Chuntian, C. & Chau, K., 2002. Three-person multiobjective conflict decision in reservoir flood control. *European Journal of Operational Research,* 142(3), pp. 625-631.

Closmann, P., Waxman, M. & Deeds, C., 1985. *Steady-state tar/water relative permeabilities in peace river cores at elevated temperature.* Las Vegas, Society of Petroleum Engineers.

Colin, M., Jules, R. & Izaskun, Z., 2015. Best Practice in Coring and Core Analysis. In: *Developments in Petroleum Science.* s.l.:Elsevier, pp. 1-15.

Corey, A., Rathjens, C., Henderson, J. & Wyllie, M., 1956. Three-phase relative permeability. *Journal of Petroleum Technology.*

Dangerfield, J. & Brown, D., 1985. The Ekofi sk Field: North Sea Oil and Gas Reservoirs. In: London: eds J. Kleepe et al., Graharm and Trotman, pp. 3-22.

Dmitri, K., 2010. *A Guide to Numerical Methods for Transport Equations.* s.l.:s.n.

Donaldson, E. C. & Alam, M., 2008. *Wettability.* s.l.:Elsevier.

Dos Santos, R. L. A., Bedrikovetsky, P. & carlos, R. H., 1997. Optimal Design and planning for Laboratory Corefloods. *Society of Petroleum Engineers.*

Ehrlich, R., 1970. *The effect of temperature on water-oil imbibition relative permeability.* s.l., s.n.

El-Sebakhy, E. A. et al., 2007. Support Vector Machines Framework for Predicting the PVT Properties of Crude Oil Systems. *Society of Petroleum Engineers.*

Enwald, H. P. E. & Almstedt, A. E., 1996. Eulerian two-phase flow theory applied to fluidization. *International Journal of Multiphase Flow,* Volume 22, pp. 21-66.

Esfahani, M. R. & Haghighi, M., 2004. Wettability evaluation of Iranian carbonate formations. *Journal of Petroleum Science and Engineering,* pp. 257-265.

Esmaeili, S., Hemanta, S., Thomas, H. & Brij, M., 2019. A data-driven model for predicting the effect of temperature on oil-water relative permeability. *Fuel,* Volume 236, pp. 264-277.

Fan, J. et al., 2019. Empirical and machine learning models for predicting daily global solar radiation from sunshine duration: A review and case study in China. *Renewable and Sustainable Energy Reviews,* Volume 100, pp. 189-212.

Farasat, A. et al., 2013. Toward an intelligent approach for determination of saturation pressure of crude oil. *Fuel Process Technology,* Volume 115, pp. 201-14.

Fayazi, A., Arabloo, M. & Mohammadi, A., 2014. Efficient estimation of natural gas compressibility factor using a rigorous method. *Journal Natural Gas Science Engineering,* Volume 16, p. 8–17.

Fayazi, A. et al., 2013. State-of-the-Art Least Square Support Vector Machine Application for Accurate Determination of Natural Gas Viscosity. *Ind Eng Chem Res,* 53(2), pp. 945-958.

Gholami, R., Shahraki, A. & Jamali, P. M., 2012. Prediction of Hydrocarbon Reservoirs Permeability Using Support Vector Machine. *Mathematical Problems in Engineering.*

Green, D. W. & Willhite, G. P., 1998. *Enhanced oil recovery.* s.l.:Society of Petroleum Engineers.

Hagoort, J., 1980. Oil recovery by gravity drainage. *Society of Petroleum Engineering Journal,* Volume 20, pp. 139-150.

Hamouda, A. A. & Karoussi, O., 2008. Effect of Temperature, Wettability and Relative Permeability on Oil Recovery from Oil-wet Chalk. *Energies,* pp. 19-34.

Hamouda, A. A., Karoussir, O. & Chukwudeme, E. A., 2008. Relative permeability as a function of temperature, initial water saturation and flooding fluid compositions for modified oil-wet chalk. *Journal of Petroleum Science and Engineering,* 63(1), pp. 61-72.

Hanga, K. M. & Yevgeniya, K., 2019. Machine learning and multi-agent systems in oil and gas industry applications: A survey. *Computer Science Review,* Volume 34.

Hann, T. & Steurer, E., 1996. Much ado about nothing? Exchange rate forecasting: Neural networks vs. linear models using monthly and weekly data. *Neurocomputing,* 10(4), pp. 323-39.

Heaviside, J. & Black, C., 1983. *Fundamentals of relative permeability: experimental and theoretical considerations.* San Francisco, California, s.n.

Henderson, G., Danesh, G., Tehrani, A. & Peden, J., 1997. The effect of velocity and interfacial tension on relative permeability of gas condensate fluids in the wellbore region. *Journal of Petroleum Science and Engineering,* Volume 17, pp. 265-273.

Honarpour, M. & Mahmood, S., 1988. Relative-permeability measurements: an overview.. *SPE Journal of Petroleum Technology,* Volume 40, p. 963–966.

Huang, D. D. & Honarpour, M. M., 1998. Capillary end effects in coreflood calculations. *Journal of Petroleum Science and Engineering,* pp. 103-117.

Idahosa, P., Oluyemi, G., Oyeneyin, M. & Prabhu, R., 2016. Rate-dependent polymer adsorption in porous media. *Journal of Petroleum Science and Engineering,* pp. 65-71.

John, R. F., 2010. Rock–Fluid Interactions. In: *Integrated Reservoir Asset Management.* s.l.:Elsevier.

Johnson, E., Bossler, D. & Naumann, V., 1959. Calculation of relative permeability from displacement experiments. *Petroleum Transaction AIME,* Volume 216, pp. 370-372.

Jones, S. & Roszelle, W., 1978. Graphical techniques for determining relative permeability from displacement experiments. *SPE Journal of Petroleum Technology,* Volume 30, pp. 807-817.

Jude, O. A. & Lyman, L. H., 1982. The Effect of Interfacial Tensions on Relative Oil/Water Permeabilities of Consolidated Porous Media. *Society of Petroleum Engineers Journal,* pp. 371-381.

Kallel, W. et al., 2016. Modelling the effect of wettability distributions on oil recovery from microporous carbonate reservoirs. *Advances in Water Resources,* Issue 95, pp. 317-328.

Keller, A. A., Broje, V. & Setty, K., 2007. Effect of advancing velocity and fluid viscosity and fluid on the dynamic contact angle of petroleum hydrocarbons. *Journal of Petroleum Science and Engineering,* pp. 201-206.

Kisi, O. & Parmar, K. S., 2016. Application of least square support vector machine and multivariate adaptive regression spline models in long term prediction of river water pollution. *J Hydrol,* Volume 534, p. 104–12.

Kuhn, M. & Johnson, K., 2013. *Applied Predictive Modeling.* New York : Springer Science+Business Media.

Kumar, M. & Inouye, T., 1994. *Low-temperature analogs of hightemperature water/oil relative permeabilities.* New Orleans, LA, Society of Petroleum Engineers.

Kumar, S., Torabzadeh, S. J. & Handy, L. L., 1985. *Relative permeability functions for high-and low-tension systems at elevated temperatures.* California, Society of Petroleum Engineers.

Lahiri, S. K. & Ghanta, K. C., 2008. The support vector regression with the parameter tuning assisted by a differential evolution technique: study of the critical velocity of a slurry flow in a pipeline. *Chemical Industry & Chemical Engineering,* 14(3), pp. 191-203.

Latifa Al-Nuaimi, L. S. O. & Mehran, S., 2018. A New Technique to Predict Relative Permeability for Two-Phase Gas/Oil System at Different Interfacial Tension. *Society of Exploration Geophysicists,* pp. 121-124.

Li, K., Shen, P. & Qing, T., 1994. A New Method for Calculating Oil-Water Relative Permeabilities with Consideration of Capillary Pressure. *Mechanics and Practice,* 16(2), pp. 46-52.

Lomeland, F., Einar, E. & Wibeke, H. T., 2005. *A New Versatile Relative Permeability Correlation.* Toronto, Canada, s.n., pp. 1-12.

Longeron, D., 1980. Influence of very low interfacial tensions on relative permeability. *Society of Petroleum Engineers Journal,* 20(05), pp. 391-401.

Lu, Y., Nariman, F. N. & Abbas, F., 2017. Effect of Temperature on Wettability of Oil/Brine/Rock Systems. *Energy Fuels,* 31(5), p. 4989–4995.

Maini, B. & Batycky, J., 1985. Effect of Temperature on Heavy-Oil/Water Relative Permeabilities in Horizontally and Vertically Drilled Core Plugs. *Journal of Petroleum Technology,* pp. 1500-1510.

Maini, B., Kokal, S. & Jha, K., 1989. *Measurements and Correlations of Three-Phase Relative Permeability at Elevated Temperatures and Pressures.* San Antonio, Texas, Society of Petroleum Engineers.

Maini, B. & Okazawa, T., 1987. Effects of temperature on heavy oil-water relative permeability of sand. *Journal of Canadian Petroleum Technology,* pp. 33-41.

Marti, L., Nayat, S.-P., José, M. M. L. & Ana, C. B. G., 2017. On the combination of support vector machines and segmentation algorithms for anomaly detection: A petroleum industry comparative study. *Journal of Applied Logic,* Volume 24, pp. 71-84.

Mehdi, H., Koederitz, L. F. & Harvey, A. H., 1982. Empirical Equations for Estimating Two-Phase Relative Permeability in Consolidated Rock. *Journal of Petroleum Technology.*

Miller, M. A. & Ramey Jr, H., 1985. Effect of temperature on oil/water relative permeabilities of unconsolidated and consolidated sands. *Society of Petroleum Engineers Journal,* 25(06), pp. 945-953.

Mingming, L. & Shuzhong, W., 2015. Pore-scale modeling of a water/oil two-phase flow in hot water flooding for enhanced oil recovery. *RSC Advances,* pp. 85373-85382.

Mohammad, A. S., Reza, M., Mohammad, A. R. & Siyamak, M., 2015. Separating Well Log Data to Train Support Vector Machines for Lithology Prediction in a Heterogeneous Carbonate Reservoir. *Iranian Journal of Oil & Gas Science and Technology,* 4(2), pp. 01-14.

Mohammadmoradi, P. B., 2016. *Effective Thermal and Electrical Conductivity of Two-Phase Saturated Porous Media.* s.l., s.n.

Mohammed, M., Khan, M. & Bashier, E., 2016. *Machine learning: algorithms and applications.* s.l.:Crc Press.

Mosavat, N., Mohsenzadeh, A. & Al-Wahaibi, Y., 2016. *Estimating Oil/Water Relative Permeability at SAGD Steam Chamber Edge.* Kuwait, Society of Petroleum Engineers .

Nait, A. M., Noureddine, Z., Hemmati-Sarapardeh, A. & Shamshirband, S., 2019. Modeling temperature-based oil-water relative permeability by integrating advanced intelligent models with grey wolf optimization: Application to thermal enhanced oil recovery processes. *Fuel,* Volume 242, pp. 649-663.

Nait, A. M., Zeraibi, N. & Redouane, K., 2018a. Optimization ofWAGprocess using dynamic proxy, genetic algorithm and ant colony optimization. *Arabian Journal for Science and Engineering,* 43(11), pp. 6399-6412.

Nguyen, V. H., Adrian, P., Mark, A. K. & Val, P. W., 2006. The effect of displacement rate on imbibition relative permeability and residual saturation. *Journal of Petroleum Science and Engineering,* pp. 54-70.

Nguyen, V. H., Sheppard, A., Knackstedt, M. A. & Pinczewski, W. V., 2005. *The effects of displacement rate and wettability on imbibition relative permeabilities.* Dallas, Texas, Society of Petroleum Engineers.

NIST, 2013. *NIST/SEMATECH.* [Online]
Available at: https://doi.org/10.18434/M32189
[Accessed 13 June 2020].

Nowroozi, S., Ranjbar, M., Hashemipour, H. & Schaffie, M., 2009. Development of a neural fuzzy system for advanced prediction of dew point pressure in gas condensate reservoirs. *Fuel Process Technology,* 90(3), p. 452–7.

Odeh, A. & Dotson, B., 1985. A method for reducing the rate effect on oil and water relative permeabilities calculated from dynamic displacement data. *J. Pet. Technol.,* pp. 2051-2058.

Olugbenga, F. & Edo, M., 2014. Wettability Effects on Capillary Pressure, Relative Permeability, and Irredcucible Saturation Using Porous Plate. *Journal of Petroleum Engineering,* Volume 2014, pp. 1-12.

Oluyemi, G. F., 2014. Conceptual Physicochemical Models for Scale Inhibitor-Formation Rock Interaction. *Petroleum Science and Technology,* pp. 253-260.

Pål, Ø. A., Dag, C. S. & Svein, M. S., 2017. Waterflooding oil-saturated core samples - Analytical solutions for steady-state capillary end effects and correction of residual saturation. *Journal of Petroleum Science and Engineering,* Volume 157, pp. 364-379.

Pan, C., Hilpert, M. & Miller, C., 2004. Lattice-Boltzmann simulation of two-phase flow in porous media. *Water Resources Research,* 40(1).

Panja, P., Velasco, R., Pathak, M. & Deo, M., 2018. Application of artificial intelligence to forecast hydrocarbon production from shales. *Petroleum,* 4(1), pp. 75-89.

Pao-Shan, Y., Shien-Tsung, C. & I-Fan, C., 2006. Support vector regression for real-time flood stage forecasting. *Journal of Hydrology,* 3.28(3-4), pp. 704-716.

Parker, J., Lenhard, R. & Kuppusamy, T., 1987. A parametric model for constitutive properties governing multiphase flow in porous media. *Water Resources Research,* pp. 618-624.

Paul, G., 2012. *Formation Evaluation MSc Course Notes: Wettability,* s.l.: s.n.

Polikar, M., Farouq, A. S. & Puttagunta, V., 1990. High-temperature relative permeabilities for Athabasca oil sands. *Society of Petroleum Engineers,* 5(01), pp. 25-32.

Qadeer, S., Dehghani, K., Ogbe, D. & Ostermann, R., 1998. *Correcting oil/water relative permeability data for capillary end effect in displacement experiments.* California, SPE.

Qiao, Y., Peng, J., Ge, L. & Wang, H., 2017. *Application of PSO LS-SVM forecasting model in oil and gas production forecast.* s.l., IEEE.

Qin, Y. et al., 2018. Experimental studies on efects of temperature on oil and water relative permeability in heavy-oil reservoirs. *Scientific Reports.*

Rafiee-Taghanaki, S. et al., 2013. Implementation of SVM framework to estimate PVT properties of reservoir oil. *Fluid Phase Equilib.,* Volume 346, p. 25–32.

Ranaee, E., Monica, R., Giovanni, M. P. & Alberto, G., 2016. Comparative assessment of three-phase oil relative permeability models. *Water Resources Research.*

Robert, G. & Jorge, F., 2012. Machine Learning and Event-Based Software Testing: Classifiers for Identifying Infeasible GUI Event Sequences. In: H. Ali & M. Atif, eds. *Advances in Computers.* s.l.:Elsevier, pp. 109-135.

Roland, L. & Guillaume, L., 2016. *Recommended procedure for determination of relative permeabilities.* Snowmass, Colorado, USA, s.n.

Roland, L., Kjetil, L., Jos, G. M. & Douglas, R., 2016. *Comparison cf four numerical simulators for scal experiments.* Snowmass, Colorado, USA, s.n.

Roland, T., 2016. *Computational Fluid Dynamics (CFD) Modelling of Critical Velocity for Sand Transport Flow Regimes in Multiphase Pipe Bends,* Aberdeen: PhD Thesis.

Rostami, A., Hemmati-Sarapardeh, A. & Shamshirband, S., 2018. Rigorous prognostication of natural gas viscosity: smart modeling and comparative study. *Fuel,* Volume 222, pp. 766-78.

Rostami, P. et al., 2019. Effect of water salinity on oil/brine interfacial behaviour during low salinity waterflooding: A mechanistic study. *Petroleum.*

Salehi, M. M., Pouria, O. & Fatemeh, N., 2017. Salinity of injection water and its impact on oil recovery absolute permeability, residual oil saturation, interfacial tension and capillary pressure. *Egyptian Journal of Petroleum,* pp. 301-312.

Sami, M. A., 2014. *Effect of oil viscosity and brine salinity/viscosity on water/oil relative permeability and residual saturations.* Abu Dhabi, Society of Petrophysicists and Well Log Analysts (SPWLA) .

Sandip, K. L. & Kartik, C. G., 2009. Support vector regression with parameter tuning assisted by differential evolution technique: Study on pressure drop of slurry flow in pipeline. *Korean Journal of Chemical Engineering,* Volume 26, p. 175–1185.

Satter, A., Iqbal, G. & Buchwalter, J., 2008. *Practical Enhanced Reservoir Engineering: Assisted with Simulation Software.* s.l.:PennWell Books.

Schembre, J. M., Tang, G. & Kovscek, A. R., 2006. Interrelationship of Temperature and Wettability on Relative Permeability of Heavy Oil in Diatomaceous Rocks. *SPE Reservoir Evaluation & Engineering,* pp. 239-250.

Schembre, J., Tang, G. & Kovscek, A., 2005. *Effect of Temperature on Relative Permeability for Heavy-Oil Diatomite Reservoirs.* Irvine, CA, Society of Petroleum Engineers.

Schembre, J., Tang, G. & Kovscek, A., 2006. Wettability Alteration and Oil Recovery by Water Imbibition at Elevated Temperatures. *Journal of Petroleum Science and Engineering.*

Sedaee Sola, B., Fariborz, R. & Babadagli, T., 2007. Temperature effects on the heavy oil/water relative permeabilities of carbonate rocks. *Journal of Petroleum Science and Engineering,* 59(1), p. 27–42.

Sendra, 2012. *Sendra User Guide,* s.l.: http://www.sendra.no.

Serapião, A. B. S., Rogério, M. T., José, R. P. M. & Ivan, R. G., 2006. *Classification of Petroleum Well Drilling Operations Using Support Vector Machine (SVM).* s.l., IEEE.

Shams, R., Esmaili, S., Rashid, S. & Suleymani, M., 2015. An intelligent modeling approach for prediction of thermal conductivity of CO2. *Journal of Natural Gas Science Engineering,* Volume 27, p. 138–50.

Shell, 2018. *Shell Helix HX5 15W-40 Technical Data Sheet.* [Online] Available at: http://www.epc.shell.com/default.asp?whichLang=EN

Shen, P., Zhu, B., Li, X.-B. & Wu, Y., 2010. An Experimental Study of the Influence of Interfacial Tension on Water–Oil Two-Phase Relative Permeability. *Transport in Porous media,* Volume 85, pp. 505-520.

Shokrollahi, A., Arabloo, M., Gharagheizi, F. & Mohammadi, A., 2013. Intelligent model for prediction of CO2–reservoir oil minimum miscibility pressure. *Fuel ,* Volume 112, p. 375–84.

Sigmund, P. & McCaffery, F., 1979. An Improved Unsteady-State Procedure for Determining the Relative-Permeability Characteristics of Heterogeneous Porous Media. *Society of Petroleum Engineers.*

Simon, P., Neill, M. & Reza, H., 2018. Chapter 8: Ocean Modelling for ResourceCharacterization. In: *Fundamentals of Ocean Renewable Energy.* s.l.:Elsevier, pp. 193-235.

Singh, M., Mani, V., Honarpour, M. & Mohanty, K., 2001. Comparison of viscous and gravity dominated gas-oil relativepermeabilities. *Journal of Petroleum Science and Engineering,* 30(2), pp. 67-81.

Smola, A. J. & Bernhard, S., 2004. A tutorial on support vector regression. *Statistics and Computing,* Volume 14, p. 199–222.

Sufi, H. A., Ramey Jr., J. H. & Brigham, E. W., 1982. *Temperature Effects on Relative Permeabilities of Oil-Water.* New Orleans, LA, Society of Petroleum Engineers.

Suykens, J. & Vandewalle, J., 1999. Least squares support vector machine classifiers. *Neural Process Lett,* Volume 9, p. 293–300.

Tang, G. & Morrow, N., 1997. Salinity, temperature, oil composition and oil recovery by waterflooding. *SPE Reservoir Engineering,* Volume 12, pp. 269-276.

Tao, T. & Watson, A., 1984. Accuracy of JBN Estimates of Relative Permeability: Part I-Error Analysis. *Society of Petroleum Engineers of AIME,* pp. 209-214.

Tarek, A., 2019. Chapter 4 - Fundamentals of Rock Properties. In: A. Tarek, ed. *Reservoir Engineering Handbook (Fifth Edition).* s.l.:Gulf Professional Publishing, pp. 167-281.

Tarek, A., 2019. Chapter 5 - Relative Permeability Concepts. In: A. Tarek, ed. *Reservoir Engineering Handbook (Fifth Edition).* s.l.:Gulf Professional Publishing, pp. 283-329.

Thomas, S., 2007. Enhanced Oil Recovery – An Overview. *Oil & Gas Science and Technology,* pp. 9-19.

Torabi, F., Mosavat, N. & Zarivnyy, O., 2016. Predicting heavy oil/water relative permeability using modified Corey-based correlations. *Fuel,* Volume 163 , pp. 196-204.

Torabzabeh, S. & Handy, L., 1984. The effect of temperature and interfacial tension on water/oil relative permeabilities of consolidated sands. *SPE Enhanced Oil Recovery Symposium.*

Tryggvason, G. et al., 2001. A Front-Tracking Method for the Computations of Multiphase Flow. *Journal of Computational Physics,* Volume 169, pp. 708-759.

Übeyli, E., 2010. Least squares support vector machine employing model-based methods coefficients for analysis of EEG signals. *Expert Syst Appl,* 37(1), p. 233–9.

Van, S. E., 1982. *Three-phase relative permeability measurements using the centrifuge method.* Tulsa, Oklahoma, s.n.

Vapnik, V., 1995. *The Nature of Statistical Learning Theory.* s.l.:Springer.

Vega, B. & Kovscek, A., 2014. Steady-State relative Permeability Measurements, Temperature Dependency and a reservoir diamite core sample evoluation. *Society of Petroleum Engineers,* pp. 1-14.

Versteeg, H. K. & Malalasekera, W., 2007. *An Introduction to Computational Fluid Dynamics (THE FINITE VOLUME METHOD).* Essex: Pearson Education Limited.

Virnovsky, G., Vatne, K., Skajaeveland, S. & Lohne, A., 1998 . *Implementation of multirate technique to measure relative permeabilities accounting for capillary effects.* New Orleans, Louisiana, Society of Petroleum Engineers.

Wael, A. et al., 2007. Fundamentals of Wettability. *Oilfield Review*, pp. 44-61.

Wang, J. & Buckley, J., 1999. Wettability and Rate Effects on End-Point Relative Permeability to water. *SCA.*

Wang, J., Dong, M. & Asghari, K., 2006. *Effect of Oil Viscosity on Heavy Oil/Water Relative Permeability Curves.* Tulsa, OK, Society Petroleum Engineers.

Watson, R. & Ertekin, T., 1988. *The Effect of Steep Temperature Gradient on Relative Permeability Measurements.* Casper, Wyoming, Society of Petroleum Engineers.

Wyllie, M., 1951. *A note on the interrelationship between wetting and non-wetting phase relative permeability,* s.l.: Journal of Petroleum Technology.

Xiao, B., Fan, J. & Ding, F., 2012. Prediction of relative permeability of unsaturated porous media based on fractal theory and Monte Carlo simulation. *Energy Fuels,* 26(11), pp. 6971-6978.

Xu, P., Qiu, S., Yu, B. & Jiang, Z., 2013. Prediction of relative permeability in unsaturated porous media with a fractal approach. *International Journal of Heat Mass Transfer ,* Volume 64, pp. 829-837.

Yasin, H., 2016. Prediction of Crude Oil Prices using Support Vector Regression (SVR) with grid search – cross validation algorithm. *Global Journal of Pure and Applied Mathematics,* 12(4), p. 3009–3020.

Zeidani, M. & Maini, B., 2016. *SAGD Relative Permeability as a Function of Temperature.* Calgary, Alberta, Society of Petroleum Engineers.

Zhang, L.-H., Jing, T., Yu, X. & Yu-long, Z., 2017. Effect of temperature on the oil–water relative permeability for sandstone reservoirs. *International Journal of Heat and Mass Transfer,* Volume 105, pp. 535-548.

Zhang, P. & Tor, A., 2006. Wettability and oil recovery from carbonates: Effects of temperature and potential determining ions. *Colloids and Surfaces A: Physicochem. Eng. Aspects,* Issue 279, pp. 179-187.

Zhao, J. & Dongsheng, W., 2017. Pore-scale simulation of wettability and interfacial tension effects on flooding process for enhanced oil recovery. *RSC Advances,* Volume 7, p. 41391– 41398.

# APPENDICES

# APPENDIX I: PRESSURE CALIBRATION

To ensure reliable and accurate pressure readings were recorded in the experiments, there was the need to calibrate the pressure sensors used for the experiments. The standard pressure calibrator/tester from general Electrics: DRUCK DPI model 615 (figure below) was used to pressure test the experimental rig and calibrate the pressure sensors.

GE DRUCK calibrator

**Pressure testing procedure**

- The DRUCK was connected to the test rig with the valve at the outlet closed after which air pressure of 50 psi was pumped into the system and held for approximately 5 minutes.
- The LCD screen indicator of the device was monitored for any pressure; if there is no drop then the system has no leak.
- When a drop in pressure is on the screen, it indicated a leakage.
- To detect the leakage, solution of LEAK-TEC detergent was sprayed on the connecting joints while looking for bubbles.
- Fittings around the detected leak were tightened and the process was repeated till no more drop in pressure was detected.

**Pressure transducers calibrate procedure**

- The rig was setup, with the differential pressure sensor, DRUCK calibrator, power supply and DAQ Assistant all linked and connected to the LABVIEW program with the PC for data logging.
- The equalising valve was closed.
- Pressure was applied by the DRUCK device to be read by the pressure sensor and recorded in the data logger starting from the lower range.
- The pressured system was held for about 2 minutes to ensure there was no pressure drop.

- The readings from the DRUCK were recorded (reference values) and compared to the measured values from the pressure sensor.
- The process repeated progressively to the upper pressure limit.
- The reference values from the DRUCK and measured values from the sensor were plotted in MS Excel (figure below) to establish the deviation of the measurement and used in tuning the LABVIEW program.

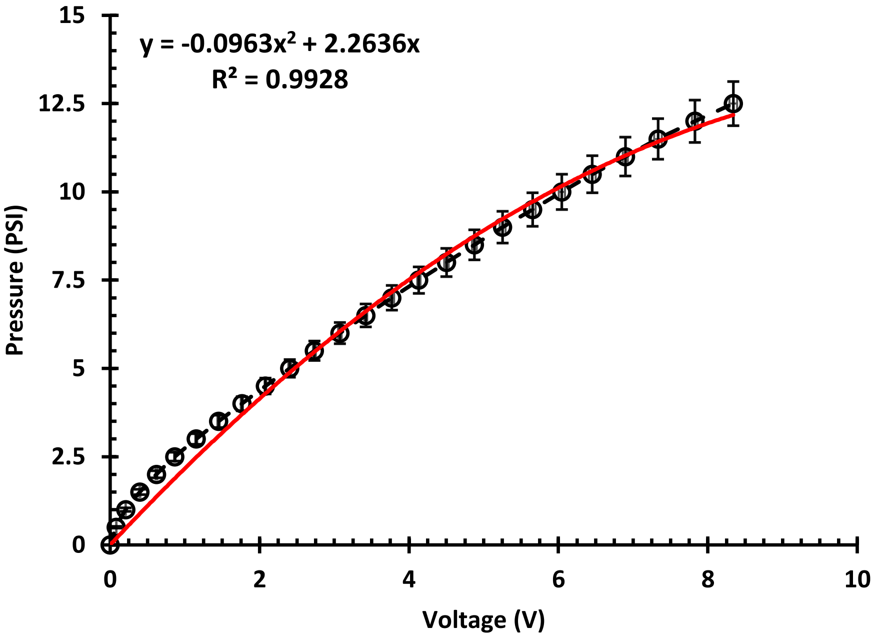

Plot of reference pressure values versus measure values by the pressure sensor.

# APPENDIX II: GRAIN SIZE ANALYSIS FROM MALVERN MASTERSIZER

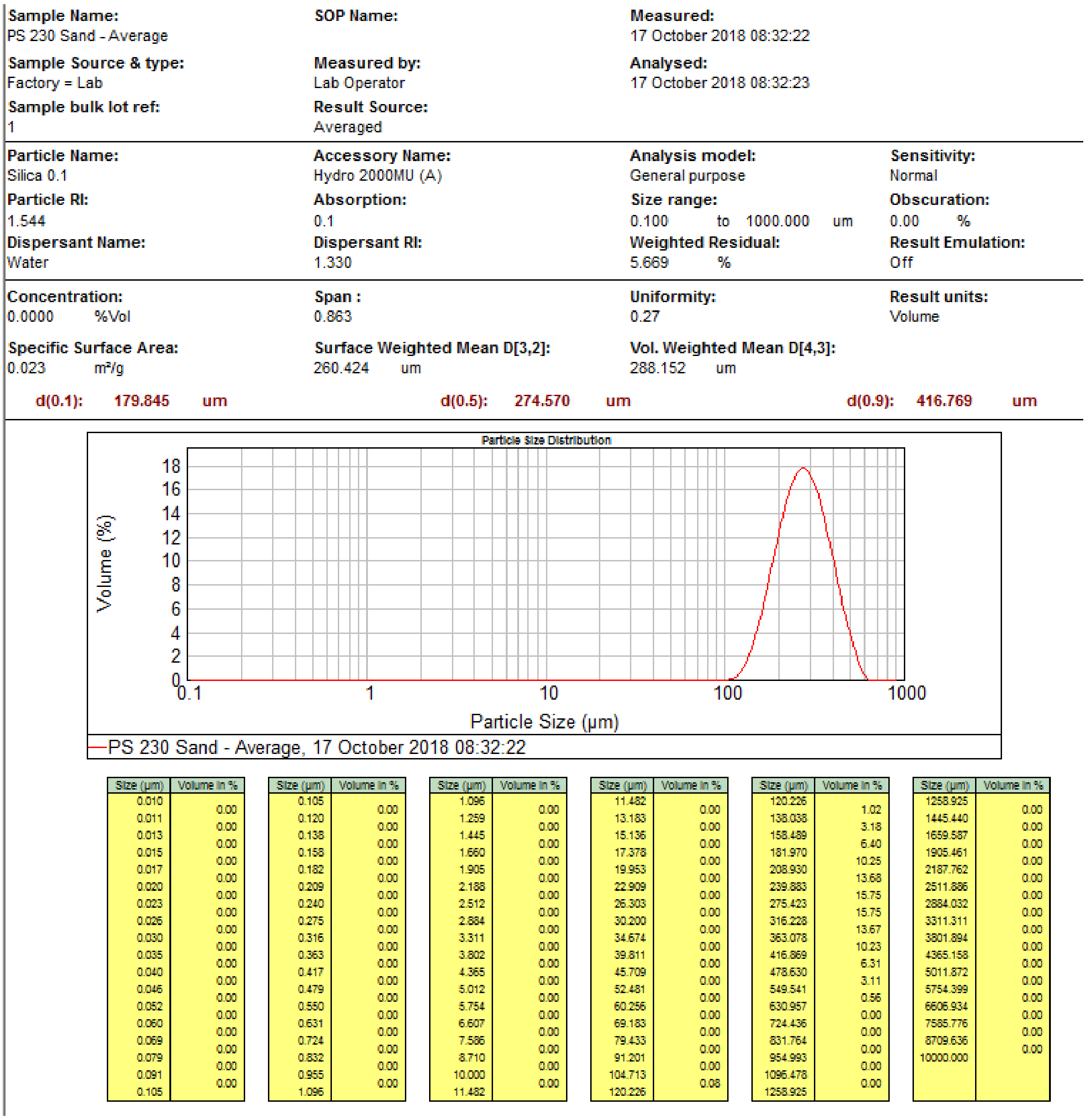

**Sample Name:** PS 230 Sand - Average

**SOP Name:**

**Measured:** 17 October 2018 08:32:22

**Sample Source & type:** Factory = Lab

**Measured by:** Lab Operator

**Analysed:** 17 October 2018 08:32:23

**Sample bulk lot ref:** 1

**Result Source:** Averaged

**Particle Name:** Silica 0.1

**Accessory Name:** Hydro 2000MU (A)

**Analysis model:** General purpose

**Sensitivity:** Normal

**Particle RI:** 1.544

**Absorption:** 0.1

**Size range:** 0.100 to 1000.000 um

**Obscuration:** 0.00 %

**Dispersant Name:** Water

**Dispersant RI:** 1.330

**Weighted Residual:** 5.669 %

**Result Emulation:** Off

**Concentration:** 0.0000 %Vol

**Span :** 0.863

**Uniformity:** 0.27

**Result units:** Volume

**Specific Surface Area:** 0.023 m²/g

**Surface Weighted Mean D[3,2]:** 260.424 um

**Vol. Weighted Mean D[4,3]:** 288.152 um

**d(0.1):** 179.845 um **d(0.5):** 274.570 um **d(0.9):** 416.769 um

| Size (μm) | Volume In % |
|---|---|
| 0.010 | 0.00 |
| 0.011 | 0.00 |
| 0.013 | 0.00 |
| 0.015 | 0.00 |
| 0.017 | 0.00 |
| 0.020 | 0.00 |
| 0.023 | 0.00 |
| 0.026 | 0.00 |
| 0.030 | 0.00 |
| 0.035 | 0.00 |
| 0.040 | 0.00 |
| 0.046 | 0.00 |
| 0.052 | 0.00 |
| 0.060 | 0.00 |
| 0.069 | 0.00 |
| 0.079 | 0.00 |
| 0.091 | 0.00 |
| 0.105 | |

| Size (μm) | Volume In % |
|---|---|
| 0.105 | 0.00 |
| 0.120 | 0.00 |
| 0.138 | 0.00 |
| 0.158 | 0.00 |
| 0.182 | 0.00 |
| 0.209 | 0.00 |
| 0.240 | 0.00 |
| 0.275 | 0.00 |
| 0.316 | 0.00 |
| 0.363 | 0.00 |
| 0.417 | 0.00 |
| 0.479 | 0.00 |
| 0.550 | 0.00 |
| 0.631 | 0.00 |
| 0.724 | 0.00 |
| 0.832 | 0.00 |
| 0.955 | 0.00 |
| 1.096 | |

| Size (μm) | Volume In % |
|---|---|
| 1.096 | 0.00 |
| 1.259 | 0.00 |
| 1.445 | 0.00 |
| 1.660 | 0.00 |
| 1.905 | 0.00 |
| 2.188 | 0.00 |
| 2.512 | 0.00 |
| 2.884 | 0.00 |
| 3.311 | 0.00 |
| 3.802 | 0.00 |
| 4.365 | 0.00 |
| 5.012 | 0.00 |
| 5.754 | 0.00 |
| 6.607 | 0.00 |
| 7.586 | 0.00 |
| 8.710 | 0.00 |
| 10.000 | 0.00 |
| 11.482 | |

| Size (μm) | Volume In % |
|---|---|
| 11.482 | 0.00 |
| 13.183 | 0.00 |
| 15.136 | 0.00 |
| 17.378 | 0.00 |
| 19.953 | 0.00 |
| 22.909 | 0.00 |
| 26.303 | 0.00 |
| 30.200 | 0.00 |
| 34.674 | 0.00 |
| 39.811 | 0.00 |
| 45.709 | 0.00 |
| 52.481 | 0.00 |
| 60.256 | 0.00 |
| 69.183 | 0.00 |
| 79.433 | 0.00 |
| 91.201 | 0.00 |
| 104.713 | 0.08 |
| 120.226 | |

| Size (μm) | Volume In % |
|---|---|
| 120.226 | 1.02 |
| 138.038 | 3.18 |
| 158.489 | 6.40 |
| 181.970 | 10.25 |
| 208.930 | 13.68 |
| 239.883 | 15.75 |
| 275.423 | 15.75 |
| 316.228 | 13.67 |
| 363.078 | 10.23 |
| 416.869 | 6.31 |
| 478.630 | 3.11 |
| 549.541 | 0.56 |
| 630.957 | 0.00 |
| 724.436 | 0.00 |
| 831.764 | 0.00 |
| 954.993 | 0.00 |
| 1096.478 | 0.00 |
| 1258.925 | |

| Size (μm) | Volume In % |
|---|---|
| 1258.925 | 0.00 |
| 1445.440 | 0.00 |
| 1659.587 | 0.00 |
| 1905.461 | 0.00 |
| 2187.762 | 0.00 |
| 2511.886 | 0.00 |
| 2884.032 | 0.00 |
| 3311.311 | 0.00 |
| 3801.894 | 0.00 |
| 4365.158 | 0.00 |
| 5011.872 | 0.00 |
| 5754.399 | 0.00 |
| 6606.934 | 0.00 |
| 7585.776 | 0.00 |
| 8709.636 | 0.00 |
| 10000.000 | |

**Sample Name:**
20/40 Sand - Average

**SOP Name:**

**Measured:**
17 October 2018 09:25:18

**Sample Source & type:**
Factory = Lab

**Measured by:**
Lab Operator

**Analysed:**
17 October 2018 09:25:19

**Sample bulk lot ref:**
1

**Result Source:**
Averaged

---

**Particle Name:**
Silica 0.1

**Accessory Name:**
Hydro 2000MU (A)

**Analysis model:**
General purpose

**Sensitivity:**
Normal

**Particle RI:**
1.544

**Absorption:**
0.1

**Size range:**
0.100 to 1000.000 um

**Obscuration:**
0.00 %

**Dispersant Name:**
Water

**Dispersant RI:**
1.330

**Weighted Residual:**
21.972 %

**Result Emulation:**
Off

---

**Concentration:**
0.0000 %Vol

**Span :**
0.836

**Uniformity:**
0.257

**Result units:**
Volume

**Specific Surface Area:**
0.012 m²/g

**Surface Weighted Mean D[3,2]:**
498.060 um

**Vol. Weighted Mean D[4,3]:**
546.574 um

**d(0.1): 343.921 um** **d(0.5): 527.638 um** **d(0.9): 784.942 um**

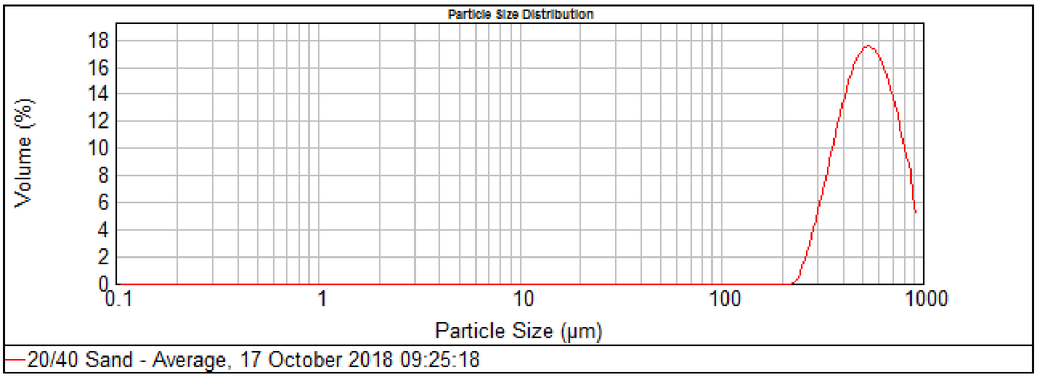

| Size (μm) | Volume In % |
|---|---|
| 0.010 | 0.00 |
| 0.011 | 0.00 |
| 0.013 | 0.00 |
| 0.015 | 0.00 |
| 0.017 | 0.00 |
| 0.020 | 0.00 |
| 0.023 | 0.00 |
| 0.026 | 0.00 |
| 0.030 | 0.00 |
| 0.035 | 0.00 |
| 0.040 | 0.00 |
| 0.046 | 0.00 |
| 0.052 | 0.00 |
| 0.060 | 0.00 |
| 0.069 | 0.00 |
| 0.079 | 0.00 |
| 0.091 | 0.00 |
| 0.105 | |

| Size (μm) | Volume In % |
|---|---|
| 0.105 | 0.00 |
| 0.120 | 0.00 |
| 0.138 | 0.00 |
| 0.158 | 0.00 |
| 0.182 | 0.00 |
| 0.209 | 0.00 |
| 0.240 | 0.00 |
| 0.275 | 0.00 |
| 0.316 | 0.00 |
| 0.363 | 0.00 |
| 0.417 | 0.00 |
| 0.479 | 0.00 |
| 0.550 | 0.00 |
| 0.631 | 0.00 |
| 0.724 | 0.00 |
| 0.832 | 0.00 |
| 0.955 | 0.00 |
| 1.096 | |

| Size (μm) | Volume In % |
|---|---|
| 1.096 | 0.00 |
| 1.259 | 0.00 |
| 1.445 | 0.00 |
| 1.660 | 0.00 |
| 1.905 | 0.00 |
| 2.188 | 0.00 |
| 2.512 | 0.00 |
| 2.884 | 0.00 |
| 3.311 | 0.00 |
| 3.802 | 0.00 |
| 4.365 | 0.00 |
| 5.012 | 0.00 |
| 5.754 | 0.00 |
| 6.607 | 0.00 |
| 7.586 | 0.00 |
| 8.710 | 0.00 |
| 10.000 | 0.00 |
| 11.482 | |

| Size (μm) | Volume In % |
|---|---|
| 11.482 | 0.00 |
| 13.183 | 0.00 |
| 15.136 | 0.00 |
| 17.378 | 0.00 |
| 19.953 | 0.00 |
| 22.909 | 0.00 |
| 26.303 | 0.00 |
| 30.200 | 0.00 |
| 34.674 | 0.00 |
| 39.811 | 0.00 |
| 45.709 | 0.00 |
| 52.481 | 0.00 |
| 60.256 | 0.00 |
| 69.183 | 0.00 |
| 79.433 | 0.00 |
| 91.201 | 0.00 |
| 104.713 | 0.00 |
| 120.226 | |

| Size (μm) | Volume In % |
|---|---|
| 120.226 | 0.00 |
| 138.038 | 0.00 |
| 158.489 | 0.00 |
| 181.970 | 0.00 |
| 208.930 | 0.00 |
| 239.883 | 1.41 |
| 275.423 | 4.29 |
| 316.228 | 7.79 |
| 363.078 | 11.32 |
| 416.869 | 14.18 |
| 478.630 | 15.68 |
| 549.541 | 15.41 |
| 630.957 | 13.49 |
| 724.436 | 10.21 |
| 831.764 | 6.22 |
| 954.993 | 0.00 |
| 1096.478 | 0.00 |
| 1258.925 | |

| Size (μm) | Volume In % |
|---|---|
| 1258.925 | 0.00 |
| 1445.440 | 0.00 |
| 1659.587 | 0.00 |
| 1905.461 | 0.00 |
| 2187.762 | 0.00 |
| 2511.886 | 0.00 |
| 2884.032 | 0.00 |
| 3311.311 | 0.00 |
| 3801.894 | 0.00 |
| 4365.158 | 0.00 |
| 5011.872 | 0.00 |
| 5754.399 | 0.00 |
| 6606.934 | 0.00 |
| 7585.776 | 0.00 |
| 8709.636 | 0.00 |
| 10000.000 | |

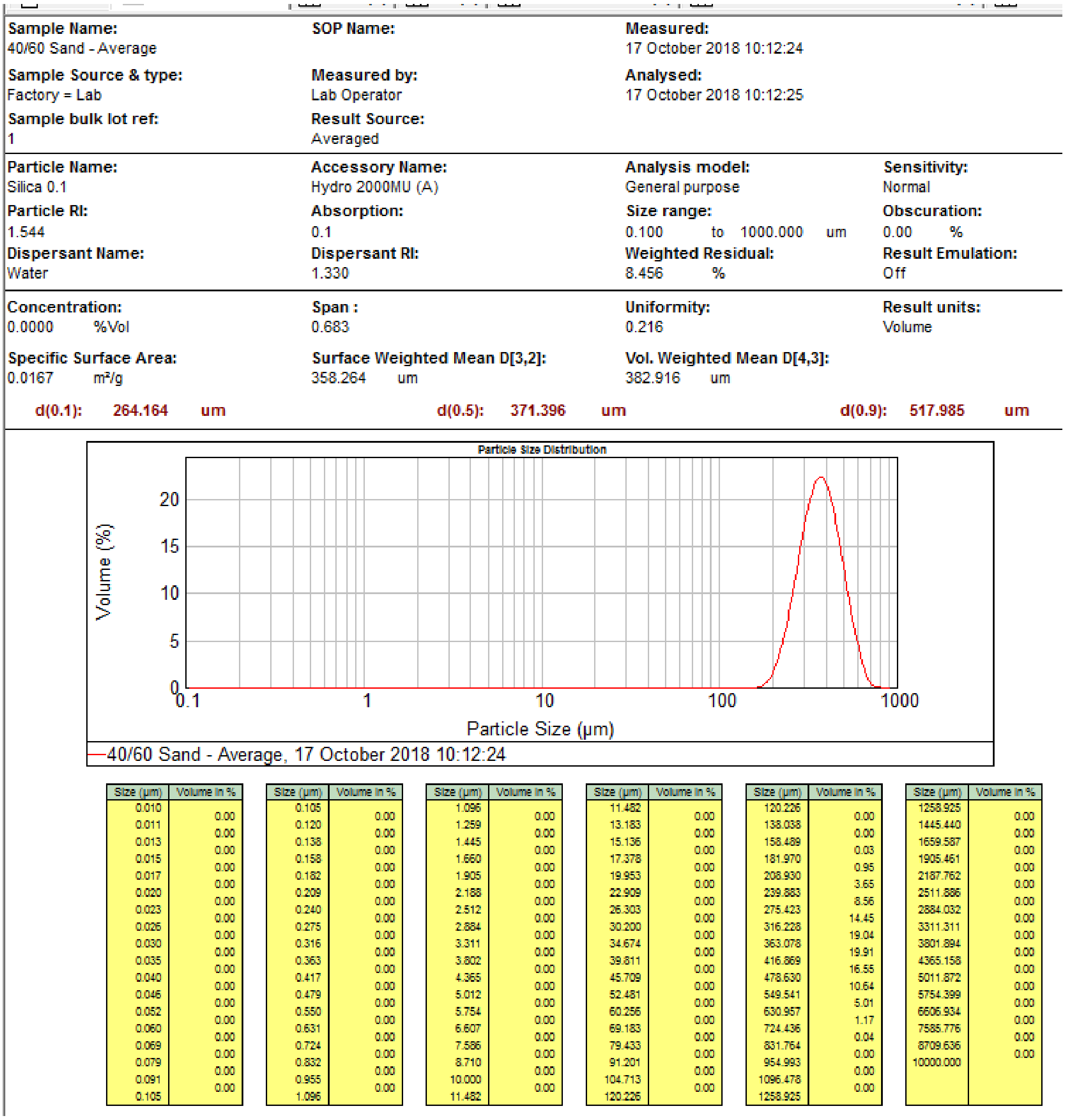

**Sample Name:**
40/60 Sand - Average

**SOP Name:**

**Measured:**
17 October 2018 10:12:24

**Sample Source & type:**
Factory = Lab

**Measured by:**
Lab Operator

**Analysed:**
17 October 2018 10:12:25

**Sample bulk lot ref:**
1

**Result Source:**
Averaged

**Particle Name:**
Silica 0.1

**Accessory Name:**
Hydro 2000MU (A)

**Analysis model:**
General purpose

**Sensitivity:**
Normal

**Particle RI:**
1.544

**Absorption:**
0.1

**Size range:**
0.100 to 1000.000 um

**Obscuration:**
0.00 %

**Dispersant Name:**
Water

**Dispersant RI:**
1.330

**Weighted Residual:**
8.456 %

**Result Emulation:**
Off

**Concentration:**
0.0000 %Vol

**Span :**
0.683

**Uniformity:**
0.216

**Result units:**
Volume

**Specific Surface Area:**
0.0167 m²/g

**Surface Weighted Mean D[3,2]:**
358.264 um

**Vol. Weighted Mean D[4,3]:**
382.916 um

**d(0.1):** 264.164 um **d(0.5):** 371.396 um **d(0.9):** 517.985 um

40/60 Sand - Average, 17 October 2018 10:12:24

| Size (μm) | Volume In % |
|---|---|
| 0.010 | 0.00 |
| 0.011 | 0.00 |
| 0.013 | 0.00 |
| 0.015 | 0.00 |
| 0.017 | 0.00 |
| 0.020 | 0.00 |
| 0.023 | 0.00 |
| 0.026 | 0.00 |
| 0.030 | 0.00 |
| 0.035 | 0.00 |
| 0.040 | 0.00 |
| 0.046 | 0.00 |
| 0.052 | 0.00 |
| 0.060 | 0.00 |
| 0.069 | 0.00 |
| 0.079 | 0.00 |
| 0.091 | 0.00 |
| 0.105 | |

| Size (μm) | Volume In % |
|---|---|
| 0.105 | 0.00 |
| 0.120 | 0.00 |
| 0.138 | 0.00 |
| 0.158 | 0.00 |
| 0.182 | 0.00 |
| 0.209 | 0.00 |
| 0.240 | 0.00 |
| 0.275 | 0.00 |
| 0.316 | 0.00 |
| 0.363 | 0.00 |
| 0.417 | 0.00 |
| 0.479 | 0.00 |
| 0.550 | 0.00 |
| 0.631 | 0.00 |
| 0.724 | 0.00 |
| 0.832 | 0.00 |
| 0.955 | 0.00 |
| 1.096 | |

| Size (μm) | Volume In % |
|---|---|
| 1.096 | 0.00 |
| 1.259 | 0.00 |
| 1.445 | 0.00 |
| 1.660 | 0.00 |
| 1.905 | 0.00 |
| 2.188 | 0.00 |
| 2.512 | 0.00 |
| 2.884 | 0.00 |
| 3.311 | 0.00 |
| 3.802 | 0.00 |
| 4.365 | 0.00 |
| 5.012 | 0.00 |
| 5.754 | 0.00 |
| 6.607 | 0.00 |
| 7.586 | 0.00 |
| 8.710 | 0.00 |
| 10.000 | 0.00 |
| 11.482 | |

| Size (μm) | Volume In % |
|---|---|
| 11.482 | 0.00 |
| 13.183 | 0.00 |
| 15.136 | 0.00 |
| 17.378 | 0.00 |
| 19.953 | 0.00 |
| 22.909 | 0.00 |
| 26.303 | 0.00 |
| 30.200 | 0.00 |
| 34.674 | 0.00 |
| 39.811 | 0.00 |
| 45.709 | 0.00 |
| 52.481 | 0.00 |
| 60.256 | 0.00 |
| 69.183 | 0.00 |
| 79.433 | 0.00 |
| 91.201 | 0.00 |
| 104.713 | 0.00 |
| 120.226 | |

| Size (μm) | Volume In % |
|---|---|
| 120.226 | 0.00 |
| 138.038 | 0.00 |
| 158.489 | 0.03 |
| 181.970 | 0.95 |
| 208.930 | 3.65 |
| 239.883 | 8.56 |
| 275.423 | 14.45 |
| 316.228 | 19.04 |
| 363.078 | 19.91 |
| 416.869 | 16.55 |
| 478.630 | 10.64 |
| 549.541 | 5.01 |
| 630.957 | 1.17 |
| 724.436 | 0.04 |
| 831.764 | 0.00 |
| 954.993 | 0.00 |
| 1096.478 | 0.00 |
| 1258.925 | |

| Size (μm) | Volume In % |
|---|---|
| 1258.925 | 0.00 |
| 1445.440 | 0.00 |
| 1659.587 | 0.00 |
| 1905.461 | 0.00 |
| 2187.762 | 0.00 |
| 2511.886 | 0.00 |
| 2884.032 | 0.00 |
| 3311.311 | 0.00 |
| 3801.894 | 0.00 |
| 4365.158 | 0.00 |
| 5011.872 | 0.00 |
| 5754.399 | 0.00 |
| 6606.934 | 0.00 |
| 7585.776 | 0.00 |
| 8709.636 | 0.00 |
| 10000.000 | |

# APPENDIX III: SIEVE ANALYSIS PROCEDURE

### Objectives of sieve analysis

1. To ascertain the grain size distribution for the test sample.
2. To determine the coefficient of uniformity for the test sample.

### Materials and equipment for sieve analysis

The following laboratory apparatus were used for the sieve analysis for the various sand samples in this experimental work.

- Sand sample
- Pan
- Mechanical shaker
- Weigh balance
- Cleaning brush
- Mesh sieves of different sizes

### Equipment selection and setup

The sieve size selection was done based on visual inspection of the specific sand grains. The selected sieves were then stacked together in descending order of diameter from top to bottom and a pan put under the last sieve to collect any grains that passes through all sieve sizes selected.

### Experimental procedure

The following was followed for the sieve analysis.

#### *Weighing of sample*

- The sample to be analysed was contained in a measuring cylinder.
- A clean pan was placed on the electronic weight balance.
- The machine reading was zeroed so that only the value of the test sample is measured.
- 200 g of grain sample was measured from the balance.

#### *Sieving of sample*

- The 200 grams of sample was poured into the sieve stack.
- The set of sieves was then placed on the mechanical shaker and tightened with the fittings.
- The mechanical shaker was set to an amplitude of 50 and vibration commenced for about 10 minutes.
- The sieved soil samples were measure in the weight balance to get the weight retained by each sieve size.
- From the measure retained weights, percentage retained was computed and plotted in MS Excel.

The procedure was repeated twice for consistency and more accurate readings.

Sieve analysis setup

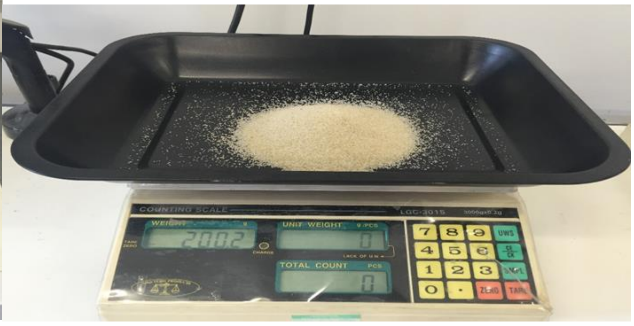

Electronic weigh balance

# APPENDIX IV: VISCOSITY DATA FROM FANN 35 VISCOMETER

| Temperature 29.8 °C | | | | | |
|---|---|---|---|---|---|
| | **RPM** | **Shear Rate, γ (s$^{-1}$)** | **Dial Reading θ** | **Shear Stress, T (dynes/cm$^{2}$)** | **Viscosity, μ (cP)** |
| 1 | 600 | 1020 | 275 | 1405.25 | 137.77 |
| 2 | 300 | 510 | 142 | 725.62 | 142.28 |
| 3 | 200 | 340 | 96 | 490.56 | 144.28 |
| 4 | 180 | 306 | 88 | 449.68 | 146.95 |
| 5 | 100 | 170 | 49 | 250.39 | 147.29 |
| 6 | 90 | 153 | 45 | 229.95 | 150.29 |
| 7 | 60 | 102 | 31 | 158.41 | 155.30 |
| 8 | 30 | 51 | 16 | 81.76 | 160.31 |
| 9 | 6 | 10.2 | 4 | 20.44 | 200.39 |
| 10 | 3 | 5.1 | 2 | 10.22 | 200.39 |
| 11 | 1.8 | 3.06 | 1.5 | 7.67 | 250.49 |
| 12 | 0.9 | 1.53 | 1 | 5.11 | 333.99 |
| **Temperature 39.1 °C** | | | | | |
| 1 | 600 | 1020 | 175 | 894.25 | 87.67 |
| 2 | 300 | 510 | 89 | 454.79 | 89.17 |
| 3 | 200 | 340 | 60 | 306.60 | 90.18 |
| 4 | 180 | 306 | 58 | 296.38 | 96.86 |
| 5 | 100 | 170 | 31 | 158.41 | 93.18 |
| 6 | 90 | 153 | 30 | 153.30 | 100.20 |
| 7 | 60 | 102 | 20 | 102.20 | 100.20 |
| 8 | 30 | 51 | 11 | 56.21 | 110.22 |
| 9 | 6 | 10.2 | 3 | 15.33 | 150.29 |
| 10 | 3 | 5.1 | 2 | 10.22 | 200.39 |
| 11 | 1.8 | 3.06 | 2 | 10.22 | 333.99 |
| 12 | 0.9 | 1.53 | 1 | 5.11 | 333.99 |
| **Temperature 49.6 °C** | | | | | |
| 1 | 600 | 1020 | 111 | 567.21 | 55.6088235 |
| 2 | 300 | 510 | 57 | 291.27 | 57.1117647 |
| 3 | 200 | 340 | 38 | 194.18 | 57.1117647 |
| 4 | 180 | 306 | 36 | 183.96 | 60.1176471 |
| 5 | 100 | 170 | 20 | 102.2 | 60.1176471 |
| 6 | 90 | 153 | 19 | 97.09 | 63.4575163 |
| 7 | 60 | 102 | 13 | 66.43 | 65.127451 |
| 8 | 30 | 51 | 7 | 35.77 | 70.1372549 |
| 9 | 6 | 10.2 | 3 | 15.33 | 150.294118 |
| 10 | 3 | 5.1 | 1 | 5.11 | 100.196078 |
| 11 | 1.8 | 3.06 | 1 | 5.11 | 166.993464 |
| 12 | 0.9 | 1.53 | - | #VALUE! | #VALUE! |

| | | | | | |
|---|---|---|---|---|---|
| **Temperature 59.4 ºC** | | | | | |
| 1 | 600 | 1020 | 77 | 393.47 | 38.5754902 |
| 2 | 300 | 510 | 40 | 204.4 | 40.0784314 |
| 3 | 200 | 340 | 27 | 137.97 | 40.5794118 |
| 4 | 180 | 306 | 25 | 127.75 | 41.748366 |
| 5 | 100 | 170 | 14 | 71.54 | 42.0823529 |
| 6 | 90 | 153 | 14 | 71.54 | 46.7581699 |
| 7 | 60 | 102 | 10 | 51.1 | 50.0980392 |
| 8 | 30 | 51 | 5 | 25.55 | 50.0980392 |
| 9 | 6 | 10.2 | 2 | 10.22 | 100.196078 |
| 10 | 3 | 5.1 | 1 | 5.11 | 100.196078 |
| 11 | 1.8 | 3.06 | 1 | 5.11 | 166.993464 |
| 12 | 0.9 | 1.53 | | 0 | 0 |
| **Temperature 69.1 ºC** | | | | | |
| 1 | 600 | 1020 | 55 | 281.05 | 27.5539216 |
| 2 | 300 | 510 | 29 | 148.19 | 29.0568627 |
| 3 | 200 | 340 | 20 | 102.2 | 30.0588235 |
| 4 | 180 | 306 | 19 | 97.09 | 31.7287582 |
| 5 | 100 | 170 | 11 | 56.21 | 33.0647059 |
| 6 | 90 | 153 | 11 | 56.21 | 36.7385621 |
| 7 | 60 | 102 | 8 | 40.88 | 40.0784314 |
| 8 | 30 | 51 | 4 | 20.44 | 40.0784314 |
| 9 | 6 | 10.2 | 2 | 10.22 | 100.196078 |
| 10 | 3 | 5.1 | 1 | 5.11 | 100.196078 |
| 11 | 1.8 | 3.06 | 1 | 5.11 | 166.993464 |
| 12 | 0.9 | 1.53 | | 0 | 0 |
| **Temperature 78.7 ºC** | | | | | |
| 1 | 600 | 1020 | 41 | 209.51 | 20.5401961 |
| 2 | 300 | 510 | 21 | 107.31 | 21.0411765 |
| 3 | 200 | 340 | 15 | 76.65 | 22.5441176 |
| 4 | 180 | 306 | 14 | 71.54 | 23.379085 |
| 5 | 100 | 170 | 8 | 40.88 | 24.0470588 |
| 6 | 90 | 153 | 8 | 40.88 | 26.7189542 |
| 7 | 60 | 102 | 5 | 25.55 | 25.0490196 |
| 8 | 30 | 51 | 3 | 15.33 | 30.0588235 |
| 9 | 6 | 10.2 | 2 | 10.22 | 100.196078 |
| 10 | 3 | 5.1 | 1 | 5.11 | 100.196078 |
| 11 | 1.8 | 3.06 | 1 | 5.11 | 166.993464 |
| 12 | 0.9 | 1.53 | | 0 | 0 |

# APPENDIX V: PRODUCTION PROFILE FROM THE EXPERIMENTAL RUNS

**40 °C**

**Mineral oil**

**Motor oil**

**0.5 cc/min**

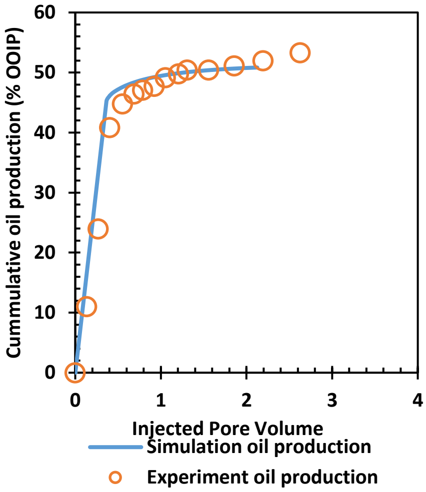

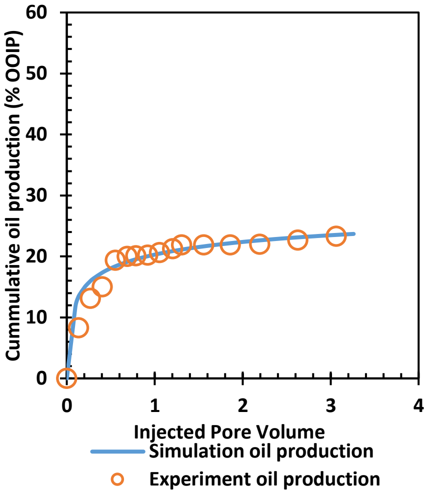

**0.75 cc/min**

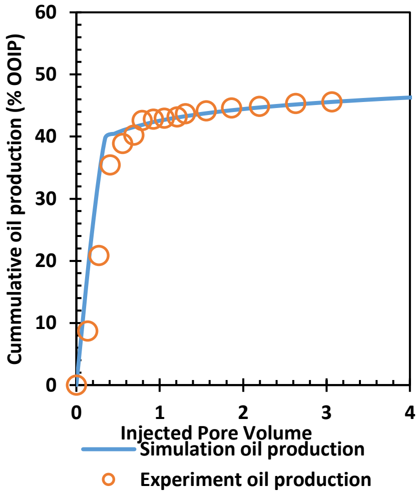

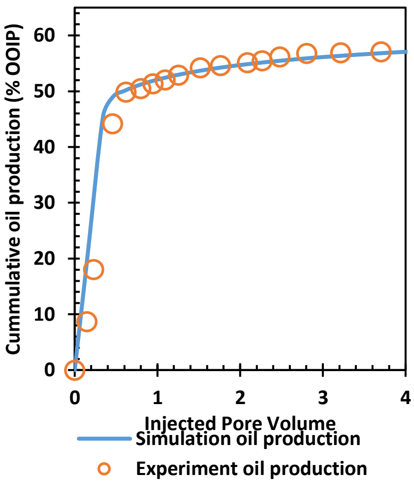

**1.00 cc/min**

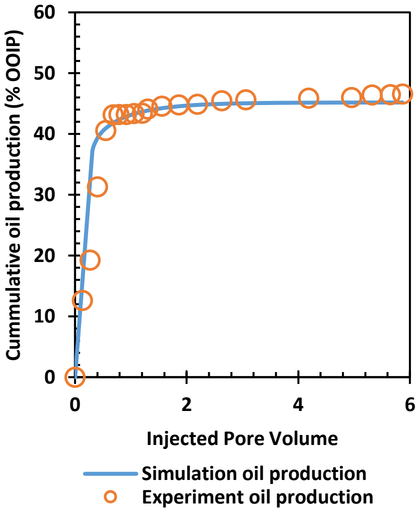

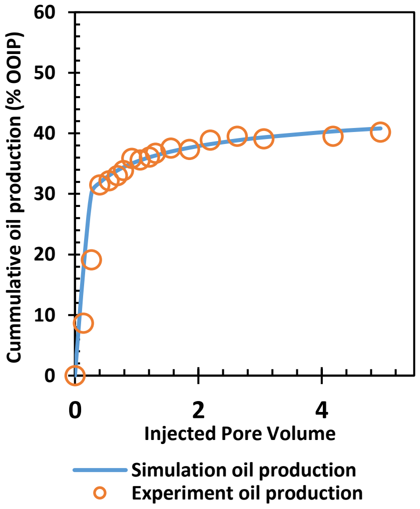

**60 °C** **Mineral oil** **Motor oil**

**0.5 cc/min**

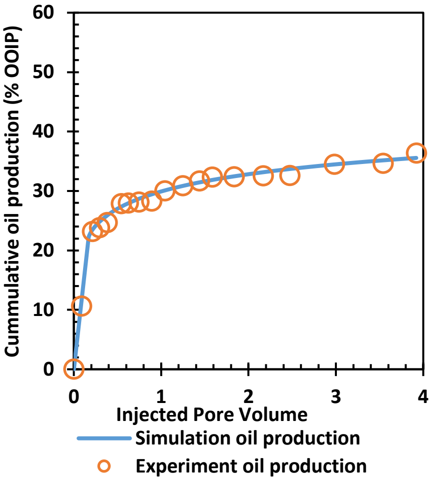

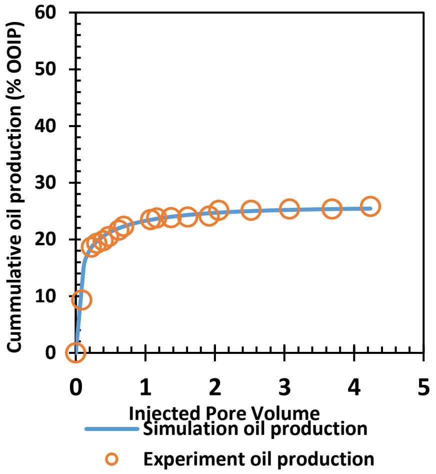

**0.75 cc/min**

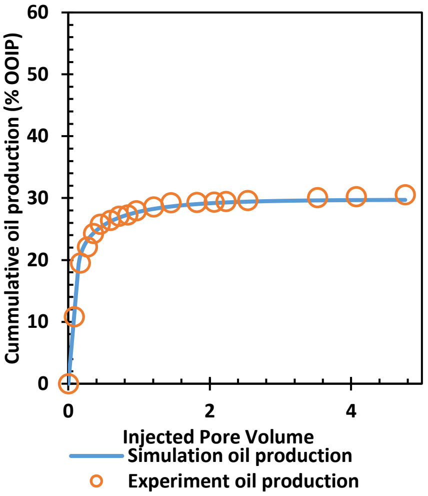

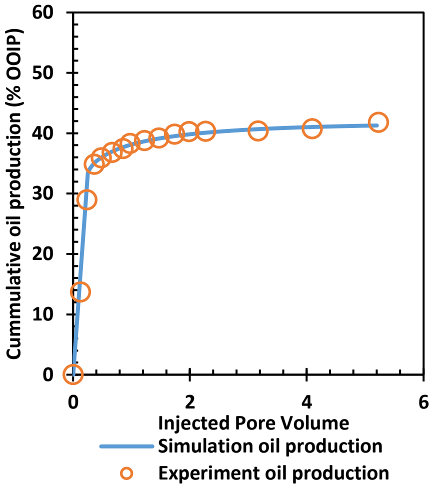

**1.00 cc/min**

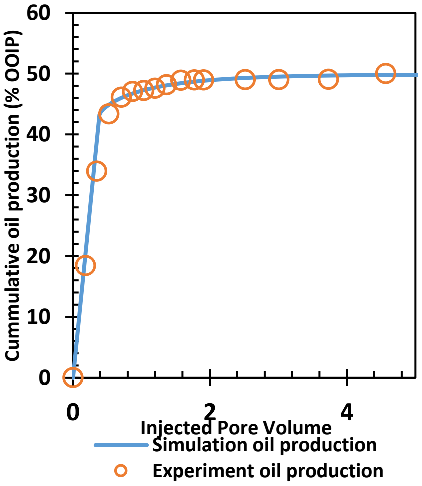

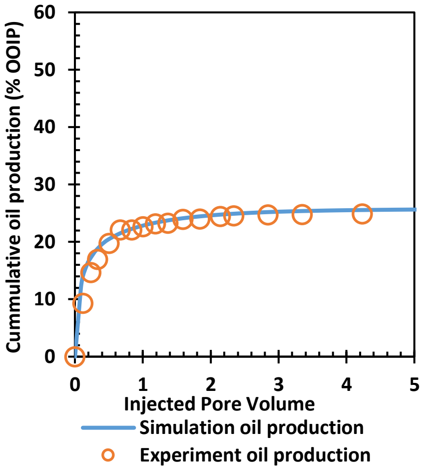

**80 °C** **Mineral oil** **Motor oil**

**0.5 cc/min**

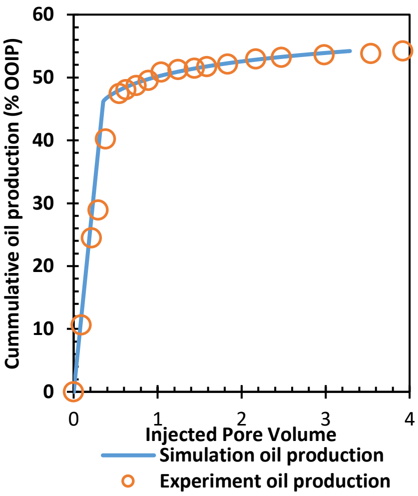

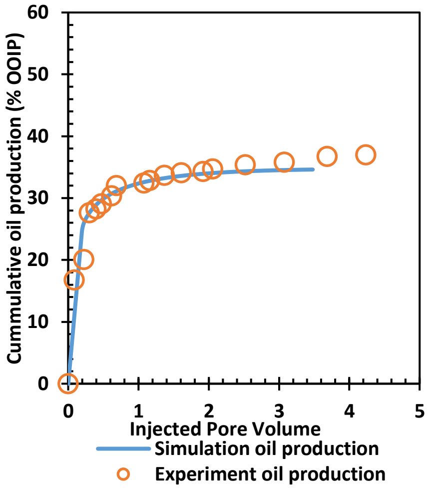

**0.75 cc/min**

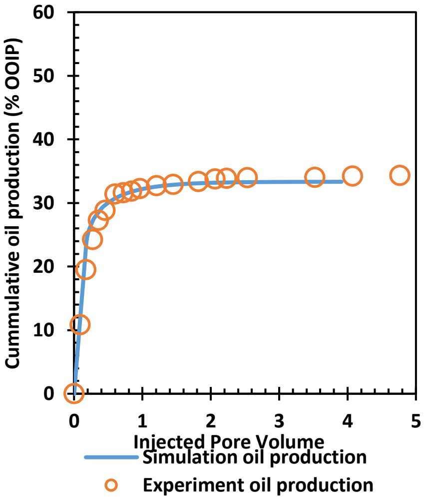

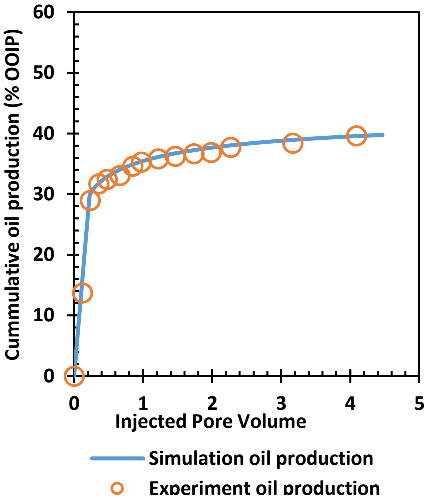

**1.00 cc/min**

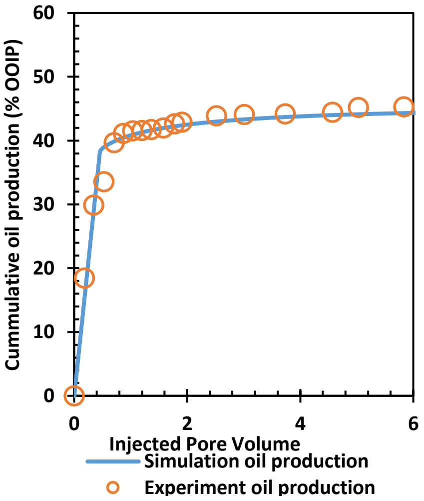

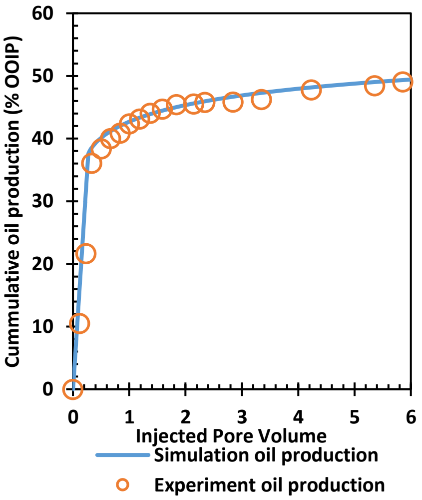

# APPENDIX VI: SATURATION PROFILE

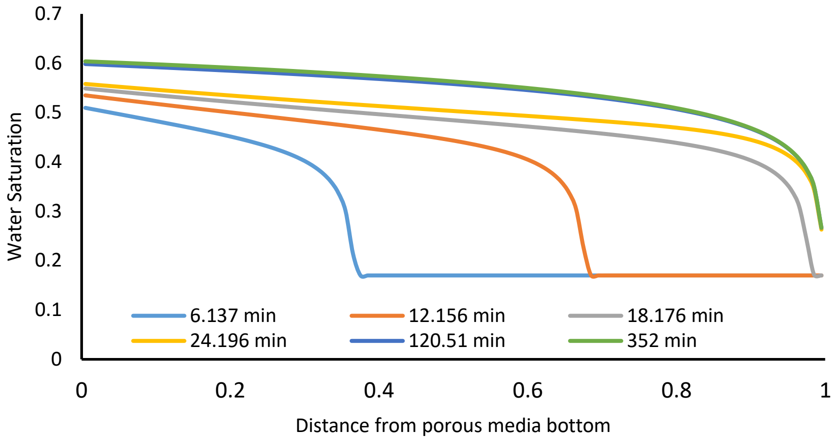

**Mineral oil @ 1.00 cc/min @ 40 °C**

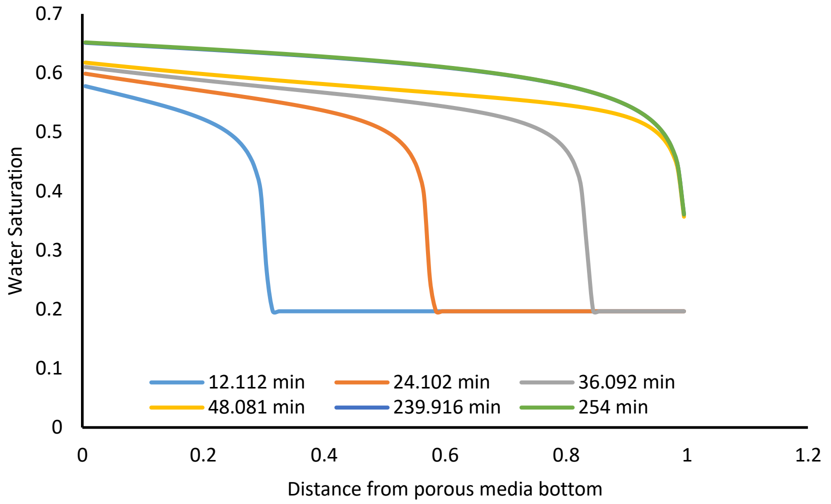

**Mineral oil @ 0.5 cc/min @ 40 °C**

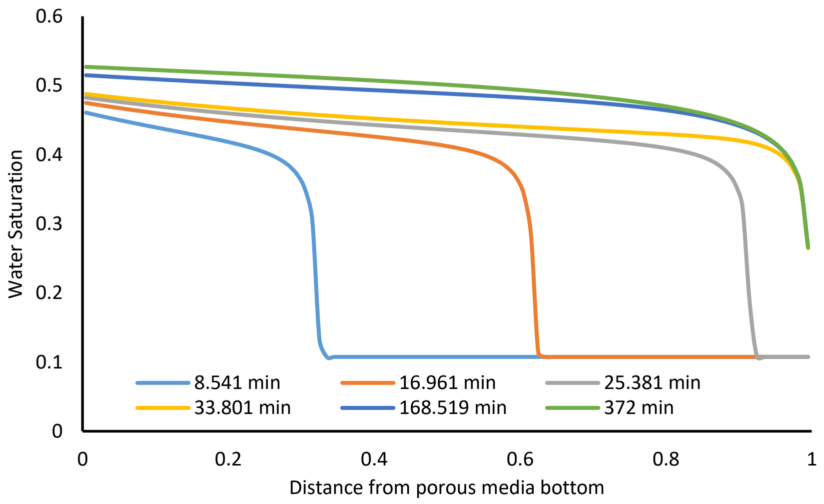

**Mineral oil @ 1.00 cc/min @ 80 °C**

Motor @ 1.00 cc/min @ 40 °C

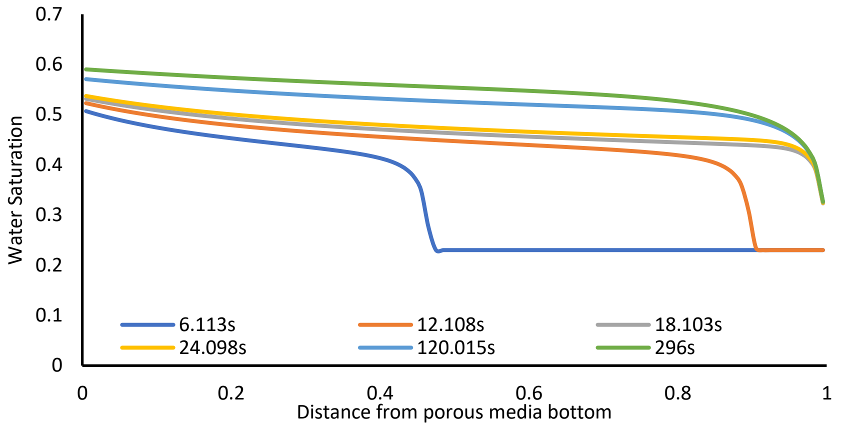

Motor oil @ 0.5 cc/min @ 40 °C

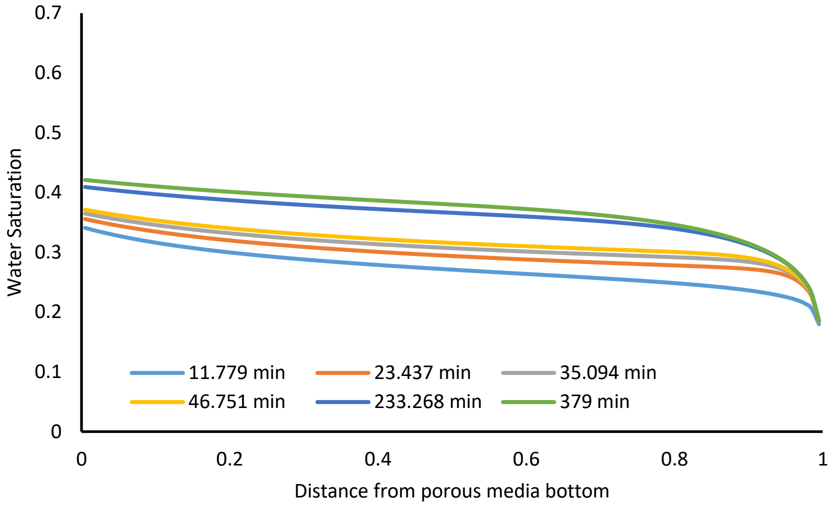

Motor oil @ 1.0 cc/min @ 80 °C

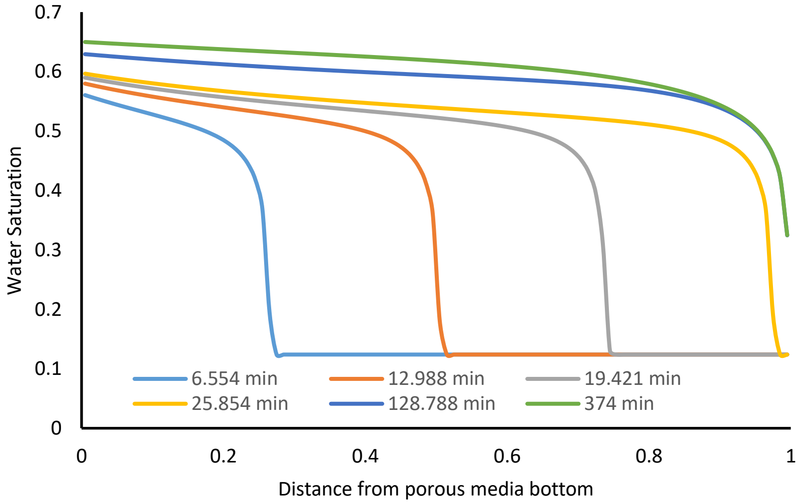

# APPENDIX VII: OIL TEMPERATURE DEPENDENT VISCOSITY UDF

```
/************************************************************/
/*                                              */
/* User-Defined Functions for temperature-dependent viscosity */
/* FLUENT 18.0                                      */
/*                                              */
/* Author: Yakubu Balogun                                 */no
/*   Date: November 2018                              */
/*                                              */
/************************************************************/
#include "udf.h"

DEFINE_PROPERTY(user_vis, cell, thread)

{

  real temp, mu;

  temp = C_T(cell, thread);

  {

/* If the temperature is high, use a small, constant viscosity */

  if (temp > 393)

     mu = 0.0125;

/* Otherwise, use a profile to get higher viscosity values */

  else if (temp >= 293)

     mu = 100607 * pow(temp, -1.913);

  else

     mu = 0.106;

}

  return mu;

}
```